THE AERONAUTICAL QUARTERLY

A Journal devoted to Aeronautics and the Allied Sciences

Volume XI AUGUST 1960 Part 3

CONTENTS

Reattachment of a Two-Dimensional Incompressible Jet to an Adjacent Flat Plate — *C. Bourque and B. G. Newman*

Analysis of Stress Concentrations at Reinforced Holes in Infinite Sheets — *W. H. Wittrick*

Limitations of the Sonic Area Rule — *L. M. Sheppard*

The Stability of the Short-Period Motion of an Airframe having Non-Linear Normal Force and Pitching Moment Curves — *P. A. T. Christopher*

Design Charts for Transient Temperature and Thermal Stress Distributions in Thermally Thick Plates — *J. S. Przemieniecki*

Further Comments on High-Lift Testing in Wind Tunnels with Particular Reference to Jet-Blowing Models — *S. F. J. Butler and J. Williams*

LONDON

ROYAL AERONAUTICAL SOCIETY

4 HAMILTON PLACE W1

15/-

THE AERONAUTICAL QUARTERLY

Editorial Board

Dr. A. M. BALLANTYNE, T.D., B.Sc., Ph.D., F.R.Ae.S., Hon.F.C.A.I., F.I.A.S. (*Chairman*)

Mr. HAYNE CONSTANT, C.B., C.B.E., M.A., F.R.S., F.R.Ae.S.

Sir HAROLD ROXBEE COX, D.Sc., D.I.C., Ph.D., F.R.Ae.S., F.I.A.S.

Sir WILLIAM FARREN, C.B., M.B.E., M.A., D.Sc., F.R.S., Hon.F.R.Ae.S., Hon.F.I.A.S.

Sir ARNOLD HALL, M.A., F.R.S., F.R.Ae.S.

Sir BENNETT MELVILL JONES, C.B.E., A.F.C., M.A., F.R.S., Hon.F.R.Ae.S., Hon.F.I.A.S.

Sir ALFRED PUGSLEY, O.B.E., D.Sc., F.R.S., F.R.Ae.S.

Sir GEOFFREY TAYLOR, M.A., D.Sc., F.R.S., Hon.F.R.Ae.S.

Dr. P. B. WALKER, C.B.E., M.A., F.R.Ae.S.

Editor—E. C. PIKE, M.A., A.F.R.Ae.S.

Editorial Referees

Aerodynamics

(a) *General*

Sir LEONARD BAIRSTOW
Mr. D. KEITH-LUCAS
Prof. W. A. MAIR
Mr. L. F. NICHOLSON
Dr. R. C. PANKHURST
Mr. E. F. RELF
Prof. E. J. RICHARDS
Dr. B. THWAITES

(b) *Fluid Motion*

Dr. G. K. BATCHELOR
Mr. A. FAGE
Dr. D. W. HOLDER
Prof. L. HOWARTH
Dr. W. P. JONES
Dr. J. W. MACCOLL
Prof. J. H. PRESTON
Prof. H. B. SQUIRE
Prof. G. TEMPLE
Prof. G. N. WARD
Prof. A. D. YOUNG

(c) *Stability and Control*

Mr. L. W. BRYANT
Mr. S. B. GATES
Mr. H. B. IRVING
Mr. G. H. LEE
Mr. M. B. MORGAN
Mr. H. H. B. M. THOMAS

Helicopters and Propellers

Prof. J. A. J. BENNETT
Mr. P. BRETT
Mr. L. G. FAIRHURST
Mr. R. HAFNER
Dr. G. S. HISLOP
Capt. R. N. LIPTROT

Instruments and Electrical Equipment

Dr. G. E. BAIRSTO
Sir GEORGE GARDNER
Dr. C. S. HUDSON
Mr. C. N. JAQUES
Mr. F. W. MEREDITH

Aircraft Design

Mr. R. BOORMAN
Mr. R. M. CLARKSON
Mr. A. N. CLIFTON
Mr. H. H. GARDNER
Mr. H. KNOWLER
Mr. W. E. W. PETTER
Mr. F. H. POLLICUTT
Dr. A. E. RUSSELL
Mr. R. S. STAFFORD
Mr. W. H. STEPHENS

Radio and Radar

Mr. J. F. ATHERTON
Mr. B. G. GATES
Dr. R. L. SMITH ROSE
Dr. A. M. UTTLEY
Sir ROBERT WATSON-WATT

Aviation Medicine

Dr. K. G. BERGIN
Dr. A. BUCHANAN BARBOUR

Meteorology

Sir DAVID BRUNT
Mr. J. K. HARDY
Prof. P. A. SHEPPARD

Sound

Mr. W. MAKINSON
Mr. F. B. GREATREX
Mr. N. FLEMING

Aircraft Propulsion

Mr. A. D. BAXTER
Mr. A. V. CLEAVER
Sir A. H. ROY FEDDEN
Dr. S. HOOKER
Mr. A. R. HOWELL
Mr. W. H. LINDSEY
Mr. P. LLOYD
Dr. A. W. MORLEY
Dr. E. S. MOULT
Mr. N. S. MUIR
Mr. F. NIXON
Mr. F. M. OWNER
Mr. H. PEARSON
Mr. H. SAMMONS
Prof. O. A. SAUNDERS
Prof. A. G. SMITH

Air Transport

Mr. A. C. CAMPBELL ORDE
Mr. P. G. MASEFIELD
Mr. N. E. ROWE
Mr. B. S. SHENSTONE
Mr. W. TYE

Aircraft Accessories

Mr. A. E. BINGHAM
Mr. W. C. CLOTHIER
Mr. H. G. CONWAY
Sir GEORGE DOWTY
Mr. R. GRAHAM
Mr. C. D. HOLLAND

Performance

Mr. H. DAVIES
Mr. D. R. NEWMAN
Mr. A. H. YATES

Flight Testing

Mr. R. R. DUDDY
Mr. P. A. HUFTON
Mr. E. T. JONES
Mr. S. SCOTT HALL
Mr. H. L. STEVENS

Structures

Prof. J. H. ARGYRIS
Mr. A. C. BROWN
Mr. H. L. COX
Mr. D. J. FARRAR
Prof. W. S. HEMP
Prof. R. HILL
Mr. H. B. HOWARD
Col. H. T. JESSOP
Mr. E. D. KEEN
Mr. F. A. KERRY
Dr. D. M. A. LEGGETT
Mr. R. L. LICKLEY
Prof. A. J. SUTTON PIPPARD
Prof. S. C. REDSHAW
Mr. R. H. SANDIFER
Sir RICHARD SOUTHWELL

Fuels and Oils

Mr. E. L. BASS
Dr. J. W. DRINKWATER
Prof. F. H. GARNER
Prof. W. E. GARNER
Dr. K. E. W. RIDLER
Dr. C. G. WILLIAMS

Materials

Dr. L. AITCHISON
Dr. N. P. ALLEN
Mr. G. FORREST
Prof. N. F. MOTT
Mr. L. ROTHERHAM
Dr. H. SUTTON
Dr. C. SYKES

Vibration and Flutter

Mr. E. G. BROADBENT
Prof. A. R. COLLAR
Prof. W. J. DUNCAN
Mr. H. TEMPLETON
Mr. M. O. W. WOLFE

Reattachment of a Two-Dimensional, Incompressible Jet to an Adjacent Flat Plate*

C. BOURQUE and B. G. NEWMAN†

SUMMARY: As part of a general investigation into Coanda effect, a study has been made of the reattachment of a two-dimensional, incompressible, turbulent jet to an adjacent, inclined, flat plate. The jet separates from the boundaries at the slot lips and reattaches to the plate downstream, a phenomenon which is associated with the lowering of the pressure between the jet and the plate accompanying the entrainment of fluid there. It is found that the flow becomes independent of both the length of the plate and the Reynolds number when these parameters are sufficiently large: the flow, scaled with respect to the width of the slot, is then uniquely determined by the plate inclination. Two approximate theories are developed for the mean pressure within the separation bubble, the position of reattachment and the increase in volume flow from the slot: the agreement with experiment is fairly satisfactory. These theories are a development of Dodds's analysis for the reattachment of a jet to a plate offset from, and parallel to, the axis of the slot and, for the purpose of comparison, a limited study is also made of this flow.

1. Introduction

Jets are frequently observed to adhere to and flow round nearby solid boundaries. This is seen, for example, when one's finger is held close to a thin stream of water issuing from a tap, or when tea is poured from a badly-designed teapot. This general class of phenomena, which may be observed in both liquid and gaseous jets, has become known as Coanda effect, after Henri Coanda the inventor, who applied it in numerous inventions[1-5]. In these applications a gas was emitted from a thin slot, one wall of which was extended as a series of straight segments of increasing length which progressively diverged from the axis of the slot. These were arranged so that the flow became reattached to the wall after each discontinuity in surface slope and thus the jet was progressively deflected. The deflection of the

*This report is abstracted from the thesis "Déviation d'un Jet Turbulent Incompressible par un Volet Incliné—Effet Coanda" presented by the first author to the Université Laval for the degree of M.Sc. The work was supported by the Defence Research Board of Canada under grant number 9550-05.

†Canadair Visiting Research Professor in Fluid Mechanics, Université Laval, 1958-59. Professor of Aerodynamics, McGill University.

Received November 1959.

THE AERONAUTICAL QUARTERLY

Editorial Board

Dr. A. M. BALLANTYNE, T.D., B.Sc., Ph.D., F.R.Ae.S., Hon.F.C.A.I., F.I.A.S. (*Chairman*)

Mr. HAYNE CONSTANT, C.B., C.B.E., M.A., F.R.S., F.R.Ae.S.

Sir HAROLD ROXBEE COX, D.Sc., D.I.C., Ph.D., F.R.Ae.S., F.I.A.S.

Sir WILLIAM FARREN, C.B., M.B.E., M.A., D.Sc., F.R.S., Hon.F.R.Ae.S., Hon.F.I.A.S.

Sir ARNOLD HALL, M.A., F.R.S., F.R.Ae.S.

Sir BENNETT MELVILL JONES, C.B.E., A.F.C., M.A., F.R.S., Hon.F.R.Ae.S., Hon.F.I.A.S.

Sir ALFRED PUGSLEY, O.B.E., D.Sc., F.R.S., F.R.Ae.S.

Sir GEOFFREY TAYLOR, M.A., D.Sc., F.R.S., Hon.F.R.Ae.S.

Dr. P. B. WALKER, C.B.E., M.A., F.R.Ae.S.

Editor—E. C. PIKE, M.A., A.F.R.Ae.S.

Editorial Referees

Aerodynamics

(a) *General*

Sir LEONARD BAIRSTOW
Mr. D. KEITH-LUCAS
Prof. W. A. MAIR
Mr. L. F. NICHOLSON
Dr. R. C. PANKHURST
Mr. E. F. RELF
Prof. E. J. RICHARDS
Dr. B. THWAITES

(b) *Field Motion*

Dr. G. K. BATCHELOR
Mr. A. FAGE
Dr. D. W. HOLDER
Prof. L. HOWARTH
Dr. W. P. JONES
Dr. J. W. MACCOLL
Prof. J. H. PRESTON
Prof. H. B. SQUIRE
Prof. G. TEMPLE
Prof. G. N. WARD
Prof. A. D. YOUNG

(c) *Stability and Control*

Mr. L. W. BRYANT
Mr. S. B. GATES
Mr. H. B. IRVING
Mr. G. H. LEE
Mr. M. B. MORIAN
Mr. H. H. B. M. THOMAS

Helicopters and Propellers

Prof. J. A. J. BENNETT
Mr. P. BRETT
Mr. L. G. FAIRHURST
Mr. R. HAFNER
Dr. G. S. HISLOP
Capt. R. N. LIPTROT

Instruments and Electrical Equipment

Dr. G. E. BAIRSTO
Sir GEORGE GARDNER
Dr. C. S. HUDSON
Mr. C. N. JAQUES
Mr. F. W. MEREDITH

Aircraft Design

Mr. R. BOOSMAN
Mr. R. M. CLARKSON
Mr. A. N. CLIFTON
Mr. H. H. GARDNER
Mr. H. KNOWLER
Mr. W. E. W. PETTER
Mr. F. H. POLLICUTT
Dr. A. E. RUSSELL
Mr. R. S. STAFFORD
Mr. W. H. STEPHENS

Radio and Radar

Mr. J. F. ATHERTON
Mr. B. G. GATES
Dr. R. L. SMITH ROSE
Dr. A. M. UTTLEY
Sir ROBERT WATSON-WATT

Aviation Medicine

Dr. K. G. BERGIN
Dr. A. BUCHANAN BARBOUR

Meteorology

Sir DAVID BRUNT
Mr. J. K. HARDY
Prof. P. A. SHEPPARD

Sound

Mr. W. MAKINSON
Mr. F. B. GREATREX
Mr. N. FLEMING

Aircraft Propulsion

Mr. A. D. BAXTER
Mr. A. V. CLEAVER
Sir A. H. ROY FEDDEN
Dr. S. HOOKER
Mr. A. R. HOWELL
Mr. W. H. LINDSEY
Mr. P. LLOYD
Dr. A. W. MORLEY
Dr. E. S. MOULT
Mr. N. S. MUIR
Mr. F. NIXON
Mr. F. M. OWNER
Mr. H. PEARSON
Mr. H. SAMMONS
Prof. O. A. SAUNDERS
Prof. A. G. SMITH

Air Transport

Mr. A. [illegible] CAMPBELL ORDE
Mr. P. G. MASEFIELD
Mr. N. E. ROWE
Mr. B. [illegible] SHENSTONE
Mr. W. TYE

Aircraft Accessories

Mr. A. E. BINGHAM
Mr. W. C. CLOTHIER
Mr. H. G. CONWAY
Sir GEORGE DOWTY
Mr. R. GRAHAM
Mr. C. D. HOLLAND

Performance

Mr. H. DAVIES
Mr. D. R. NEWMAN
Mr. A. H. YATES

Flight Testing

Mr. R. R. DUDDY
Mr. P. A. HUFTON
Mr. E. T. JONES
Mr. S. SCOTT HALL
Mr. H. L. STEVENS

Structures

Prof. J. H. ARGYRIS
Mr. A. C. BROWN
Mr. H. L. COX
Mr. D. J. FARRAR
Prof. W. S. HEMP
Prof. R. HILL
Mr. H. B. HOWARD
Col. H. T. JESSOP
Mr. E. D. KEEN
Mr. F. A. KERRY
Dr. D. M. A. LEGGETT
Mr. R. L. LICKLEY
Prof. A. J. SUTTON PIPPARD
Prof. S. C. REDSHAW
Mr. R. H. SANDIFER
Sir RICHARD SOUTHWELL

Fuels and Oils

Mr. E. L. BASS
Dr. J. W. DRINKWATER
Prof. F. H. GARNER
Prof. W. E. GARNER
Dr. K. E. W. RIDLER
Dr. C. G. WILLIAMS

Materials

Dr. L. AITCHISON
Dr. N. P. ALLEN
Mr. G. FORREST
Prof. N. F. MOTT
Mr. L. ROTHERHAM
Dr. H. SUTTON
Dr. C. SYKES

Vibration and Flutter

Mr. E. G. BROADBENT
Prof. A. R. COLLAR
Prof. W. J. DUNCAN
Mr. H. TEMPLETON
Mr. M. O. W. WOLFE

Reattachment of a Two-Dimensional, Incompressible Jet to an Adjacent Flat Plate*

C. BOURQUE and B. G. NEWMAN†

SUMMARY: As part of a general investigation into Coanda effect, a study has been made of the reattachment of a two-dimensional, incompressible, turbulent jet to an adjacent, inclined, flat plate. The jet separates from the boundaries at the slot lips and reattaches to the plate downstream, a phenomenon which is associated with the lowering of the pressure between the jet and the plate accompanying the entrainment of fluid there. It is found that the flow becomes independent of both the length of the plate and the Reynolds number when these parameters are sufficiently large: the flow, scaled with respect to the width of the slot, is then uniquely determined by the plate inclination. Two approximate theories are developed for the mean pressure within the separation bubble, the position of reattachment and the increase in volume flow from the slot: the agreement with experiment is fairly satisfactory. These theories are a development of Dodds's analysis for the reattachment of a jet to a plate offset from, and parallel to, the axis of the slot and, for the purpose of comparison, a limited study is also made of this flow.

1. Introduction

Jets are frequently observed to adhere to and flow round nearby solid boundaries. This is seen, for example, when one's finger is held close to a thin stream of water issuing from a tap, or when tea is poured from a badly-designed teapot. This general class of phenomena, which may be observed in both liquid and gaseous jets, has become known as Coanda effect, after Henri Coanda the inventor, who applied it in numerous inventions[1-5]. In these applications a gas was emitted from a thin slot, one wall of which was extended as a series of straight segments of increasing length which progressively diverged from the axis of the slot. These were arranged so that the flow became reattached to the wall after each discontinuity in surface slope and thus the jet was progressively deflected. The deflection of the

---

*This report is abstracted from the thesis "Déviation d'un Jet Turbulent Incompressible par un Volet Incliné—Effet Coanda" presented by the first author to the Université Laval for the degree of M.Sc. The work was supported by the Defence Research Board of Canada under grant number 9550-05.

†Canadair Visiting Research Professor in Fluid Mechanics, Université Laval, 1958-59. Professor of Aerodynamics, McGill University.

Received November 1959.

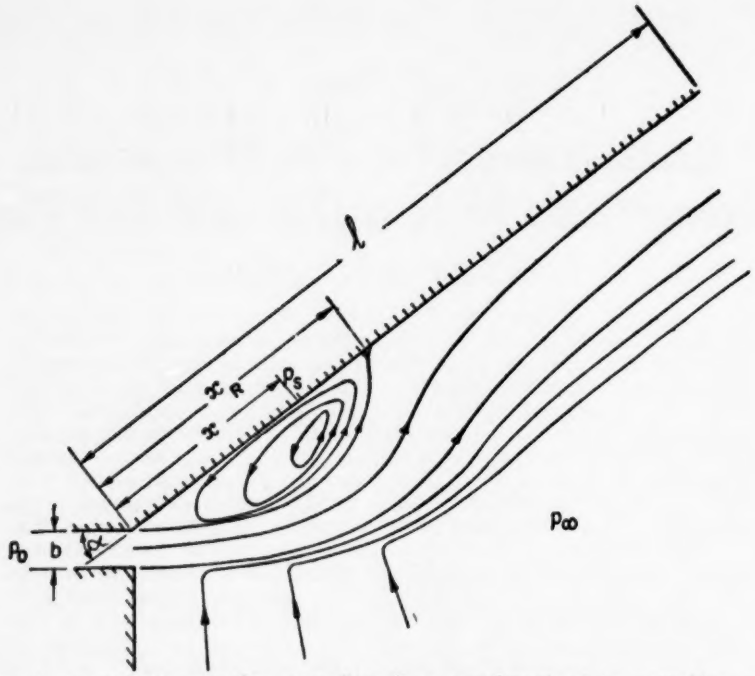

FIGURE 1. Approximate mean-flow streamlines for a two-dimensional jet reattaching to an inclined flat plate.

flow at the slot and at each subsequent corner is associated with a reduced wall pressure and thus, for given upstream conditions, the mass flow from the slot is greater than that of a free jet if the flow is subsonic. Furthermore, the quantity of fluid entrained by the jet from the surroundings is apparently increased when the jet is deflected. These features were exploited by Coanda in both two-dimensional and axisymmetric situations to improve the scavenging of internal combustion engines, to augment the thrust of a nozzle with induced flow[6], to increase the maximum lift coefficient of a wing and to achieve possible improvements in the performance of other devices. A critical review of these devices has been given by Voedisch[5]. It should be noted that in these applications the surrounding fluid is either moving or at rest.

Although a jet is probably deflected more efficiently by a curved surface[7-9], there is nevertheless considerable interest in Coanda's particular wall geometry, the simplest form of which consists of a single flat plate inclined at an angle to the axis of a two-dimensional slot. The flow from this slot with the surrounding fluid at rest is the main topic of the present paper (Fig. 1).

After leaving the slot the flow separates from the surface and, if the plate is sufficiently long and its inclination is sufficiently small, the jet curves towards the

plate and eventually reattaches to it, enclosing a separation bubble. The forces on the plate associated with this flow have been measured by von Glahn[8] and a physical explanation of the behaviour has been given by Squire[7]. Imagine the jet flowing freely, *i.e.* completely separated from the plate. After leaving the slot the highly unstable shear layers on both sides of the jet quickly become turbulent and the surrounding fluid is rapidly entrained. That fluid which is entrained near the plate is slightly accelerated there and thus the static pressure on the wall becomes less than that of the surroundings, with the minimum pressure some distance from the corner. In consequence the jet curves towards the wall, which further reduces the pressure there. Thus eventually, if the wall is long enough, the flow reattaches to it, enclosing a separation bubble. It is clear from this explanation that the establishment of the flow depends on the maintenance of approximately two-dimensional conditions, in particular the prevention of spanwise flow parallel to the length of the slot. In practice such flow is prevented by the use of end plates or similar devices. It is found experimentally that, at large plate inclinations, the flow can be of the type just described or can be fully detached, depending on how it is initiated. For example, if reattached flow is established at a low inclination and the plate angle is then increased, the flow will remain attached to a relatively high angle. On the other hand if the flow is initially detached from the plate and the angle of inclination is reduced, the flow will spontaneously reattach to the plate at a smaller angle.

A potential theory for this flow has been given by Metral[3] in which the jet is assumed to be fully attached to the wall. The pressure at the sharp corner is thus infinitely negative and the theoretical mass flow is too large. The theory is developed by examining the flow in the hodograph plane and is similar to analyses for flow round other curved surfaces which have been given by Lighthill[11] and Yen[12]. Of necessity the theory cannot predict the reattachment of the jet to the surface or the details of the flow near the sharp corner. In order to do this the entrainment of surrounding fluid by the jet must be included in the analysis. Entrainment between a shear layer and its surroundings is fundamental to the understanding of a variety of viscous flows. For example, an approximate theory using the concept of entrainment for a two-dimensional turbulent boundary layer has been given by Head[13]. An entrainment theory for a jet issuing parallel to and offset from a flat plate (Fig. 2) has been developed recently by Dodds[14]*. In this latter case the jet reattaches to the plate, enclosing a separation bubble, and the theory predicts the mean pressure within the bubble and the position of reattachment of the mean flow streamline which divides that flow which proceeds downstream along the plate from that which recirculates within the bubble. This is the dividing streamline identified by Chapman and his associates in their study of separated flows[15].

The purpose of the present paper is to apply Dodds's theory to the Coanda deflection of a jet by a flat plate and to compare the predictions with experiment.

**Note added in proof*: A similar analysis has also been made recently by H. R. Chaplin "The Effect of Jet Mixing on the Annular Jet", David Taylor Model Basin Report 1375, 1959.

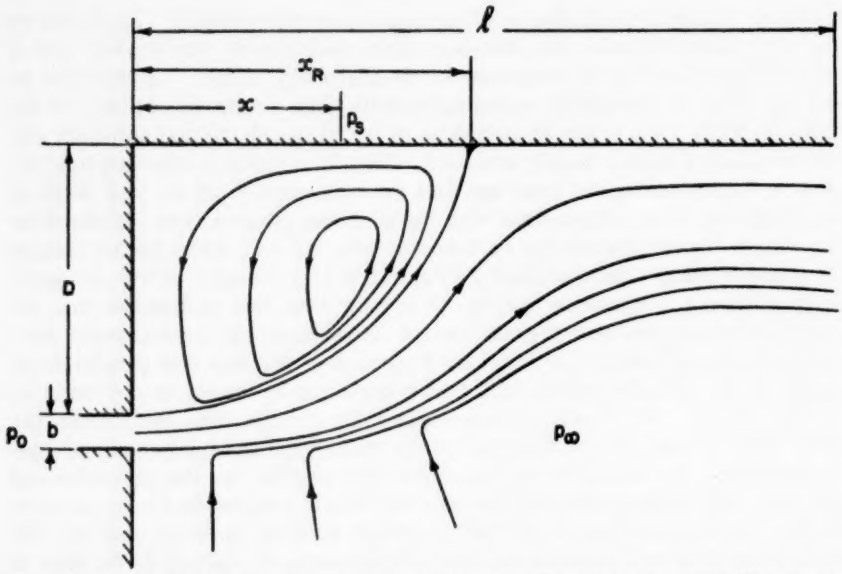

FIGURE 2. Approximate mean-flow streamlines for a two-dimensional jet reattaching to an offset parallel plate.

In doing this the original theory has been extended and, for the purpose of comparison, some measurements have also been made of the flow which Dodds studied. In addition both flows have been examined from the viewpoint of dimensional analysis to isolate the relative importance of the various parameters. The experimental investigation has been confined to an air jet at speeds low enough for the flow to be effectively incompressible.

NOTATION

- b width of the slot
- C_p pressure coefficient: $C_{pB}=(p_B-p_\infty)/(p_0-p_\infty)$ $C_{ps}=(p_s-p_\infty)/(p_0-p_\infty)$
- D distance of the offset plate from the axis of the slot
- J jet momentum per unit span of slot (suffixes 1, 2 and 3 refer to the momenta shown in Figs. 3 and 4)
- l length of the plate
- p static pressure
- p_0 stagnation pressure of the fluid supplying the jet
- p_B theoretical static pressure within the separation bubble
- p_s static pressure on the surface of the plate
- p_∞ static pressure of the surrounding fluid at rest

r theoretical radius of the centre line of the reattaching jet

Q volume flow from the slot with plate in position

Q_0 volume flow from the slot for a free jet

R Reynolds number, $=[(p_0-p_\infty)\,b^2/(\rho\nu^2)]^{1/2}$

s arc length measured along the centre line of the jet

s_0 distance of the slot exit from the hypothetical origin of the jet

$t=\tanh\{\sigma y/(s+s_0)\}$ on the dividing streamline: suffix 1 refers to the particular value of $y=y_1$ shown in Fig. 4

u mean velocity parallel to the axis of the jet or parallel to the plate after reattachment

u_m maximum value of u in the wall jet after reattachment

x distance measured along the plate from the corner in each case

x_R value of x at the reattachment point

y distance from the jet axis

z distance from the plate

$z_{m/2}$ larger value of z for which $u=u_m/2$ in the reattached wall jet

z_m value of z at $u=u_m$

α angle between the inclined plate and the axis of the slot

θ angle at which the centre line of the jet theoretically impinges on the plate (Fig. 4)

ν kinematic viscosity of the fluid

ρ density of the fluid

σ parameter for a free turbulent jet (equation (7))

2. Dimensional Analysis of the Two Flows

Consider the flow shown in Fig. 1, in which a two-dimensional jet reattaches to an adjacent flat plate inclined at an angle α to the axis of the slot. If the ratio of the supply pressure p_0 to the ambient pressure p_∞ is less than about 1·1, the flow may be treated as incompressible and the following parameters are then sufficient to define the flow:—

p_0-p_∞, the supply pressure measured relative to the surroundings

b, the width of the slot

l, the length of the flat plate

α, the angular inclination of the plate to the axis of the slot

ρ, the density of the fluid

ν, the kinematic viscosity of the fluid.

The surface pressure p_s at distance x from the sharp corner, when expressed non-dimensionally as

$$C_{ps} \equiv \frac{p_s - p_\infty}{p_0 - p_\infty},$$

is a function of four non-dimensional combinations of the parameters and hence may be written

$$C_{ps} = f\left\{\alpha, \frac{x}{b}, \frac{l}{b}, \left[\frac{(p_0 - p_\infty)\, b^2}{\rho \nu^2}\right]^{1/2}\right\} \quad . \quad . \quad . \quad . \quad . \quad (1)$$

Similarly the distance x_R of the point of reattachment of the mean dividing streamline from the corner may be written

$$\frac{x_R}{b} = f\left\{\alpha, \frac{l}{b}, \left[\frac{(p_0 - p_\infty)\, b^2}{\rho \nu^2}\right]^{1/2}\right\} \quad . \quad . \quad . \quad . \quad . \quad (2)$$

In some cases it is possible to simplify these equations. If the length of the plate l is sufficiently large compared with x_R, the surface pressure becomes equal to p_s before the end of the plate and an arbitrary increase in the length of the plate has no effect on the flow near the corner. Thus the parameter l/b is no longer important and may be omitted from equations (1) and (2). Furthermore, if the Reynolds number $R = [(p_0 - p_\infty)\, b^2/(\rho \nu^2)]^{1/2}$ is sufficiently large, the flow may be expected to become insensitive to variations of fluid viscosity, so that R may be omitted from the equations[16]. It should be noted that the associated limiting value of R may itself be a function of α.

With these simplifications, the equations become

$$C_{ps} = f\left\{\alpha, \frac{x}{b}\right\} \quad . \quad . \quad . \quad . \quad . \quad . \quad . \quad (1a)$$

$$\frac{x_R}{b} = f\{\alpha\} \quad . \quad . \quad . \quad . \quad . \quad . \quad . \quad . \quad (2a)$$

A similar set of equations can be stated for the second flow, in which a two-dimensional jet reattaches to a parallel flat plate offset from the jet axis (Fig. 2). The parameter D/b replaces the plate inclination α.

$$C_{ps} = f\left\{\frac{D}{b}, \frac{x}{b}, \frac{l}{b}, \left[\frac{(p_0 - p_\infty)\, b^2}{\rho \nu^2}\right]^{1/2}\right\} \quad . \quad . \quad . \quad . \quad (3)$$

$$\frac{x_R}{b} = f\left\{\frac{D}{b}, \frac{l}{b}, \left[\frac{(p_0 - p_\infty)\, b^2}{\rho \nu^2}\right]^{1/2}\right\} \quad . \quad . \quad . \quad . \quad (4)$$

As before, when l/b and R are sufficiently large, the equations simplify to

$$C_{ps}=f\left\{\frac{D}{b},\frac{x}{b}\right\} \quad . \quad . \quad . \quad . \quad . \quad . \quad . \quad . \quad . \quad (3a)$$

$$\frac{x_R}{b}=f\left\{\frac{D}{b}\right\} . \quad . \quad . \quad . \quad . \quad . \quad . \quad . \quad . \quad . \quad (4a)$$

A further simplification is possible when D/b is large. In this case variations of the separate parameters b and p_0-p_∞ will not appreciably affect the flow as long as their product $b(p_0-p_\infty)$, which is approximately the jet momentum per unit length of slot, is maintained constant[9, 17]. This is equivalent to stating that the separate parameters b and p_0-p_∞ may be replaced by the single parameter $b(p_0-p_\infty)$ and is only permissible if the slot width is small compared with the dimensions of the separation bubble; otherwise, the hypothetical change in slot position associated with a change of slot width b would be significant.

With this simplification,

$$\frac{(p_s-p_\infty)D}{(p_0-p_\infty)b}=f\left\{\frac{x}{D},\frac{l}{D},\left[\frac{(p_0-p_\infty)bD}{\rho v^2}\right]^{1/2}\right\} \quad . \quad . \quad . \quad (5)$$

$$\frac{x_R}{D}=f\left\{\frac{l}{D},\left[\frac{(p_0-p_\infty)bD}{\rho v^2}\right]^{1/2}\right\} \quad . \quad . \quad . \quad . \quad (6)$$

When l/D and $[(p_0-p_\infty)bD/(\rho v^2)]^{1/2}$ are each sufficiently large,

$$\frac{(p_s-p_\infty)D}{(p_0-p_\infty)b}=f\left(\frac{x}{D}\right) . \quad . \quad . \quad . \quad . \quad . \quad . \quad (5a)$$

$$\frac{x_R}{D}=\text{constant}. \quad . \quad . \quad . \quad . \quad . \quad . \quad (6a)$$

3. Theoretical Analysis of the Two Flows

3.1. General

Two theories are given and both are extensions of Dodds's analysis[14] for the flow shown in Fig. 2.

The following assumptions are made:—

(*i*) The jet flow is incompressible and the mean flow is two-dimensional.

(*ii*) The velocity is uniform at the exit from the slot, *i.e.* the increase in velocity associated with the reduced pressure within the separation bubble is neglected. Thus the jet momentum per unit length $J=2(p_0-p_\infty)b$.

(*iii*) The pressure within the separation bubble is uniform and the centre line of the jet is a circular arc of radius r. The width of the jet is thus small compared

with r, which is similar to Taylor's assumption for a two-dimensional jet blowing across a uniform flow[17].

(*iv*) The jet entrains a similar amount of fluid from the surroundings as a free jet and the velocity distribution is similar to that of a free jet. The jet momentum is therefore conserved[17].

(*v*) Entrainment within the bubble ceases, and the flow divides, where the extended centre line of the jet intersects the plate.

(*vi*) The force parallel to the plate due to the skin friction of the forward and backward flow near reattachment is negligible compared with the jet momentum. This is a plausible assumption since the flow tends to become independent of viscosity at high Reynolds numbers.

The simplest, and probably the most accurate, analysis of a free jet is that due to Görtler, who assumed that the turbulent eddy viscosity was constant across the jet at each downstream station.

The distribution of velocity parallel to the axis of the jet is given by[18]

$$u=\left[\frac{3J\sigma}{4\rho\,(s+s_0)}\right]^{1/2}\operatorname{sech}^2\frac{\sigma y}{s+s_0}, \qquad . \quad . \quad . \quad (7)$$

where

s is the axial distance from the slot,

s_0 is the distance of the slot downstream of the hypothetical origin of the jet where the flow emerges with momentum J from an infinitely thin slot ($b \longrightarrow 0$),

y is distance measured perpendicular to the axis of the jet,

σ is a constant. Sufficiently far downstream in a free jet it has the value 7·7 (Ref. 18). In the present theory, however, σ is left as a floating constant, which permits some variation in the rate of entrainment due to the curvature of the jet.

The mean volume flow between the centre line of the jet and the reattaching streamline is, by definition, constant and equal to $\frac{1}{2}(Jb/\rho)^{1/2}$.

Thus the equation of this streamline is

$$t^2=\frac{\sigma b}{3\,(s+s_0)}, \quad \text{where } t=\tanh\frac{\sigma y}{s+s_0} \qquad . \quad . \quad . \quad . \quad (8)$$

An approximate value of s_0 may be obtained by equating the hypothetical total volume flow in the jet at $s=0$ to the efflux from the slot, $(Jb/\rho)^{1/2}$.

This gives $s_0 = \sigma b/3$ and the reattachment streamline is given by

$$\frac{3s}{\sigma b} = \frac{1}{t^2} - 1 \qquad . \quad . \quad . \quad . \quad . \quad (9)$$

The two flows are now examined separately.

3.2. Reattachment of a Jet to a Plate Parallel to and Offset from the Axis of the Slot

The mathematical model of the flow is shown in Fig. 3.

First Theory

For the first theory the momentum principle is applied locally at the point of reattachment, and the pressure difference between the surroundings and the bubble, $p_\infty - p_B$, is neglected.

$$\text{Thus} \quad J\cos\theta = J_1 - J_2 = \int_{-\infty}^{y} \rho u^2 dy - \int_{y}^{\infty} \rho u^2 dy, \qquad . \quad . \quad (10)$$

where θ is the angle at which the jet impinges on the plate, J_1 is the flow momentum proceeding downstream along the plate, J_2 is the flow momentum returned within the bubble at the point of reattachment, and y identifies the dividing streamline and is given by equations (8) and (9).

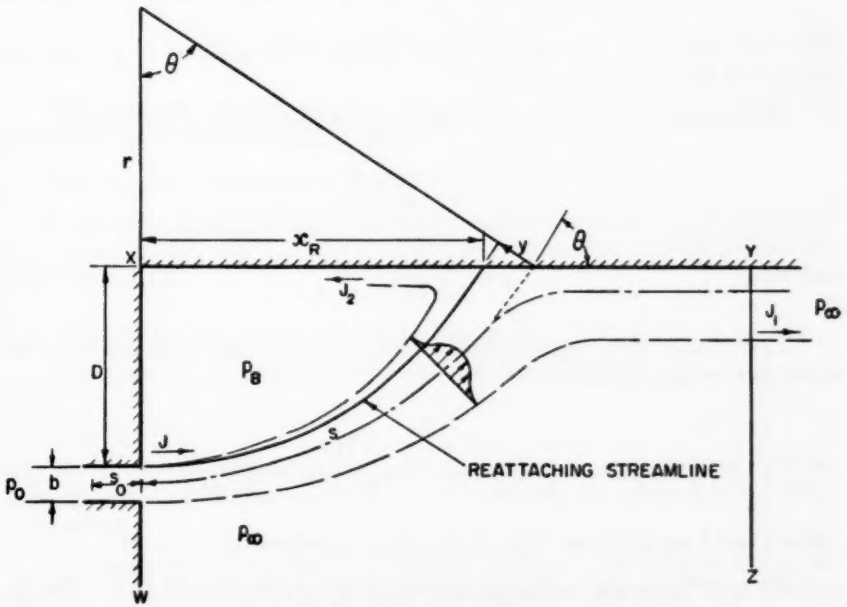

FIGURE 3. Mathematical model for an offset parallel plate.

Substituting equation (7) in equation (10) gives

$$\cos\theta = \frac{3}{2}t - \frac{1}{2}t^3, \qquad (11)$$

where t is given by equation (8).

The following geometrical relationships can be stated from Fig. 3:—

$$s = r\theta \qquad (12)$$

$$D + b/2 = r(1 - \cos\theta). \qquad (13)$$

Substituting relation (12) in equation (9) gives

$$\frac{b}{r} = \frac{3\theta}{\sigma\left(\frac{1}{t^2} - 1\right)}, \qquad (14)$$

and substituting relation (13) in equation (14) gives

$$\frac{D}{b} = \frac{\sigma\left(\frac{1}{t^2} - 1\right)\left(1 - \cos\theta\right)}{3\theta} - \frac{1}{2}, \qquad (15)$$

where t is related to θ by equation (11). Hence a unique value of b/r may be determined for each value of D/b.

The pressure difference across the jet is, by assumption (*iii*) of Section 3.1,

$$p_\infty - p_B = \frac{J}{r}$$

and thus

$$C_{pB} \equiv \frac{p_B - p_\infty}{p_0 - p_\infty} = -2\frac{b}{r} \qquad (16)$$

The distance of the point of reattachment of the dividing streamline from the corner is given approximately by

$$\frac{x_R}{b} = \frac{r}{b}\sin\theta - \frac{y}{b\sin\theta} = \frac{\sigma\left(\frac{1}{t^2} - 1\right)\sin\theta}{3\theta} - \frac{\tanh^{-1} t}{3t^2\sin\theta}, \qquad (17)$$

where t and θ are known in terms of D/b from equations (11) and (15).

Thus, both C_{pB} and x_R/b may be determined as functions of D/b. The increased volume flow from the slot, which was neglected as one of the original

assumptions, may nevertheless be computed approximately. For small values of C_{pB} the ratio of the volume flow Q to the volume flow Q_0 of a free jet with the same values of $p_0 - p_\infty$ and b is

$$\frac{Q}{Q_0} = 1 - \frac{1}{4} C_{pB} \quad . \quad . \quad . \quad . \quad . \quad (18)$$

Second Theory

For the second theory the momentum principle is applied to the control volume $WXYZ$ (Fig. 3) and in this case account is taken of the force arising from the pressure difference $p_\infty - p_B$. It is assumed that the bubble pressure p_B acts to the centre line of the jet and then changes discontinuously to the pressure of the surroundings, p.

The momentum equation is therefore

$$J - J_1 = (p_\infty - p_B)\left(D + \frac{b}{2}\right).$$

p_s before the end of the plate and an arbitrary increase in the length of the plate has Introducing $p_\infty - p_B = J/r$ and equation (7), this becomes

$$\frac{1}{2} - \frac{3}{4} t + \frac{1}{4} t^3 = \frac{1}{r}\left(D + \frac{b}{2}\right) = 1 - \cos\theta,$$

from equation (13).

$$\text{Thus} \quad \cos\theta = \frac{1}{2} + \frac{3}{4} t - \frac{1}{4} t^3 \quad . \quad . \quad . \quad . \quad . \quad (19)$$

Equation (19) replaces equation (11) in the first theory: the remaining equations are carried over without change.

Once again C_{pB}, x_R/b and Q/Q_0 may be determined as functions of D/b.

It should be noted that both the theories may be expected to be inaccurate at small values of D/b; this is due, in particular, to the failure of assumptions (*iii*) and (*v*) of Section 3.1.

3.3. The Reattachment of a Jet to an Inclined Flat Plate

The mathematical model for this flow is shown in Fig. 4.

First Theory

The momentum principle is once again applied locally at the point of reattachment and equation (11), giving the angle θ at which the jet impinges on the plate, is unaltered.

The geometrical relationships are different, however. Referring to Fig. 4, the arc $OA = s = r(\alpha + \theta)$, where α is the angle of inclination of the plate. It is possible to proceed by stating the exact geometrical relationship between θ and α; however,

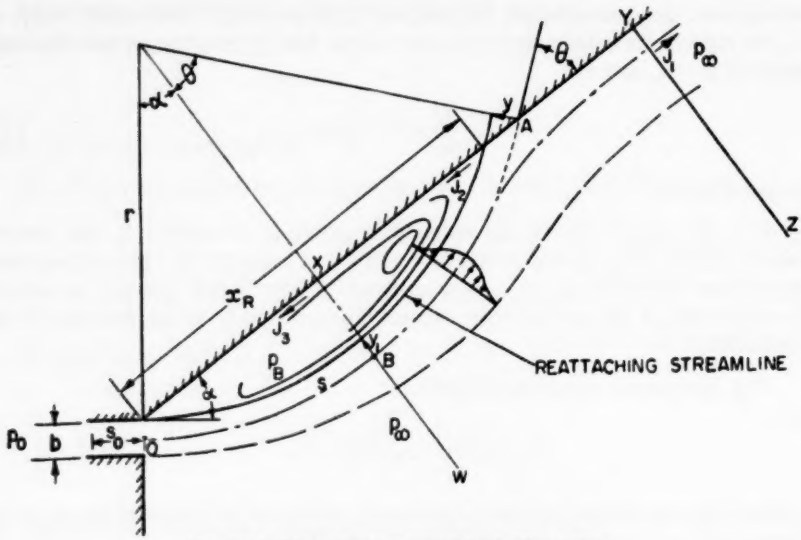

FIGURE 4. Mathematical model for inclined plate.

since the assumptions of the analysis are such that it is only valid if r is very much greater than the jet width, it is reasonable to put $\theta=\alpha$. The small error introduced fortunately reduces the error associated with assumption (v) and results in a more accurate theory for $\alpha>20°$.

Hence
$$s=2r\alpha \quad . \quad . \quad . \quad . \quad . \quad . \quad . \quad . \quad (20)$$

Substituting this in equations (9) and (16),

$$C_{pB}=\frac{-12\alpha}{\sigma\left(\frac{1}{t^2}-1\right)}, \quad . \quad . \quad . \quad . \quad . \quad . \quad (21)$$

where t is related to α by equation (11), which becomes

$$\cos\alpha=\frac{3}{2}t-\frac{1}{2}t^3 \quad . \quad . \quad . \quad . \quad . \quad . \quad (22)$$

This distance of the point of reattachment from the sharp corner is given approximately by

$$\frac{x_R}{b}=\frac{\sigma\left(\frac{1}{t^2}-1\right)}{3\alpha}\sin\alpha-\frac{\tanh^{-1}t}{3t^2\sin\alpha} \quad . \quad . \quad . \quad (23)$$

The increased volume flow, as in the previous case, is

$$\frac{Q}{Q_0} = 1 - \frac{1}{4} C_{pB}. \qquad . \quad . \quad . \quad . \quad (18)$$

Second Theory

This is similar to the second theory for the previous flow, the momentum principle being applied to the control volume $WXYZ$ shown in Fig. 4. Once again the bubble pressure is assumed to act to the centre line of the jet and there to change discontinuously to p_∞.

In applying the momentum theorem, account must now be taken of the momentum J_3 flowing back along the plate.

$$J - (J_1 - J_3) = (p_\infty - p_B)\, r\,(1 - \cos\alpha) \quad . \quad . \quad . \quad . \quad (24)$$

Since the pressure within the bubble is constant, J_3 equals the momentum inboard of the reattaching or dividing streamline at the plane WX.

$$J_3 = \int_{y_1}^{\infty} \rho u^2 dy, \qquad . \quad . \quad . \quad . \quad . \quad (25)$$

where y_1 identifies the position of the dividing streamline as it crosses plane WX.

With the aid of equations (7) and (25), and introducing $p_\infty - p_B = J/r$, equation (24) reduces to

$$\cos\alpha = \frac{1}{4}[3\,(t + t_1) - (t^3 + t_1^3)], \quad \text{where } t_1 = \tanh \frac{\sigma y_1}{r\alpha + s_0} \qquad . \quad . \quad (26)$$

Since the arc distance OA is twice the arc distance OB, equation (9) gives the following relation between t and t_1:—

$$t^2 = \frac{t_1^2}{2 - t_1^2} \qquad . \quad . \quad . \quad . \quad . \quad . \quad (27)$$

Equations (26) and (27) replace equation (22) of the first theory and the remaining expressions for C_{pB}, x_B/b and Q/Q_0 (equations (21), (23) and (18)) are unchanged.

Once again it should be noted that both these theories may be expected to become inaccurate at small values of α, for then the centre line of the jet is no longer approximately circular, the pressure difference $p_\infty - p_B$ differs significantly from J/r and the entrainment within the bubble ceases relatively close to the corner.

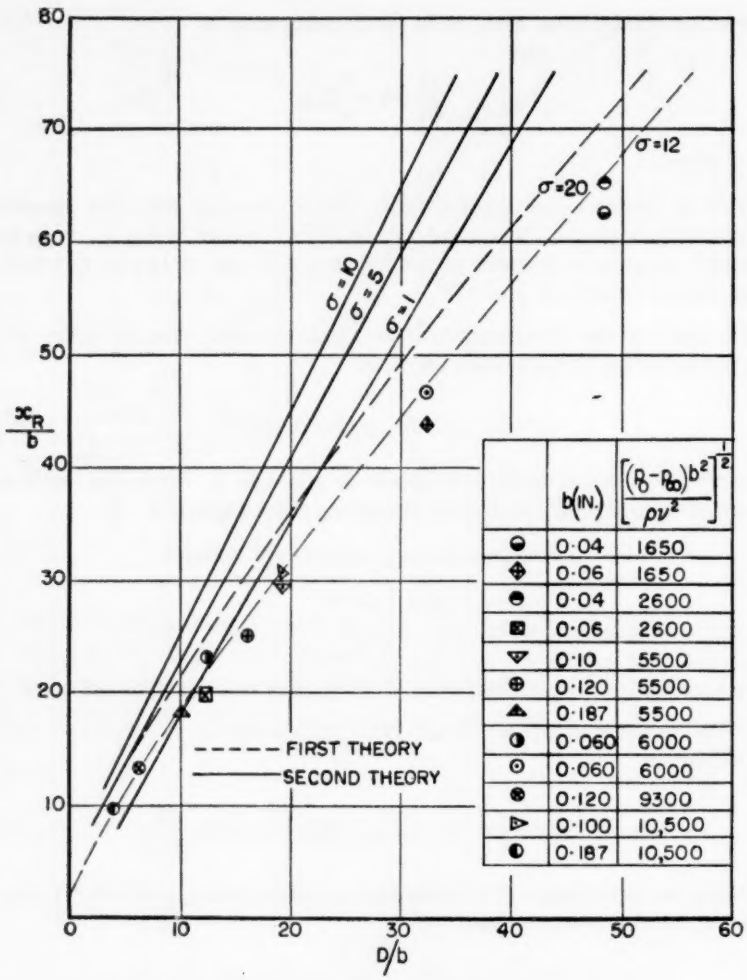

FIGURE 5. Reattachment distance for the offset parallel plate. $l = 12$ in.

4. Details of the Experimental Investigation

The apparatus which was used to investigate the two flows is described in the Appendix. For the inclined plate the investigation was comprehensive and included measurements of the surface pressure p_s, the reattachment distance x_R and the increase in exit volume flow Q/Q_0 for various slot widths b, plate lengths l, plate angles α, and supply pressures $p_0 - p_\infty$. In addition the range of values of α and l/b for which either fully-separated or reattached flow is possible, was determined at high Reynolds numbers. The velocity distribution downstream of reattachment

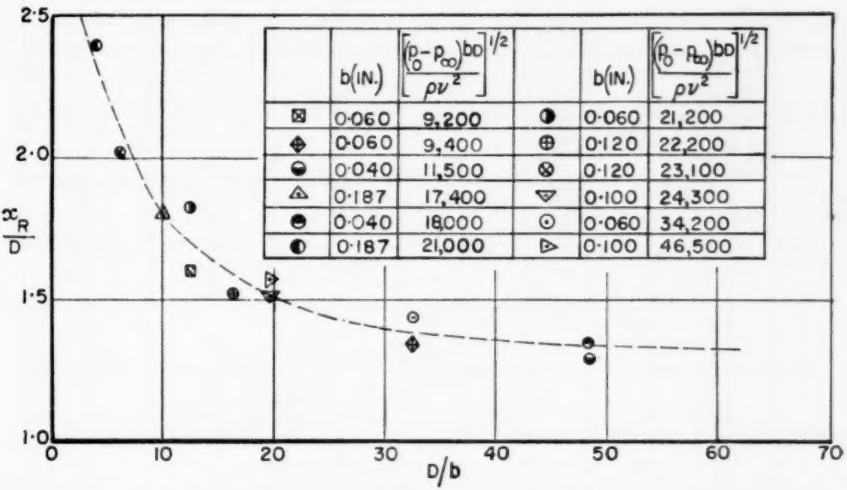

FIGURE 6. Alternative presentation of the reattachment distance for the offset parallel plate. $l=12$ in.

was also measured. For the offset parallel plate the surface pressure and reattachment distance were measured for various slot widths, offset distances D and supply pressures, using a "long" plate. The effect of plate length was not investigated as the main purpose of these measurements was to obtain a comparison with the theory valid for long plates and high Reynolds numbers. Undoubtedly for this case also there exists a range of D/b and l/b for which both fully-separated and reattached flows are possible, but this was not investigated.

All the measurements were made at incompressible speeds with $p_0/p_\infty < 1{\cdot}05$.

5. Discussion of the Experimental Results and Comparison with Theory

5.1. Reattachment of a Jet to a Parallel Flat Plate Offset from the Axis of the Jet (Fig. 2)

Figure 5 gives the distance from the slot to the point of reattachment of the dividing streamline for various slot widths b, offset distances D, and supply pressures (p_0-p_∞). The results have been plotted non-dimensionally in accordance with equation (4) and indicate that for these measurements the flow was independent of both l/b and the Reynolds numbers $[(p_0-p_\infty)\,b^2/(\rho\nu^2)]^{1/2}$, when the latter were sufficiently large, in agreement with equation (4*a*). The limiting value of l/b, which is a function of D/b, has not been determined. All that can be said is that the plate length is unimportant when l is greater than $3{\cdot}8\,x_R$, but this is unlikely to be the lower limit. The limiting value of R varies from about 6,000 at $D/b=12$ to 2,500 at $D/b=50$.

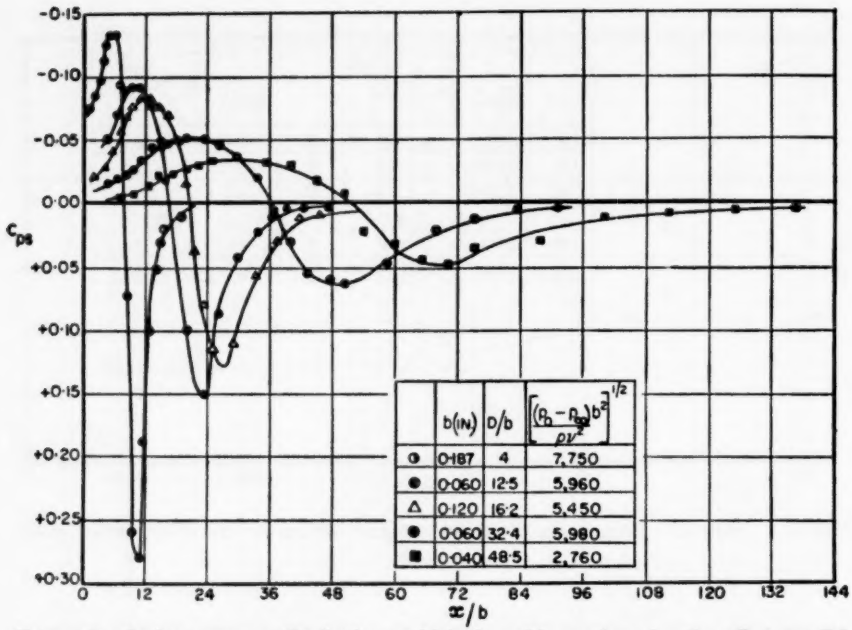

FIGURE 7. Surface pressure distribution at high Reynolds numbers for the offset parallel plate. $l = 12$ in.

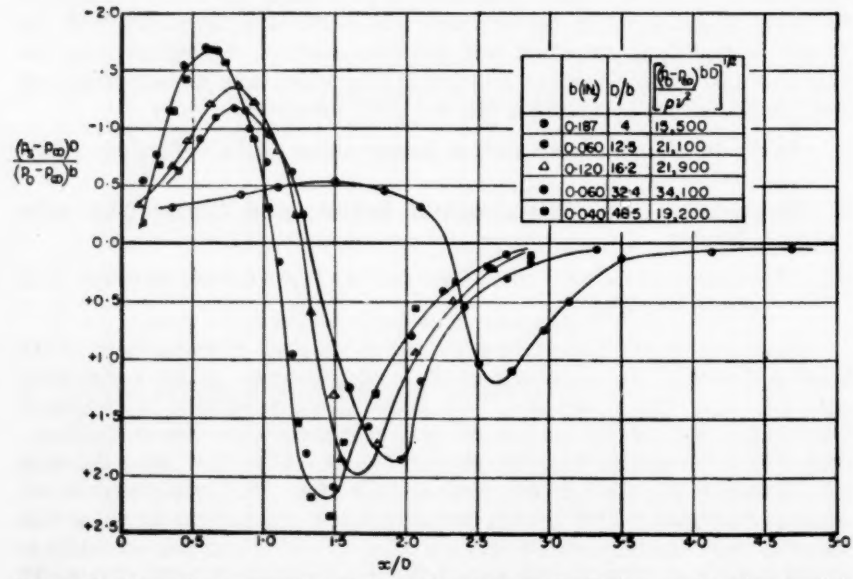

FIGURE 8. Alternative presentation of the surface pressure distribution on the offset parallel plate. $l = 12$ in.

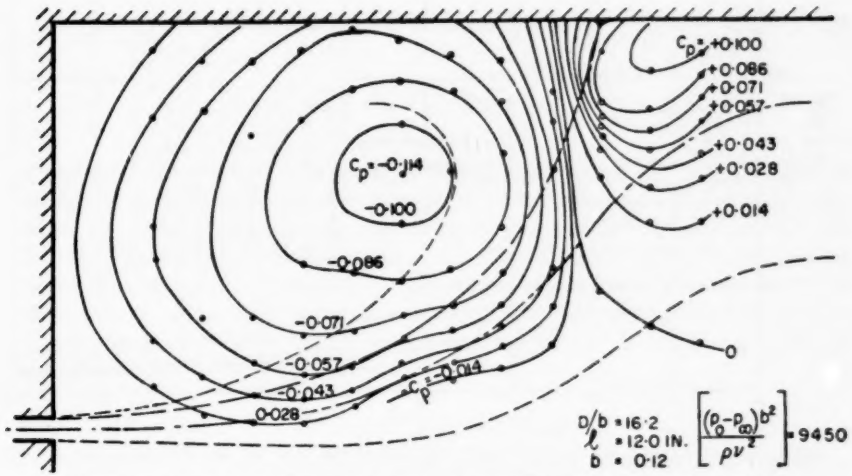

FIGURE 9. Approximate contours of constant pressure within the separation bubble.

For large values of D/b, the dimensional analysis indicates that x_R/D becomes a constant at large l/D and $[(p_0-p_\infty)\,bD/(\rho\nu^2)]^{1/2}$ (equation (6*a*)). The results are replotted in these co-ordinates in Fig. 6 and it appears that the limiting value of D/b is about 35 and the limiting value of the appropriate Reynolds number $[(p_0-p_\infty)\,bD/(\rho\nu^2)]^{1/2}$ is about 2×10^4 and appears to be approximately constant even for small values of D/b. It should be noted that the fact that these results plot in accordance with the dimensional analysis is an indication that the flow was effectively two-dimensional, for otherwise an additional parameter, slot length divided by slot width, would be of importance.

The distribution of pressure on the surface of the plate, plotted as $C_{ps}=(p_s-p_\infty)/(p_0-p_\infty)$ is given in Fig. 7 for various values of D/b when l/b and R are large. Once again the results are in accordance with the simplified dimensional analysis (equation (3*a*)). Fig. 8 also indicates that when D/b exceeds about 35 the pressure distribution plotted in the form $\{(p_s-p)\,D/(p_0-p)\,b\}$ is a function of x/D only and is independent of D/b in accordance with equation (5*a*).

The contours of constant static pressure within the separation bubble for $D/b=16{\cdot}2$ are shown in Fig. 9. The pressure was measured by means of a plate fitted with pressure taps and mounted in the centre of the jet in the plane of two-dimensional flow (*see* Appendix). No great accuracy can be claimed for these measurements: the pressure taps were of necessity relatively close to the leading edge of the plate and furthermore it appears that the secondary flow associated with the presence of the plate caused the length of the bubble to decrease by about 15 per cent. Nevertheless the general shape of the contour is no doubt a good indication of the true pressure distribution. The estimated position of the jet and the reattaching streamline are indicated in dotted lines in Fig. 9 and are based on the known position of reattachment. The mean streamlines within the bubble are

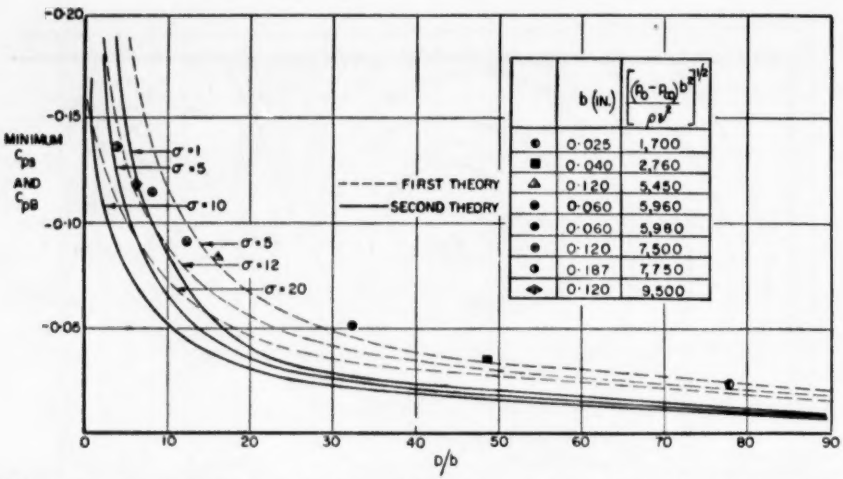

FIGURE 10. Comparison between the theoretical bubble pressure and the minimum pressure on the offset parallel plate. $l = 12$ in.

indicated qualitatively in Fig. 2 and are similar to those associated with a vortex situated near the point of reattachment. The back flow within the bubble decelerates on approaching the rear wall which joins the plate to the slot, and thus the pressure rises into the corner. The pressure on the surface of the plate is smallest opposite the centre of the hypothetical vortex. It is seen that this physical model of the flow satisfactorily explains the pressure distribution within the bubble shown in Fig. 9. It should be noted that the point of reattachment only corresponds to the position of maximum surface pressure when the jet impinges on the plate at an angle approaching 90° (*i.e.* D/b is large). For small D/b it more nearly corresponds to the position where the pressure coefficient changes sign.

In relating the bubble pressure and reattachment distance to the theories in Section 3.2, it is evident that the basic assumption of a uniform pressure within the bubble in incorrect. However the minimum pressure on this surface is roughly the mean pressure within the bubble (Fig. 9) and therefore this particular pressure is chosen for comparison with the theories in Fig. 10. The measured reattachment distances are also compared in Fig. 5. It is apparent that the first theory, with σ having the plausible value of 12, compares very favourably with the reattachment distance, and is approximately correct for the minimum surface pressure, although smaller values of σ give better agreement for the middle range of D/b. The second theory is less satisfactory and requires very low values of σ: this is associated with the assumption that the low bubble pressure acts on the rear wall which joins the plate to the slot, whereas in reality the pressure on this wall is much higher than the mean bubble pressure*. Both theories are incorrect when $D/b \longrightarrow 0$, for then the minimum $C_{ps} \simeq 0$ and is not a large negative value as predicted.

Note added in proof: Indeed Chaplin has effectively combined the two theories to predict the pressure on the rear wall.

Applying the momentum principle perpendicular to the plate suggests that

$$\int_0^{l/b} C_{ps}\, d\,(x/b)=0;$$

however the measured distribution gives non-zero values for this integral. This is thought to be associated with the momentum of the entrained fluid perpendicular to the plate and to a much lesser extent to the skin friction on the rear wall and the outgoing momentum perpendicular to the plate in the wall jet. It is interesting to note that Sigalla[20] also detected a moderately high pressure near the slot for a plane wall jet, presumably for the same reason. It should be noted that the neglect of this momentum has no effect on the first theory and a small, but probably negligible, effect on the second theory.

5.2. Reattachment of a Jet to an Inclined Plate

As mentioned in the Introduction, there is a range of values of α, depending on l/b, for which the jet may or may not be reattached to the plate. The angle at which a free jet spontaneously reattaches to the plate, and the maximum angle for which reattached flow is possible, are shown in Fig. 11. These measurements were made at a sufficiently high Reynolds number for the flow to be insensitive

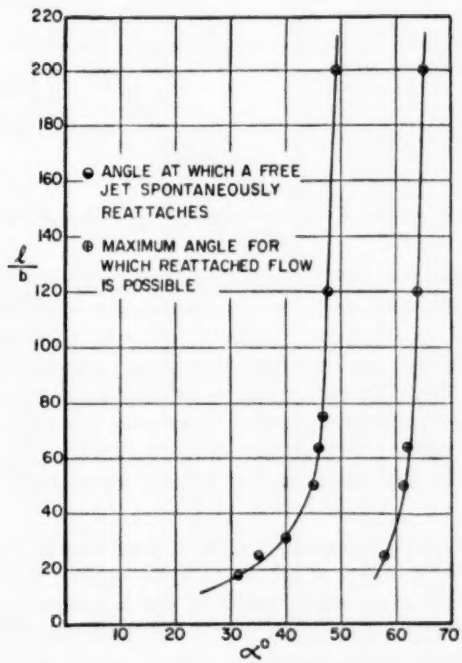

Figure 11. Zones of flow at high Reynolds numbers for the inclined plate.

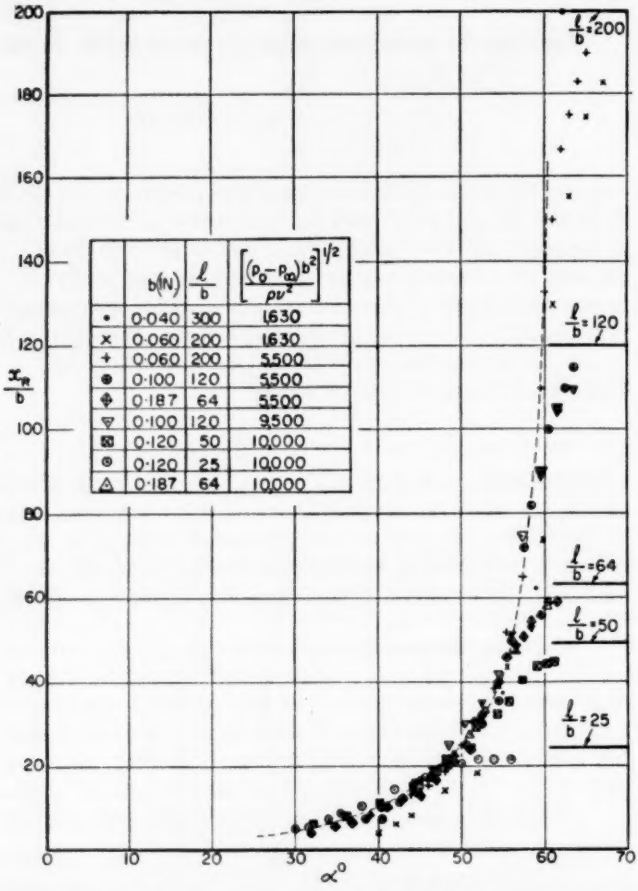

FIGURE 12. Reattachment distance for the inclined plate.

to variations in this parameter. The two curves shown divide the figure into three regions. To the left the jet is always reattached, forming a separation bubble, and to the right it is always separated as a free jet. In the central region, the jet is separated or reattached depending on how the flow is started. For example, reattached flow may always be obtained in this region by guiding the flow round the sharp corner temporarily with an additional surface: conversely it can always be separated by temporarily introducing a large disturbance downstream. For all the remaining work which is to be described, the flow in the central region is reattached.

The reattachment distances x_R for various slot widths b, plate lengths l and supply pressures $(p_0 - p_\infty)$ are shown in Fig. 12 as a function of the angle of inclination of the plate α. The results are presented in terms of the non-dimensional parameters given in equation (2). Only the results for the lowest Reynolds number deviate significantly from the other results, indicating that R is no longer a

significant parameter when it is sufficiently large. Furthermore all the results lie on one curve (*i.e.* are insensitive to l/b) when x_R is smaller than about $0{\cdot}7l$ for all values of α and thus the limiting value of l/b at any given α may be detemined as $1{\cdot}4$ times the value of x_R/b given by this curve. The results are therefore in agreement with the prediction of equation (2*a*). No results were obtained for $\alpha < 30°$ because the bubble of separation was too small, even with the largest available slot width.

The distributions of pressure on the surface of the plate for $\alpha = 35°$, $45°$, $55°$, $62\frac{1}{2}°$ are shown in Figs. 13, 14, 15, 16. The first three figures are for values of l/b sufficiently large for this parameter to be unimportant and thus show the effect of changes of R only. It is noted that when R exceeds about 5,500 the curves become independent of R (equation (1*a*)). Once again the results indicate that the flow was effectively two-dimensional. With one exception the results shown in Fig. 16 were all made at the same high R and thus show the effect of variations of

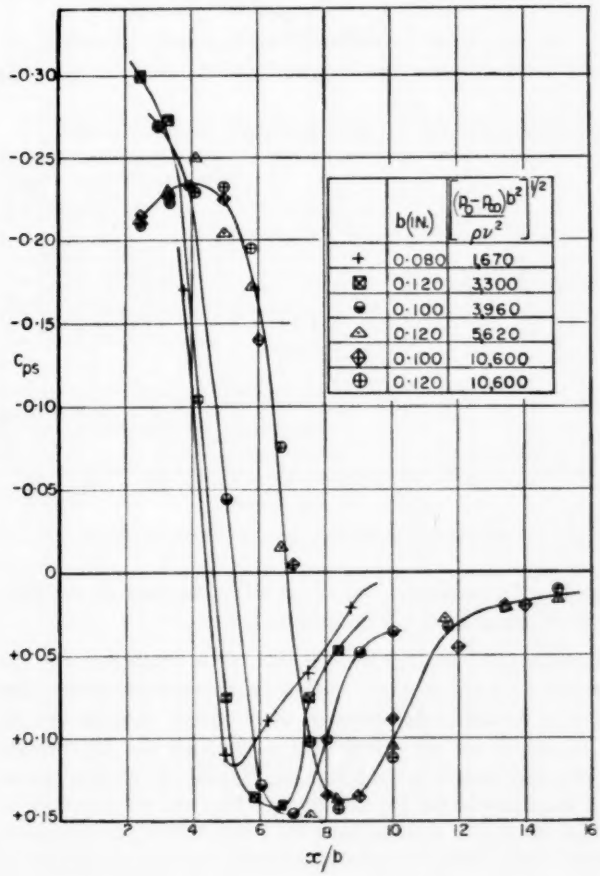

FIGURE 13. Surface pressure distribution on the inclined plate. $l = 12$ in., $\alpha = 35°$.

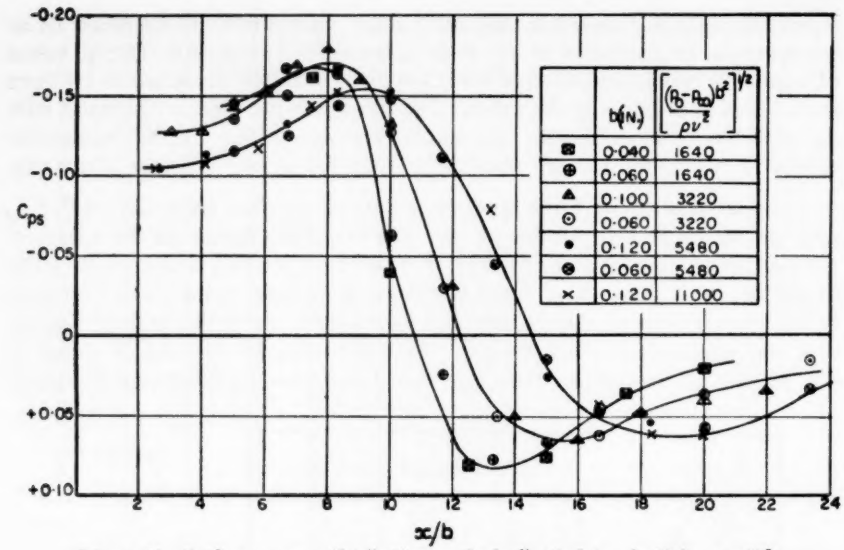

FIGURE 14. Surface pressure distribution on the inclined plate. $l=12$ in., $\alpha=45°$.

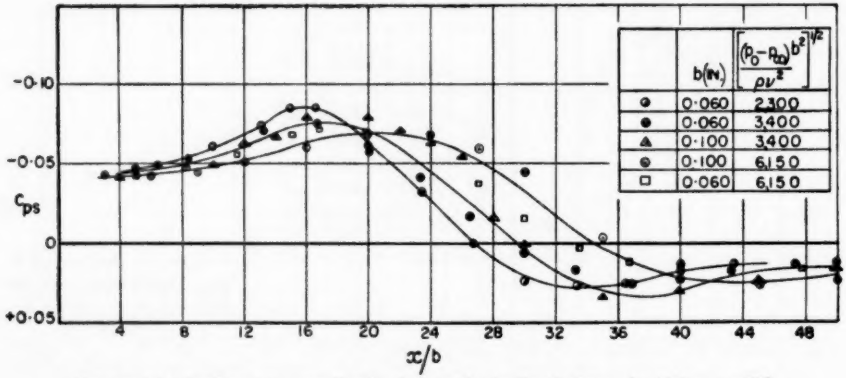

FIGURE 15. Surface pressure distribution on the inclined plate. $l=12$ in., $\alpha=55°$.

l/b only. Reference to Fig. 12 indicates that at $\alpha=62\frac{1}{2}°$ the flow is certainly influenced by the length of the plate when l/b is less than 200.

The universal reattachment distance for large R and l/b is compared with the two theories for various values of σ in Fig. 17. As all the theoretical curves cross the experimental curve, it is apparent that none of them strictly predicts the reattachment distance at all angles for one value of σ. Although the appropriate values of σ will not be identical with that for a free jet, because of the flow curvature and possibly altered transition in the jet, nevertheless they are not expected to differ appreciably from the value 7.7. On this basis the second theory is preferable to the first.

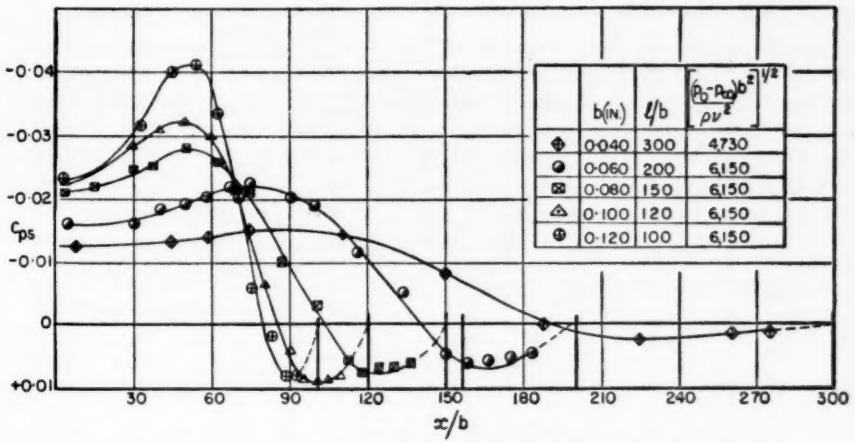

FIGURE 16. Surface pressure distribution on the inclined plate. $l=12$ in., $\alpha=62\frac{1}{2}°$.

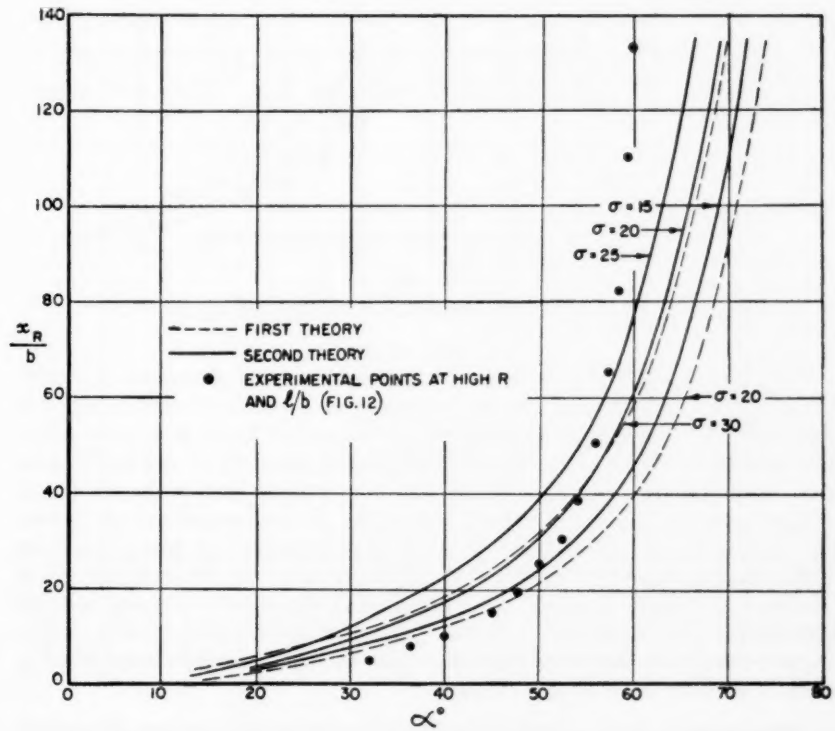

FIGURE 17. The reattachment distance on the inclined plate: comparison with theory.

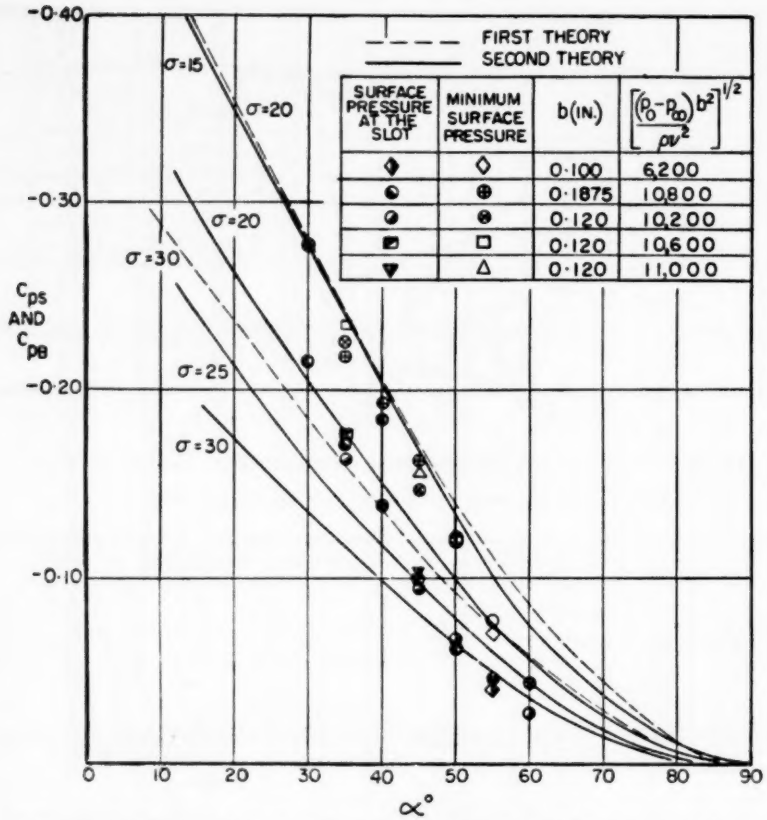

FIGURE 18. Pressure within the separation bubble for the inclined plate. $l=12$ in.

The variation of surface pressure in the neighbourhood of the slot is smaller than in the previous case and thus the assumption of a constant bubble pressure is more acceptable. The point of reattachment corresponds to the position of maximum surface pressure for large α and to the position where $C_p=0$ for small values of α, which behaviour is similar to the first flow, and the general distribution of pressure may be associated with the curvature of the streamlines as before. Unfortunately it was impossible to measure the distribution of pressure within the bubble because, when the bubble was sufficiently large, the pressure differences were small and highly oscillatory. For comparison with the two theories, both the minimum pressure on the surface and the pressure at the slot determined by extrapolation, have been plotted in Fig. 18. Once again the second theory requires values of σ closer to those of a free jet.

Measurements of the increase in volume flow due to the presence of the plate are given as a function of α in Fig. 19. The increase is very small and could not

be measured with great accuracy. It is interesting to note that the maximum increase occurs at $\alpha \simeq 25°$. Two theoretical curves from the second theory, for the values of σ which gave best agreement with the pressure at the corner, are also shown in the figure and the agreement is fair for values of α between 20° and 50°. The theory is in error at low values of α because the basic assumptions fail. It is also possible to compare the results with the potential flow analysis due to Metral[3] and it is noted that this theory gives increments which are far in excess of those achieved in practice. Viewed in this light, the present entrainment theory is a decided improvement for α greater than about 10°.

In this case the application of the principle of momentum perpendicular to the plate suggests that, for large l/b,

$$-\int_0^{l/b} C_{ps}\, d\,(x/b) = 2 \sin \alpha.$$

However, the integrated surface pressure distributions are, in general, less than $2 \sin \alpha$, although the agreement is fairly good for the largest value of α. Once again therefore the incoming momentum of the entrained fluid perpendicular to the jet is apparently significant.

Referring to Figs. 12, 13, 14 and 15, the effect of a reduction of R below those values for which it is an insignificant parameter, is to reduce the reattachment

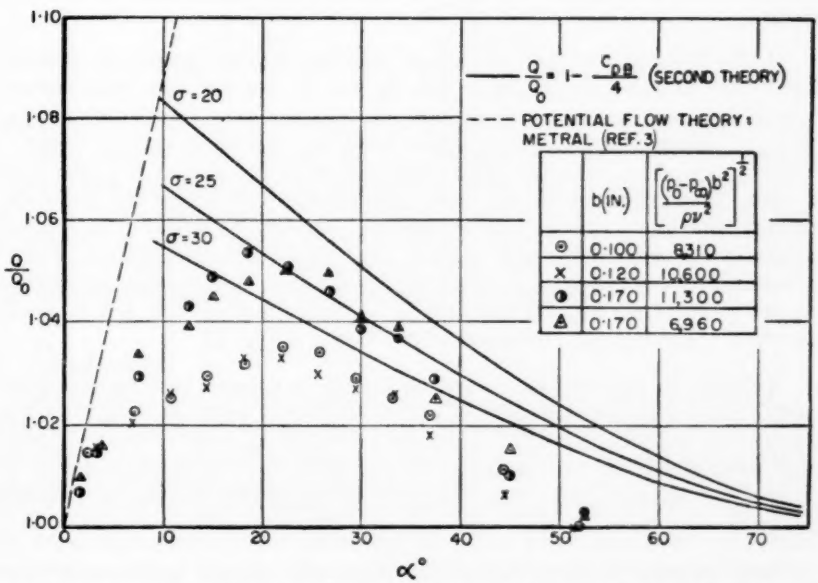

FIGURE 19. Increase in volume flow from the slot due to the presence of the inclined plate. $l = 12$ in.

distance x_R/b and to increase the numerical value of the minimum C_{ps} within the bubble, both of which are associated with an increased curvature of the jet. The reason for this variation is not well understood. It is likely to be associated with the skin friction in the region of reattachment, but a variation in the right direction would be obtained only if the total skin friction associated with the back flow was greater than that associated with the flow proceeding downstream in the vicinity of the reattachment point.

In Figs. 12 and 16 it is seen that, for a given value of α, the effect of a reduction of l/b below the limiting value is to reduce x_R/b and to increase $(-C_{ps})$ in the bubble: it is thus similar to the effect of a reduction of R. In this case the explanation is as follows. When the point of reattachment is near the end of the plate the final direction of the flow is inclined at an angle greater than α to the axis of the slot, because the flow outboard of the reattaching streamline is no longer constrained to depart in the direction of the plate. This statement is supported by the fact that

$$-\int_0^{l/b} C_{ps}\, d\,(x/b)$$

in Fig. 16 increases as l/b decreases. Thus the final momentum in the direction of the plate is reduced. According to the theoretical ideas of Section 3.3, this is associated with a reduction of both the bubble pressure and the reattachment distance.

It was observed that the distribution of surface pressure and of the position of reattachment were fairly steady in time for $\alpha < 35°$, but fluctuated with increasing amplitude as α was increased, until the reattachment point reached the limiting value $0{\cdot}7l$. From then on the fluctuations decreased until the flow finally failed to reattach to the plate. The magnitude of the maximum fluctuations in x_R was ± 20 per cent. The oscillations are due to the high turbulence in the jet and to a lesser extent to variations in the position of transition, both of which lead to fluctuations in the effective value of the plate angle α. The fluctuations are therefore roughly proportional to $dx_R/d\alpha$ and it is interesting to note that, on this basis, the description just given of the increase and decrease of the fluctuations with α is in agreement with the curves for each value of l/b shown in Fig. 12.

Referring to the right hand curve in Fig. 11, it is noted that the maximum possible plate angle for reattached flow does not vary a great deal with l/b. For example, for $l/b=25$, $\alpha_{max}=57°$, while for $l/b=200$, $\alpha_{max}=65°$. The maximum angle which has so far been obtained experimentally is 75°, corresponding to an l/b of approximately 2,000. The theories of course predict 90° for an infinitely long plate.

Pitot traverses of the reattached flow have been made at angles $\alpha=30°$ and 45° for $l \gg x_R$. The traverses were made far enough downstream for the static pressure to be sensibly atmospheric, as indicated by Figs. 13 and 14. The

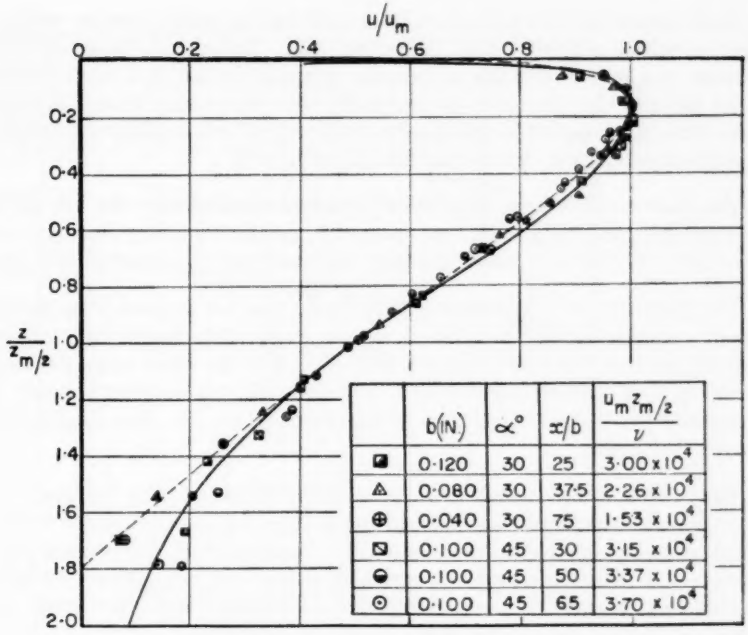

—— Glauert's theory[21] for $z_m/z_{m/2}=0{\cdot}14$

- - - - mean profile from the measurements of Förthmann[19] and Sigalla[20]. $u_m z_{m/2}/\nu=4$ to 11×10^4.

FIGURE 20. Velocity profiles downstream of reattachment.

computed velocity profiles are presented non-dimensionally in Fig. 20 in terms of the maximum velocity u_m and the distance $z_{m/2}$, which is the larger value of z at which $u=\frac{1}{2}u_m$. Plotted in this way the profiles are similar and in good agreement with the mean profile representing the measurements of a wall jet by Förthmann[19] and by Sigalla[20] at slightly higher Reynolds numbers and with Glauert's[21] theory for $z_m/z_{m/2}=0{\cdot}14$, where z_m is the value of z at $u=u_m$. Thus it appears that a conventional wall jet is obtained far downstream of reattachment.

6. Conclusions

The reattachment of an incompressible, two-dimensional jet to a neighbouring surface is associated with the entrainment of surrounding fluid by the jet. For a jet reattaching to an adjacent inclined flat plate, it is found that the flow becomes independent of the Reynolds number at the slot, $[(p_0-p_\infty)b^2/(\rho\nu^2)]^{1/2}$, when this exceeds about 5,500 and independent of the non-dimensional length of the plate, l/b, when this exceeds a value which depends on the plate angle α and which may be determined from Fig. 12. For a jet reattaching to an offset parallel flat plate the flow becomes independent of D/b, l/b and Reynolds number when these are sufficiently large, the limiting value of D/b being about 35.

Approximate theories have been developed for the mean pressure within the separation bubble and the position of reattachment. These are based on the known properties of a free jet and the momentum principle applied to a control volume. For the point of reattachment, the agreement with experiment is very satisfactory for the offset plate, using the first theory, for $D/b > 3$ and is fairly satisfactory for the inclined plate, using the second theory, for $\alpha > 25°$.

The increase in volume flow from the slot associated with the low pressure on the inclined plate has a maximum value of 5 per cent for a long plate and occurs at $\alpha \simeq 25°$. This is very much less than that predicted by potential flow theory.

The flows exhibit a hysteresis phenomenon. For the inclined plate there is a range of α at each l/b for which the jet may be either reattached or fully separated, depending on how the flow is started (Fig. 11). For the offset plate the same is presumably true with D/b replacing α, although this was not investigated. The phenomenon may be of importance when deciding on the plate length in any practical application.

The present theories could usefully be improved, particularly for small values of α or D/b, and could also be extended to the case of a compressible subsonic jet. It might also be interesting to examine the importance of entrainment for the deflection of a sonic or a supersonic jet round a sharp corner, although the existing potential flow theories[3, 4] are probably more satisfactory and there is, of course, no increase in mass flow in this case.

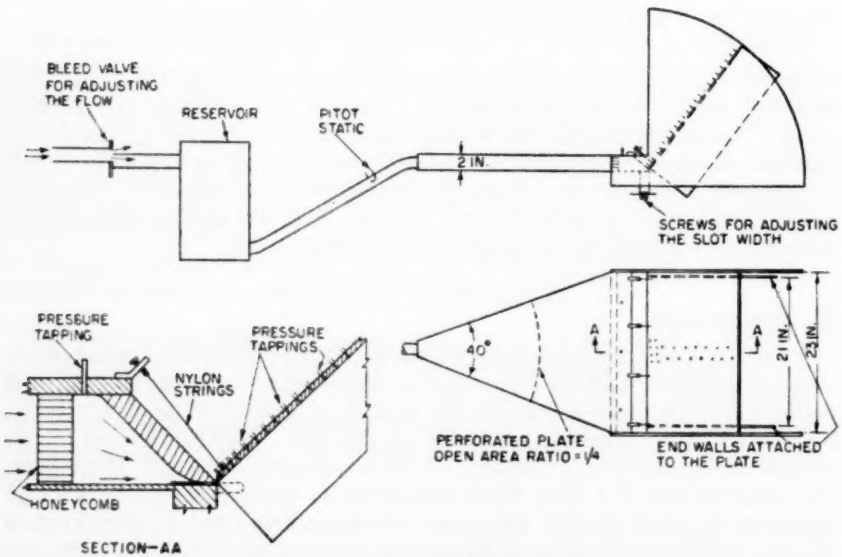

FIGURE 21. Sketch of the apparatus.

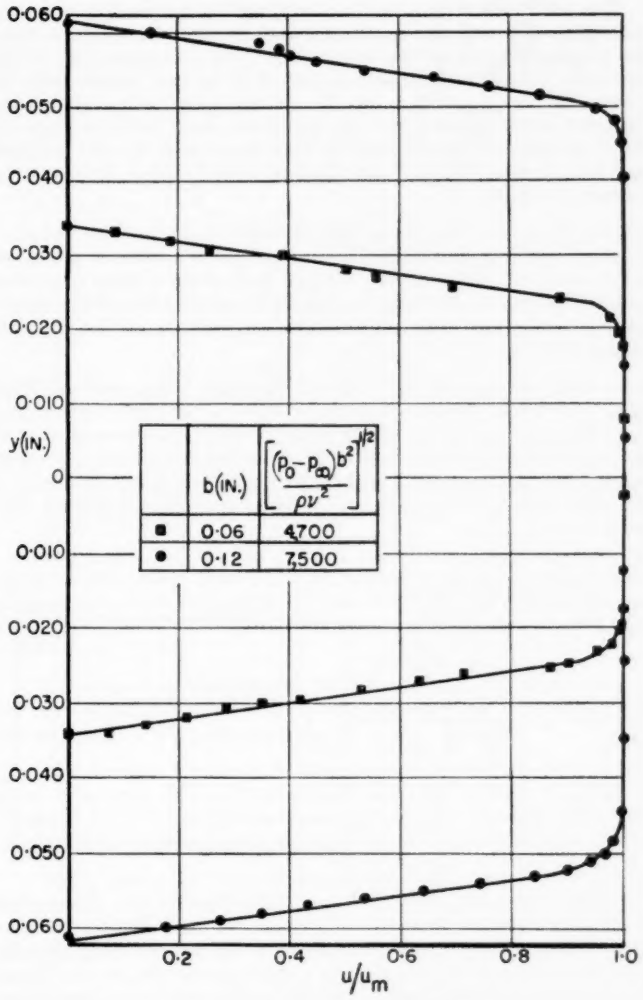

FIGURE 22. Velocity profile at the exit from the slot with a free jet.

Appendix

APPARATUS AND EXPERIMENTAL PROCEDURE

The apparatus, shown schematically in Fig. 21, was designed to produce a quasi two-dimensional jet under those conditions which have been examined theoretically. Air was supplied from a centrifugal compressor driven by a constant speed, three-phase motor. The flow to the apparatus was controlled by a bleed valve situated upstream of a large reservoir: the reservoir reduced the fluctuations in total pressure to an acceptable level of less than one per cent.

In order to obtain a uniform velocity at the slot, the flow was decelerated by means of a 40° expansion, in which a perforated plate was placed to inhibit separation of the

flow from the walls. This was followed by a short uniform settling space which contained a deep-cell honeycomb. The flow was then accelerated into the slot, the width of which was adjustable: the minimum value of the contraction ratio, corresponding to the maximum slot width, was 11:1. This arrangement proved to be very satisfactory; the pressures given by three pressure tappings across the settling space were identical and equal to the total pressure in the centre of the jet, which was itself uniform along the length of the slot. With the flow issuing as a free jet, Pitot traverses at the slot indicated that the flow emerged with laminar boundary layers about 0·010 in. thick. Traverses for two slot widths are shown in Fig. 22.

The effective length of the slot was 21 in. and its width could be varied up to a maximum value of 0·19 in. The lips were surface ground and the slot width in the centre was *less* than that at the ends by 0·005 in. with wind off and, at the highest stagnation pressure (20 in. water), was *greater* by 0·003 in., due mainly to deformation of the top lip. Most of the readings were made at an intermediate stagnation pressure and the variation of slot width was roughly 0·002 in.

Three plates were used, respectively 3, 6 and 12 in. long. They were cut from "Perspex" plastic sheet, $\frac{1}{4}$ in. thick. Pressure tappings of 0·015 in. diameter were drilled in the longest plate, the holes being closest together near the slot. The plywood sides of the setting space were extended to form large end walls. These were insufficient, however, to completely prevent inflow from the sides, as detected by tufts, and it was necessary to attach additional end walls directly to the plates in order to produce satisfactory two-dimensional conditions.

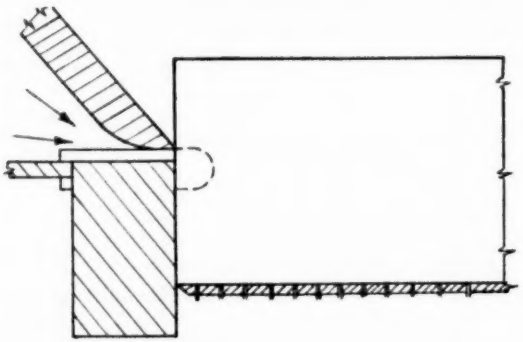

FIGURE 23. Mounting for a parallel offset plate.

The plates could be mounted either parallel to the axis of the slot and some distance from it (Figs. 2 and 23) or inclined to the axis to form a sharp corner with the top lip of the slot (Figs. 1 and 21). The outside of the top lip and the leading edge of the plates were chamfered at 45° so that they could abut to form the sharp corner in the latter case. The leading edge of the plate was held in position against the suction force on the plate by means of the four nylon strings shown in Fig. 21. The sharp corner was sealed at the back of the plate with adhesive tape.

In each case a desired slot width was set with feeler gauges. The pressure in the settling space was measured on a vertical alcohol manometer to an accuracy of one per cent. The surface pressure on the plate was measured with a vertical multi-tube manometer, filled with alcohol and fitted with a freezing device. The oscillation of those tubes connected to the tappings near reattachment were about 20 per cent of the mean, and care was taken to freeze the manometer to give approximately the mean pressure distribution.

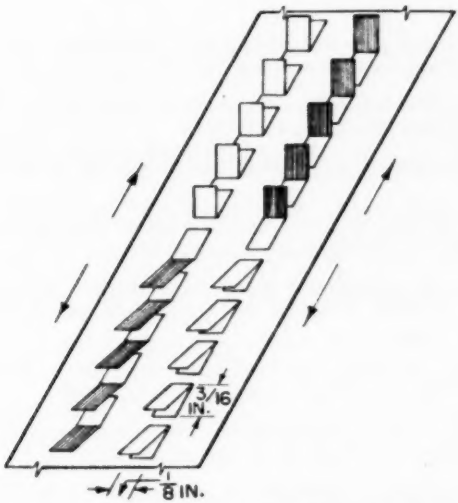

FIGURE 24. Paper flags for determining the position of reattachment.

The position of reattachment of the dividing streamline was determined by using small flexible paper flags (two-dimensional tufts) fixed to the surface with hinge lines perpendicular to the direction of mean flow (Fig. 24). These indicated the instantaneous division of forward and backward flow and the mean position of reattachment could readily be estimated.

The mass flow through the slot was measured in terms of the pressure difference between a central Pitot tube and a wall static tapping in the circular pipe which connected the apparatus to the large reservoir.

The velocity profile downstream of reattachment was measured with a round Pitot tube with internally sharpened lips and external diameter 0·028 in. This was mounted on a dial-gauge traversing gear. The traverses were made where the static pressure was sensibly equal to the pressure of the surroundings.

The pressure distribution within the separation bubble for the offset plate was determined with an additional $\frac{1}{4}$ in. thick plate fitted with three pressure tappings and rounded leading edge, mounted in the centre of the plate and parallel to the end walls. The taps were situated at $\frac{1}{2}$ in. from the leading edge.

REFERENCES

1. YOUNG, D. W. and ZONARS, D. Wind Tunnel Tests of the Coanda Wing and Nozzle. U.S.A.F. Technical Report 6199, September 1950.

2. SPROULE, R. S., ADDERLEY, J. W. and ROBINSON, S. T. The Coanda Effect. C.I.O.S., S.H.A.E.F., Item No. 5, 1944.

3. METRAL, A. Sur un Phénomène de Déviation des Veines Fluides et ses Applications. Effet Coanda. Cabinet Technique du Ministère de l'Air, November 1938.

4. METRAL, A. and ZERNER, F. L'Effet Coanda. Publications Scientifiques et Techniques du Ministère de l'Air, No. 218, 1948; Ministry of Supply TIB/T4027, 1953.

5. VOEDISCH, A. Analytical Investigation of the Coanda Effect. Air Materiel Command, U.S.A.F. Wright Field, Technical Report F-TR-2155-ND, 1948.

6. VON KÁRMÁN, T. *Theoretical Remarks on Thrust Augmentation.* Reissner Anniversary Volume, Edwards, Ann Arbor, Michigan, 1949.

7. SQUIRE, H. B. Jet Flow and its Effect on Aircraft. *Aircraft Engineering,* Vol. 22, March 1950.

8. VON GLAHN, U. H. Use of the Coanda Effect for Jet Deflection and Vertical Lift with Multiple-Flat-Plate and Curved-Plate Deflection Surfaces. N.A.C.A. T.N. 4377, 1958.

9. NEWMAN, B. G. The Deflection of Plane Jets by Adjacent Boundaries—Coanda Effect. *Boundary Layer Control Principles and Applications,* edited by G. V. Lachmann, Pergamon Press, in print.

10. VON GLAHN, U. H. Use of the Coanda Effect for Obtaining Jet Deflection and Lift with a Single Flat-Plate Deflection Surface. N.A.C.A. T.N. 4272, 1958.

11. LIGHTHILL, M. J. Notes on the Deflection of Jets by Insertion of Curved Surfaces and on the Design of Bends in Wind Tunnels. R. & M. 2105, 1945.

12. YEN, K. T. A Theoretical Evaluation of the Coanda Nozzle. Rensselaer Polytechnic Institute, T.R. AE5501, July 1955.

13. HEAD, M. R. Entrainment in the Turbulent Boundary Layer. A.R.C. 20,383, September 1958.

14. DODDS, J. I. Private communication, 1958.

15. CHAPMAN, D. R., KUEHN, D. M. and LARSON, H. K. Investigation of Separated Flows in Supersonic and Subsonic Streams with Emphasis on the Effect of Transition. N.A.C.A. T.N. 3869, 1957.

16. TOWNSEND, A. A. *The Structure of Turbulent Shear Flow.* Cambridge University Press, 1956.

17. TAYLOR, G. I. The Use of a Vertical Air Jet as a Windscreen. Mémoires sur la Mécanique des Fluides, offerts à Riabouchinsky, Ministère de l'Air, 1954.

18. SCHLICHTING, H. *Boundary-Layer Theory.* Pergamon Press, p. 498, 1955.

19. FÖRTHMANN, E. Uber turbulente Strahlausbreitung. *Ingenieur-Archiv,* Vol. 5, pp. 42-54, 1934; N.A.C.A. T.M. 789, 1936.

20. SIGALLA, A. Measurements of Skin Friction in a Plane Turbulent Wall Jet. *Journal of the Royal Aeronautical Society,* Vol. 62, December 1958.

21. GLAUERT, M. B. The Wall Jet. *Journal of Fluid Mechanics,* Vol. 1, 1956.

Analysis of Stress Concentrations at Reinforced Holes in Infinite Sheets

W. H. WITTRICK, M.A., Ph.D., F.A.A., A.F.R.Ae.S., A.F.I.A.S.

(Department of Aeronautical Engineering, University of Sydney)

SUMMARY: Equations are derived which enable the stresses around a compactly reinforced hole in an infinite sheet to be computed. The only restrictions placed on the shape of the hole are that it has at least one axis of symmetry and that the region outside it can be conformally mapped on to the region outside the unit circle by a transformation function in the form of a polynomial of any order. This admits a very wide range of holes of practical importance, including circles, ellipses, and squares, triangles and rectangles with rounded corners. Two loading cases are treated; the first corresponds to uniform tensions at infinity in directions parallel and perpendicular to the axis of symmetry of the hole, and the second to uniform shear at infinity in these directions. Superposition of these basic loading cases enables the stresses to be determined for any uniform state of stress at infinity. The equations are in an ideal form for use with a digital computer.

1. Introduction

Considerable interest attaches to the problem of determining the stress concentration arising at a hole in an infinite sheet, subjected to stresses at infinity. In practice a reinforcing member is usually provided around the hole boundary in order to reduce the stress concentration.

Mansfield[1] has shown how, for any given state of stress in the sheet, the hole may be designed in such a way that its presence leaves the state of stress unchanged. The hole is then said to be a neutral one, and its shape and the distribution of reinforcement around its boundary are dictated by the state of stress for which it is designed. With any other loading the hole is no longer neutral. Mansfield's theory leads in some cases to practically possible holes, the best known example being for a uniform state of stress with both principal stresses of the same sign. The hole is then elliptical, with a ratio of axes equal to the square root of the ratio of the principal stresses and the major axis in the direction of the greater principal stress. Such a hole could be used, for example, for a window in a pressure cabin, in which the predominant loading is due to the pressurisation, with a hoop tensile stress roughly equal to twice the longitudinal stress.

Received March 1960.

In practice, however, neutral holes suffer from three disadvantages. First, the reinforcement required is invariably non-uniform and therefore undesirable from a manufacturing point of view. Second, the weight of reinforcement required is often rather excessive and it is known[2] that a smaller amount of uniform reinforcement can lead to holes having stress concentration factors only slightly in excess of unity. Finally, the shape of the neutral hole may be unfavourable for reasons quite apart from strength considerations. There is little doubt that these arguments, and particularly the weight penalty which must be paid for a neutral hole, have led designers to accept compromise solutions, with different shapes and a uniform reinforcement having as small a weight as possible consistent with an acceptable stress concentration factor.

At the present time only elliptical and circular reinforced holes have been analysed to any great extent[2, 3] and the information available to the designer for other shapes of hole is rather meagre. The analysis of this paper is intended as a means of rectifying this deficiency. It has been made as general as possible, to cover holes of different shapes, with any reinforcement, and with any uniform state of stress at infinity.

The only assumptions made about the shape of the hole are, first, that it has at least one axis of symmetry and, second, that the region outside the hole may be mapped on to the region outside the unit circle by means of a polynomial transformation function of arbitrary order. The assumption of symmetry is not a serious restriction, since the great majority of holes of interest in practice have the required amount of symmetry. The second assumption is more restrictive but, nevertheless, a large number of practical shapes can be approximated to by this type of transformation function, particularly squares and triangles with rounded corners[4].

The reinforcement is assumed to be compact, which means that its flexural rigidity is sufficiently small for the shear force in the reinforcement to be neglected in comparison with the tension. This forms the basis for most previous work on reinforced holes.

The stress system at infinity is assumed to be uniform but otherwise arbitrary. However, it was found to be convenient to analyse separately the two cases of tensions at infinity, parallel and perpendicular to the axis of symmetry of the hole, and shear at infinity in these directions. The principle of superposition then enables any state of stress at infinity to be analysed.

The equations given are in an ideal form for solving on a digital computer. In fact it is possible to write a general programme which will enable the stresses to be computed around an arbitrary hole, conforming to the given restrictions, merely by specifying the coefficients of the polynomial transformation function, the cross-sectional area of the reinforcement, and the state of stress at infinity.

NOTATION

x, y Cartesian co-ordinates

s, n co-ordinates tangential and normal to the hole boundary

$z = x + iy$

t thickness of the sheet

A cross-sectional area of the reinforcement

r local radius of curvature of the hole boundary

X, Y co-ordinates of points on the hole boundary, made non-dimensional by dividing by R

G shear modulus

μ Poisson's ratio

ξ angle between the x-axis and the tangent to the hole

ζ complex co-ordinate in the circle plane

θ polar angle in the circle plane

$\sigma = e^{i\theta}$, complex co-ordinate on the unit circle

$\Omega(\zeta)$ transformation function

R constant determining the size of the hole, *see* equation (6)

c_j real constants in the transformation function ($j = -1, 0, 1, \ldots . N$), *see* equation (6)

F Airy stress function

$\Phi_0(z), \chi_0(z)$ complex stress functions, *see* equation (1)

$\Psi_0(z) = \chi_0'(z)$

$\Phi(\zeta) = \Phi_0(z)$

$\Psi(\zeta) = \Psi_0(z)$

a_n, b_n real constants in the expansions of $\Phi(\zeta)$ and $\Psi(\zeta)$, for the case of tensions at infinity, *see* equations (25) and (26)

p_n, q_n real constants in the expansions of $\Phi(\zeta)$ and $\Psi(\zeta)$, for the case of shear at infinity, *see* equations (39) and (40)

f_1, f_2 applied tensile stresses at infinity in the x, y directions

S applied shear stress at infinity in the x, y directions

T tension in the reinforcement

$P = \dot{X}^2 + \dot{Y}^2$

$$Q = 2P^{-1/2}\left[\frac{Rt}{A} + (1+\mu)\frac{R}{r}\right]^{-1}$$

A prime ($'$) denotes differentiation

A dot denotes differentiation with respect to θ

A bar denotes the complex conjugate value.

2. Equations of Plane Stress in Complex Form

In this section the basic equations of the two-dimensional theory of elasticity in complex form[5] will be summarised.

In terms of the complex variables z and $\bar{z}$, defined by the equations

$$z = x + iy, \qquad \bar{z} = x - iy,$$

the biharmonic equation for the Airy stress function F becomes

$$\frac{\partial^4 F}{\partial z^2 \partial \bar{z}^2} = 0.$$

Its general (real) solution is

$$F = \bar{z}\Phi_0(z) + z\overline{\Phi_0(z)} + \chi_0(z) + \overline{\chi_0(z)}, \quad . \quad . \quad . \quad . \quad (1)$$

where $\Phi_0(z)$ and $\chi_0(z)$ are two arbitrary analytic functions, and a bar denotes the complex conjugate.

The stresses $\widehat{xx}$, $\widehat{yy}$ and $\widehat{xy}$ are given by the equations

$$\widehat{xx} + \widehat{yy} = 4\frac{\partial^2 F}{\partial z \partial \bar{z}} = 4[\Phi_0'(z) + \overline{\Phi_0'(z)}], \quad . \quad . \quad . \quad (2)$$

$$\widehat{yy} - \widehat{xx} + 2i\widehat{xy} = 4\frac{\partial^2 F}{\partial z^2} = 4[\bar{z}\Phi_0''(z) + \Psi_0'(z)], \quad . \quad . \quad (3)$$

where $\Psi_0(z) = \chi_0'(z)$

and a prime (′) denotes differentiation.

The displacements u and v of a point in the x and y directions are given by the equation

$$G(u + iv) = \kappa\Phi_0(z) - z\overline{\Phi_0'(z)} - \overline{\Psi_0(z)}, \quad . \quad . \quad . \quad (4)$$

where G is the shear modulus and κ is a constant depending on the value of Poisson's ratio μ. For the case of plane stress

$$\kappa = \frac{3 - \mu}{1 + \mu}.$$

The only other basic relation required expresses the fact that the sum of the direct stresses at a point in any two perpendicular directions is constant, independent of the orientation; thus

$$\widehat{ss} + \widehat{nn} = \widehat{xx} + \widehat{yy}, \quad . \quad . \quad . \quad . \quad . \quad (5)$$

where s and n are any two perpendicular directions.

3. Transformation of the Equations

Let the region outside the hole in the z-plane be mapped on to the region outside the unit circle in the ζ-plane by means of a transformation function

$$z=\Omega(\zeta)=R\sum_{-1}^{N} c_j\zeta^{-j}, \quad . \quad . \quad . \quad . \quad . \quad (6)$$

in which R is a constant, having the dimensions of a length, whose magnitude determines the size of the hole, and the dimensionless coefficients c_j determine the shape of the hole. As mentioned previously, it will be assumed that the hole has at least one axis of symmetry, and the x-axis will be chosen to coincide with it. The effect of this is to ensure that R and all the c_j coefficients are real, thereby simplifying the subsequent analysis considerably. In practice and without loss of generality, the values $c_{-1}=1$ and $c_0=0$ may be postulated.

Let $$\Phi_0(z)=\Phi_0[\Omega(\zeta)]=\Phi(\zeta)$$

and $$\Psi_0(z)=\Psi_0[\Omega(\zeta)]=\Psi(\zeta).$$

It can be shown[5] that the functions $\Phi(\zeta)$ and $\Psi(\zeta)$ are expressible in the form

$$\Phi(\zeta)=R(\alpha\zeta+a_0+a_1\zeta^{-1}+a_2\zeta^{-2}+\ldots.), \quad . \quad . \quad . \quad (7)$$

$$\Psi(\zeta)=R(\beta\zeta+b_0+b_1\zeta^{-1}+b_2\zeta^{-2}+\ldots.), \quad . \quad . \quad . \quad (8)$$

provided that the stress at infinity is finite and that the resultants in both the x and y directions of any tractions which may be applied to the hole boundary are zero. The constants α and β may be expressed in terms of the stresses at infinity by means of the equations

$$\alpha=\frac{1}{8}(f_1+f_2)+iC. \quad . \quad . \quad . \quad . \quad . \quad (9)$$

$$\beta=\frac{1}{4}(f_2-f_1+2iS) \quad . \quad . \quad . \quad . \quad . \quad (10)$$

where f_1, f_2 and S are the values of $\widehat{xx}$, $\widehat{yy}$ and $\widehat{xy}$ respectively at infinity and C is an arbitrary real constant. It can be shown from equation (4) that the values of C, a_0 and b_0 correspond to rigid body movements which do not affect the stresses and can therefore be disregarded.

It can also be shown[5] that if the resultant moment, about the origin, of the tractions applied to the hole boundary is zero, the real part of the function

$$z\bar{z}\Phi_0'(z)+z\Psi_0(z)-\chi_0(z)$$

is single-valued.

Now the functions $\Phi_0'(z)$ and $\Psi_0(z)$ are both single-valued, as can be seen from equations (7) and (8). This follows because the stress components are single-valued. Hence the real part of $\chi_0(z)$ must be single-valued.

$$\text{Now} \quad \chi_0(z) = \int \Psi_0(z)\, dz = \int \Psi(\zeta)\, \Omega'(\zeta)\, d\zeta$$

$$= R^2 \int (\beta\zeta + b_0 + b_1\zeta^{-1} + b_2\zeta^{-2} + \ldots)(c_{-1} - c_1\zeta^{-2} - 2c_2\zeta^{-3} - \ldots)\, d\zeta.$$

The term in ζ^{-1} in the integrand of this expression will, when integrated, give rise to a term in $\log \zeta$ which increases by $2\pi i$ on making any anti-clockwise circuit surrounding the origin. It follows therefore that

$$\mathcal{I}(b_1 c_{-1} - \beta c_1) = 0,$$

where $\mathcal{I}$ denotes the imaginary part.

But all the c_i coefficients are real and, from equation (10), the imaginary part of β is $\frac{1}{2}iS$. Hence it follows that

$$\mathcal{I}(b_1) = \frac{c_1}{2c_{-1}} iS, \qquad (11)$$

4. Boundary Conditions

Consider the equilibrium of an element ds of the boundary reinforcement, with a triangular element of the attached sheet, as shown in Fig. 1. It will be assumed that the shear force in the reinforcement may be neglected in comparison with the tension T.

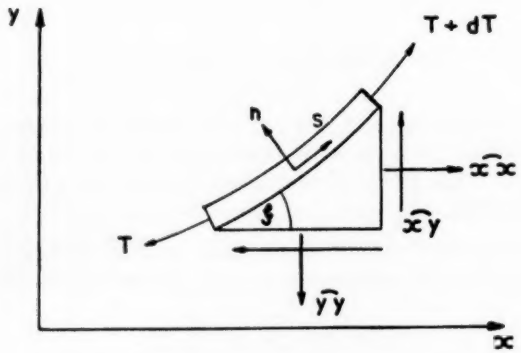

FIGURE 1. Element of reinforcement and attached sheet.

For equilibrium of the element in the y direction

$$d(T\sin\xi) = t(\widehat{yy}\,dx - \widehat{xy}\,dy)$$

$$= t\left(\frac{\partial^2 F}{\partial x^2}dx + \frac{\partial^2 F}{\partial x \partial y}dy\right) = t\,d(\partial F/\partial x),$$

where t is the sheet thickness and ξ is the slope of the boundary.

Similarly, for equilibrium in the x direction,

$$d(T\cos\xi) = -td(\partial F/\partial y).$$

Multiplication of the first equation by $-i$ and addition to the second gives

$$d(Te^{-i\xi}) = -itd\left(\frac{\partial F}{\partial x} - i\frac{\partial F}{\partial y}\right) = -2itd\left(\frac{\partial F}{\partial z}\right).$$

Integration of this equation and substitution of equation (1) now gives the equation

$$\frac{T}{2t} = -i\,e^{i\xi}\,[\overline{\Phi_0(z)} + \bar{z}\,\Phi_0'(z) + \Psi_0(z)] \quad . \quad . \quad . \quad (12)$$

For future reference it may be noted that the constant of integration has been incorporated in the function $\Phi_0(z)$.

Since T is essentially real, the first boundary condition expresses the fact that the *right-hand side of equation* (12) *is real*. It will be seen later that this enables the function $\Psi_0(z)$ to be determined in terms of $\Phi_0(z)$.

The secondary boundary condition arises from the equality of strain of the reinforcement and of the sheet to which it is attached, from which the following equation is obtained:—

$$\frac{T}{A} = \widehat{ss} - \mu\,\widehat{nn}, \quad . \quad . \quad . \quad . \quad . \quad . \quad (13)$$

where A is the cross-sectional area of the reinforcement and the s and n directions are shown in Fig. 1. Consider now the equilibrium of an element of reinforcement alone, as shown in Fig. 2. Resolving in the n and s directions,

$$\widehat{nn} = \frac{T}{rt} \quad . \quad . \quad . \quad . \quad . \quad . \quad . \quad (14)$$

and $$\widehat{sn} = \frac{1}{t}\frac{dT}{ds} \quad . \quad . \quad . \quad . \quad . \quad . \quad . \quad (15)$$

where r is the local radius of curvature of the boundary.

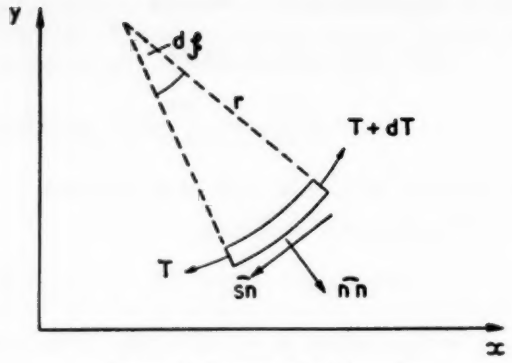

FIGURE 2. Element of reinforcement.

Combining equations (13) and (14), the second boundary condition may now be written in the more convenient form

$$T\left[\frac{1}{A}+\frac{1+\mu}{rt}\right]=\widehat{ss}+\widehat{nn} \quad . \quad . \quad . \quad . \quad . \quad (16)$$

where T is given by equation (12) and $(\widehat{ss}+\widehat{nn})$ by equations (2) and (5).

5. Geometry of the Hole

Some expressions concerning the geometry of the hole will now be derived in terms of the transformation function.

Let the x and y co-ordinates of a point on the boundary of the hole be denoted by XR and YR, where X and Y are non-dimensional.

On the unit circle

$$\zeta=e^{i\theta}=\sigma, \text{ say}, \quad . \quad . \quad . \quad . \quad . \quad (17)$$

so that, on separating real and imaginary parts of equation (6),

$$X=\sum_{-1}^{N} c_j\cos j\theta, \qquad Y=-\sum_{-1}^{N} c_j\sin j\theta. \quad . \quad . \quad (18)$$

Hence $$\dot{X}=-\sum_{-1}^{N} jc_j\sin j\theta, \qquad \dot{Y}=-\sum_{-1}^{N} jc_j\cos j\theta \quad . \quad . \quad (19)$$

and $$\ddot{X}=-\sum_{-1}^{N} j^2c_j\cos j\theta, \qquad \ddot{Y}=\sum_{-1}^{N} j^2c_j\sin j\theta, \quad . \quad . \quad . \quad (20)$$

where dots denote differentiation with respect to θ.

The slope ξ of the boundary of the hole is given by

$$e^{i\xi} = \frac{dz}{|dz|} = \frac{\Omega'(\sigma)\, d\sigma}{|\Omega'(\sigma)|\, |d\sigma|}.$$

Now $\quad d\sigma = i\sigma d\theta \quad$ and $\quad |d\sigma| = d\theta.$

Hence $$-ie^{i\xi} = \frac{\sigma\Omega'(\sigma)}{|\Omega'(\sigma)|} \qquad (21)$$

Also $$\Omega'(\sigma) = \frac{d\theta}{d\sigma}\frac{d}{d\theta}\Omega(\sigma) = \frac{R(\dot{X}+i\dot{Y})}{i\sigma}.$$

Hence $$|\Omega'(\sigma)| = RP^{1/2}, \qquad (22)$$

where $$P = \dot{X}^2 + \dot{Y}^2. \qquad (23)$$

The radius of curvature r of the boundary is readily shown to be given by the equation

$$\frac{R}{r} = P^{-3/2}(\dot{X}\ddot{Y} - \dot{Y}\ddot{X}). \qquad (24)$$

6. The Case of Tensions at Infinity

Consider first the case where the stress system at infinity consists of tensions f_1 and f_2 in the x and y directions, with no shear stress ($S = 0$).

From equations (7) to (10), therefore

$$\Phi_0(z) = \Phi(\zeta) = R\left[\frac{1}{8}(f_1+f_2)\zeta + a_0 + a_1\zeta^{-1} + a_2\zeta^{-2} + \ldots\right]. \qquad (25)$$

$$\Psi_0(z) = \Psi(\zeta) = R\left[\frac{1}{4}(f_2-f_1)\zeta + b_1\zeta^{-1} + b_2\zeta^{-2} + \ldots\right] \qquad (26)$$

It may be noted that although a_0 does not affect the stresses it is necessary to retain it in order to account for the constant of integration involved in the derivation of equation (12).

Because of the symmetry of the hole and of the loading about the x-axis, it is clear that if the displacements at a point z_0 are u_0 and v_0, then at the image point $\bar{z}_0$ the displacements are u_0 and $-v_0$. Using equation (4) it is then a simple matter to show that

$$\Phi_0(z) = \overline{\Phi}_0(z), \qquad \Psi_0(z) = \overline{\Psi}_0(z).$$

This means that all the a_n and b_n coefficients in equations (25) and (26) are real.

Since $S=0$ and b_1 is real, equation (11) is automatically satisfied.

$$\text{Now} \quad \Phi_0'(z)=\frac{d}{dz}\Phi_0(z)=\frac{d}{d\zeta}\Phi(\zeta)\frac{d\zeta}{dz}=\frac{\Phi'(\zeta)}{\Omega'(\zeta)}.$$

Hence, on using equations (21) and (22), equation (12) for the tension in the reinforcement becomes

$$\frac{TRP^{1/2}}{2t}=\sigma\Omega'(\sigma)\left[\overline{\Phi(\sigma)}+\Psi(\sigma)\right]+\sigma\overline{\Omega(\sigma)}\,\Phi'(\sigma). \qquad . \quad . \quad (27)$$

The right-hand side of this equation must be real. Hence, using the fact that $\bar{\sigma}=1/\sigma$, the following boundary equation is obtained

$$\sigma\Omega'(\sigma)\left[\Phi\left(\frac{1}{\sigma}\right)+\Psi(\sigma)\right]-\frac{1}{\sigma}\Omega'\left(\frac{1}{\sigma}\right)\left[\Phi(\sigma)+\Psi\left(\frac{1}{\sigma}\right)\right]+$$
$$+\sigma\Omega\left(\frac{1}{\sigma}\right)\Phi'(\sigma)-\frac{1}{\sigma}\Omega(\sigma)\Phi'\left(\frac{1}{\sigma}\right)=0. \quad . \quad (28)$$

This equation is multiplied throughout by $d\sigma/[2\pi i(\sigma-\zeta)]$, where $|\zeta|\geqslant 1$, and integrated round the unit circle. Then, on using equations (6), (25) and (26) and the known properties of Cauchy integrals[5], it is found that

$$\zeta\Omega'(\zeta)\Psi(\zeta)=\frac{1}{8}(f_1+f_2)\left[\frac{1}{\zeta}\Omega(\zeta)+\zeta\Omega\left(\frac{1}{\zeta}\right)-\Omega'(\zeta)-\Omega'\left(\frac{1}{\zeta}\right)\right]+\frac{1}{\zeta}\Omega'\left(\frac{1}{\zeta}\right)\Phi(\zeta)-$$
$$-\zeta\Omega\left(\frac{1}{\zeta}\right)\Phi'(\zeta)+b_1R^2+R^2\sum_{n=0}^{N-1}\left[a_n\sum_{j=n+1}^{N}(j-n)\,c_j\left(\zeta^{j-n}+\zeta^{n-j}\right)\right]. \quad (29)$$

Thus, the function $\Psi(\zeta)$ has now been determined completely in terms of $\Phi(\zeta)$, apart from the coefficient b_1 which remains unknown.

Substitution of equations (6), (25) and (29) into equation (27) now gives the following expression for the tension T:—

$$\frac{TP^{1/2}}{4Rt}=\frac{1}{8}(f_1+f_2)\sum_{-1}^{N}c_j\cos(j+1)\theta+\frac{1}{8}(f_2-f_1)(2c_{-1}\cos 2\theta-c_1)+\frac{1}{2}b_1-$$
$$-\sum_{n=0}^{\infty}\left[a_n\sum_{j=-1}^{N}j\,c_j\cos(n-j)\theta\right]+\sum_{n=0}^{N-1}\left[a_n\sum_{j=n+1}^{N}(j-n)\,c_j\cos(j-n)\theta\right]. \quad (30)$$

The sum of the direct stresses in the sheet at the boundary of the hole is given by

$$\widehat{ss}+\widehat{nn}=4\left[\Phi_0'(z)+\overline{\Phi_0'(z)}\right]$$
$$=4\left[\frac{\Phi'(\sigma)}{\Omega'(\sigma)}+\overline{\frac{\Phi'(\sigma)}{\Omega'(\sigma)}}\right].$$

Hence, on noting that

$$\Omega'(\sigma)\,\overline{\Omega'(\sigma)} = |\Omega'(\sigma)|^2,$$

and using equation (22),

$$\frac{PR^2}{4}(\widehat{ss}+\widehat{nn}) = \overline{\Omega'(\sigma)}\,\Phi'(\sigma) + \Omega'(\sigma)\,\overline{\Phi'(\sigma)}.$$

Substitution of equations (6) and (25) now gives the equation

$$\frac{P}{8}(\widehat{ss}+\widehat{nn}) = -\frac{1}{8}(f_1+f_2)\sum_{-1}^{N} jc_j\cos(j+1)\theta + \sum_{n=1}^{\infty}\left[na_n\sum_{j=-1}^{N} jc_j\cos(n-j)\theta\right] \quad . \quad (31)$$

Now the strain boundary condition on the hole, equation (16), can be written in the form

$$\frac{TP^{1/2}}{4Rt} = Q\,\frac{P}{8}(\widehat{ss}+\widehat{nn}), \quad . \quad . \quad . \quad . \quad (32)$$

$$\text{where} \qquad Q = 2P^{-1/2}\left[\frac{Rt}{A}+(1+\mu)\frac{R}{r}\right]^{-1} . \quad . \quad . \quad (33)$$

Substitution of equations (30) and (31) into (32) then gives

$$\tfrac{1}{2}b_1 - \sum_{n=0}^{\infty}\left[a_n(1+nQ)\sum_{j=-1}^{N} jc_j\cos(n-j)\theta\right] + \sum_{n=0}^{N-1}\left[a_n\sum_{j=n+1}^{N}(j-n)\,c_j\cos(j-n)\theta\right] +$$

$$+\frac{1}{8}(f_1+f_2)\sum_{-1}^{N} c_j(1+jQ)\cos(j+1)\theta + \frac{1}{8}(f_2-f_1)(2c_{-1}\cos 2\theta - c_1) = 0.$$

$$. \quad . \quad . \quad (34)$$

Equation (34) enables the unknowns b_1 and the a_n to be determined. It should be noted however that, in general, P, r and therefore Q are functions of θ, which makes it impossible to compare coefficients of the various cosine terms directly in equation (34). Theoretically Q could be expanded as a cosine series itself and the resulting products of cosines in equation (34) could be expressed in terms of the sums of cosines. Then, after comparing coefficients, an infinite number of infinite simultaneous equations in the unknowns would result. However, even in the simple case of an elliptical hole, this process is far too lengthy and complicated to be a practical possibility. Furthermore, only an approximate solution could be obtained in this way, by retaining only a finite number of a_n coefficients and an appropriate number of simultaneous equations.

A far simpler and more direct approach to the problem is to retain only a finite number, say m, of the a_n coefficients in the first place and to satisfy equation (34) at $(m+1)$ points in the range $0 \leqslant \theta \leqslant \pi$, say at $\theta = 0, \pi/m, 2\pi/m, \ldots, \pi$. In this way

sufficient simultaneous equations can be derived to determine the values of b_1 and the a_n. This procedure is ideal for use with a digital computer and was successfully employed for obtaining the stresses around reinforced elliptical holes[2, 3]. If it is expected that, over some region of the boundary, rapid variations of stress may occur, as in a square hole with only slightly rounded corners, the procedure can be modified by satisfying equation (34) at smaller intervals of θ in this region. A good guide to whether a sufficient number of the a_n coefficients has been retained, for the required accuracy, is the convergence of a_n to zero as n increases. Also, if there is any doubt about whether the chosen intervals of θ are small enough, a check can be made after the determination of the unknowns to see how closely equation (34) is satisfied at the middle points of the intervals.

There are certain special cases in which Q is constant. For example, if the hole is unreinforced, then $A=0$ and $Q=0$. If the hole is circular, with a uniform reinforcing member, then P, r, A, and therefore Q, are constant. Also, it can be shown[2] that any elliptical hole designed to be neutral for some particular ratio λ of f_1/f_2 is of such a shape, and has a reinforcing member with such an area distribution, that the variations of P, r, and A with θ cancel each other out and leave Q constant with the value $2/(\lambda+\lambda^{-1})$. If, for whatever reason, Q happens to be constant, the unknowns can be determined directly from equation (34) by comparing coefficients of the various cosine terms. In this case it is easily seen that $a_n=0$ if $n>N$, so that the series for $\Phi(\zeta)$ terminates at a finite number of terms.

Once the unknown coefficients a_n have been determined, the sum of the direct stresses, $(\widehat{ss}+\widehat{nn})$, in the sheet at the boundary of the hole may be computed from equation (31). The tension T in the reinforcement follows from equation (32).

$$\text{Thus} \qquad \frac{T}{Rt} = \frac{1}{2} QP^{1/2} (\widehat{ss}+\widehat{nn}). \qquad . \quad . \quad (35)$$

Equation (14) then gives the stress $\widehat{nn}$ and, knowing both this and $(\widehat{ss}+\widehat{nn})$, the stress $\widehat{ss}$ can be computed.

Finally, an expression for the shear stress $\widehat{sn}$ on the boundary can be obtained from equation (15).

$$\text{Now} \qquad ds = |dz| = |\Omega' (\sigma)\, d\sigma| = RP^{1/2} d\theta.$$

$$\text{Hence} \qquad \widehat{sn} = \frac{1}{RtP^{1/2}} \frac{dT}{d\theta}$$

$$= 4P^{-1/2} \frac{d}{d\theta}\left[\frac{TP^{1/2}}{4Rt} P^{-1/2}\right]$$

$$= \frac{4}{P} \frac{d}{d\theta}\left(\frac{TP^{1/2}}{4Rt}\right) - \frac{2}{P^2} \frac{TP^{1/2}}{4Rt} \frac{dP}{d\theta}.$$

Using equation (32) this becomes

$$\widehat{sn} = \frac{4}{P} \frac{d}{d\theta}\left(\frac{TP^{1/2}}{4Rt}\right) - \frac{Q}{4P} (\widehat{ss}+\widehat{nn}) \frac{dP}{d\theta} \qquad . \quad . \quad . \quad (36)$$

Also, from equation (30),

$$\frac{d}{d\theta}\left(\frac{TP^{1/2}}{4Rt}\right) = -\frac{1}{8}(f_1+f_2)\sum_{-1}^{N}(j+1)\,c_j\sin(j+1)\,\theta - \frac{1}{2}(f_2-f_1)\;c_{-1}\sin 2\theta + \\ + \sum_{n=0}^{\infty}\left[a_n\sum_{j=-1}^{N} j\,(n-j)\,c_j\sin(n-j)\,\theta\right] - \sum_{n=0}^{N-1}\left[a_n\sum_{j=n+1}^{N}(j-n)^2 c_j\sin(j-n)\,\theta\right]. \quad . \quad . \quad . \quad (37)$$

From equation (23),

$$\frac{dP}{d\theta} = 2(\dot{X}\ddot{X}+\dot{Y}\ddot{Y}). \quad . \quad . \quad . \quad . \quad (38)$$

Equations (36), (37) and (38) enable $\widehat{sn}$ to be computed.

7. The Case of Shear at Infinity

Consider now the case where the stress system at infinity consists of a pure shear stress S, with no tensions ($f_1 = f_2 = 0$).

The symmetry is now such that if the displacements at a point z_0 are u_0 and v_0, then at the image point $\bar{z}_0$ the displacements are $-u_0$ and v_0. It then follows from equation (4) that

$$\Phi_0(z) = -\overline{\Phi}_0(z), \qquad \Psi_0(z) = -\overline{\Psi}_0(z).$$

Hence the coefficients in equations (7) and (8) are purely imaginary and, on using equations (9) and (10), the expansions of $\Phi(\zeta)$ and $\Psi(\zeta)$ may be written in the form

$$\Phi(\zeta) = iRS(p_0 + p_1\zeta^{-1} + p_2\zeta^{-2} + \ldots) \quad . \quad . \quad . \quad (39)$$

$$\Psi(\zeta) = iRS\left(\frac{1}{2}\zeta + q_1\zeta^{-1} + q_2\zeta^{-2} + \ldots\right), \quad . \quad . \quad . \quad (40)$$

where the p_n and q_n coefficients are real.

Comparing equations (8) and (40) it is seen that

$$b_1 = iq_1S.$$

Hence, equation (11) gives

$$q_1 = \frac{c_1}{2c_{-1}} \quad . \quad . \quad . \quad . \quad . \quad . \quad . \quad (41)$$

The analysis now follows a course exactly similar to that of the preceding section. The fact that the right-hand side of equation (27) is real gives $\Psi(\zeta)$ in terms of $\Phi(\zeta)$. Thus

$$\zeta\Omega'(\zeta)\Psi(\zeta)=\frac{1}{2}iR^2S(\zeta^2-\zeta^{-2})+\frac{1}{\zeta}\Omega'\left(\frac{1}{\zeta}\right)\Phi(\zeta)-\zeta\Omega\left(\frac{1}{\zeta}\right)\Phi'(\zeta)+$$

$$+iR^2S\sum_{n=0}^{N-1}\left[p_n\sum_{j=n+1}^{N}(j-n)\,c_j(\zeta^{j-n}-\zeta^{n-j})\right]. \quad . \quad (42)$$

The tension T in the reinforcement is given by

$$\frac{TP^{1/2}}{4Rt}=-\frac{1}{2}S\sin 2\theta+S\sum_{n=0}^{\infty}\left[p_n\sum_{j=-1}^{N}jc_j\sin(j-n)\theta\right]-$$

$$-S\sum_{n=0}^{N-1}\left[p_n\sum_{j=n+1}^{N}(j-n)\,c_j\sin(j-n)\theta\right]. \quad (43)$$

The sum of the two direct stresses in the sheet at the boundary of the hole is given by the equation

$$\frac{P}{8}(\widehat{ss}+\widehat{nn})=-S\sum_{n=0}^{\infty}[np_n\sum_{j=-1}^{N}jc_j\sin(j-n)\theta]. \quad . \quad . \quad . \quad (44)$$

Substitution of equations (43) and (44) into equation (32) then gives the following equation for the determination of the unknowns p_n.

$$\sum_{n=0}^{\infty}\left[p_n(1+nQ)\sum_{j=-1}^{N}jc_j\sin(j-n)\theta\right]-\sum_{n=0}^{N-1}\left[p_n\sum_{j=n+1}^{N}(j-n)\,c_j\sin(j-n)\theta\right]=\frac{1}{2}\sin 2\theta.$$

$$. \quad . \quad . \quad (45)$$

Knowing the p_n coefficients, the sum of the direct stresses $(\widehat{ss}+\widehat{nn})$ can be computed from (44). Equation (35) then gives the tension T, and $\widehat{nn}$ follows from equation (14). Knowing $(\widehat{ss}+\widehat{nn})$ and $\widehat{nn}$, the stress $\widehat{ss}$ can be computed.

The shear stress $\widehat{sn}$ at the boundary is given by equation (36) where, in this case,

$$\frac{d}{d\theta}\left(\frac{TP^{1/2}}{4Rt}\right)=-S\cos 2\theta+S\sum_{n=0}^{\infty}\left[p_n\sum_{j=-1}^{N}j(j-n)\,c_j\cos(j-n)\theta\right]-$$

$$-S\sum_{n=0}^{N-1}\left[p_n\sum_{j=n+1}^{N}(j-n)^2c_j\cos(j-n)\theta\right]. \quad (46)$$

As before, since Q is in general a function of θ, only an approximate solution is possible, by retaining a finite number, say $(m-1)$, of the p_n coefficients and satisfying equation (45) at $(m-1)$ points in the range $0 < \theta < \pi$, say at $\theta = \pi/m, 2\pi/m, \ldots, (m-1)\pi/m$. The equation is automatically satisfied at $\theta = 0$ and π.

If Q happens to be constant, for any of the reasons previously described, the unknowns p_n can be obtained from equation (45) by comparing coefficients of the various cosine terms. As in the case of tensions at infinity, it is readily seen that $p_n = 0$ if $n > N$ and the series for $\Phi(\zeta)$ terminates at a finite number of terms.

References

1. Mansfield, E. H. Neutral Holes in Plane Sheet—Reinforced Holes which are Elastically Equivalent to the Uncut Sheet. *Quarterly Journal of Mechanics and Applied Mathematics*, Vol. 6, p. 370, 1953.
2. Wittrick, W. H. Stresses Around Reinforced Elliptical Holes, with Applications to Pressure Cabin Windows. *The Aeronautical Quarterly*, Vol. X, p. 373, 1959.
3. Wittrick, W. H. The Stresses Around Reinforced Elliptical Holes in Plane Sheet. Aeronautical Research Laboratories (Melbourne) Report A.R.L. SM 267.
4. Wittrick, W. H. Some Simple Transformation Functions for Square and Triangular Holes with Rounded Corners. *The Aeronautical Quarterly*, Vol. XI, May 1960.
5. Muskhelishvili, N. I. *Some Basic Problems of the Mathematical Theory of Elasticity*. Noordhoff, Groningen, Holland, 1953.

Limitations of the Sonic Area Rule

L. M. SHEPPARD

(Weapons Research Establishment, South Australia)

SUMMARY: Recent free flight tests have provided information on the applicability of the sonic area rule to non-lifting configurations. An analysis of results for the sonic wave drag of swept-back, tapered wings has suggested that the sonic area rule is applicable to thin wing and slender body combinations provided that the product of the wing span/length ratio and the cube root of the thickness/chord ratio is less than unity. The wing span/length ratio was found to be a much more useful slenderness parameter than the aspect ratio.

When the wing has a round-nosed section, theoretical considerations predict the existence of a so-called leading edge drag force varying with Mach number. One would expect such a wing to have the same sonic drag-rise as the equivalent body with an identical cross-sectional area distribution. Some test results do not confirm this drag-rise equivalence. It appears that the transonic drag-rise of the leading edge force is much greater than that predicted by theory.

Tests on one basic wing-body combination, with different body cross-sectional shapes of the same area, suggest that the cross-sectional shape, of a smooth slender body, has no influence on the transonic wave drag of a configuration.

1. Introduction

The sonic area rule[1, 2] predicts that the sonic wave drag of a non-lifting wing-body combination depends primarily on its cross-sectional area distribution. Whitcomb[1] showed that the rule does enable configurations with low sonic drag-rise to be designed. Lord[2] examined the theoretical design of low drag combinations as well as the estimation of sonic wave drag.

It is very important to know what limitations should be placed on the applicability of the sonic area rule, otherwise ineffective designs and incorrect drag estimates could occur. Spreiter[3] and Page[4] investigated the range of applicability of the rule for rectangular and delta wings respectively. The range of applicability of the sonic area rule for swept-back, tapered wings is investigated here by analysing some experimental results obtained by the Aerodynamics Division, Weapons Research Establishment[5, 6]. Other results obtained at the same time provide information on the influence of round-nosed wing sections and the body cross-sectional shape.

The wind tunnel and free flight experimental results utilised in this paper are discussed in Section 2. An examination of the range of applicability of the sonic

Received December 1959.

area rule is made in Section 3. Section 4 presents a discussion of some data on wings with round-nosed sections. Finally, in Section 5, some brief remarks are made on the influence of body cross-sectional shape.

NOTATION

A aspect ratio

C_D wave drag coefficient, $=D_{wave}/(qS)$

ΔC_D drag-rise coefficient, $=(D/qS)-(D/qS)_{M=0.8}$

D total drag

D_{wave} wave drag

M free stream Mach number

$q=\frac{1}{2}\rho V^2$

S wing area

σ slenderness parameter, span/length

V free stream velocity

$\Lambda_{1/2}$ angle of mid-chord sweepback

ρ free stream density

τ thickness/chord ratio

2. Experimental Results

Limitations of the sonic area rule can be investigated by analysing suitable experimental data. Possible sources of such data are wind tunnel and free flight tests. It is fortunate that some suitable test results do exist and these are discussed here.

The wind tunnel data presented by Spreiter[3] and Page[4] were obtained at Reynolds numbers, based on the mean wing aerodynamic chord, of one to two million. Page's transonic tunnel results apply to delta wings and are more accurate than the transonic bump results, for rectangular wings, used by Spreiter. Thickness/chord ratios varied from 2 per cent to 10 per cent and the aspect ratios from $\frac{1}{2}$ to 6.

The free flight results[5, 6] were obtained at a Reynolds number, based on the mean wing aerodynamic chord, of about six million. All body-alone drag results are considerably more accurate than the wing drag results, the maximum errors of which could be 25 per cent. The bodies had thickness/length ratios between 6 per cent and 8 per cent, while the wings of the wing-body combinations had 6 per cent to 12·5 per cent thickness/chord ratios. Wing aspect ratio varied from 2 to 4. All the test vehicles were accelerated up to speed by 3 in. cordite rocket motors. During the subsequent coasting flight the total vehicle drag was derived by a double differentiation of the trajectory, as determined from three-station reflection Doppler.

Wing drag was determined from the difference between the drags of the wing-body combination and the basic body alone, interference effects on the drag being negligible.

It must be noted that some accurate experimental drag results for swept-back, tapered wings are still desirable because of the rather poor accuracy of the free flight results[6].

3. Range of Applicability

The range of applicability of the sonic area rule for rectangular wings has been investigated by Spreiter[3]. If the drag-rise depends solely on the cross-sectional area distribution then, for a given family of wings, it can be shown[3] that $[\Delta C_D/(A\tau^2)]_{M=1}$ would be constant, independent of $A\tau^{1/3}$. Here ΔC_D is the drag-rise coefficient based on the exposed wing area, A is the aspect ratio, τ is the thickness/chord ratio and M denotes the free stream Mach number. A simpler derivation of this result can be obtained from the theoretical version[2] of the sonic area rule. This version treats wave drag, not drag-rise. Since it is derived from supersonic theory it satisfies the first-order supersonic similarity law and so[7] the wave drag parameter $C_D/(A\tau^2)$ must be a constant for a given wing family. Therefore, the sonic area rule would be expected to be applicable where $C_D/(A\tau^2)$, or $\Delta C_D/(A\tau^2)$, is independent of $A\tau^{1/3}$.

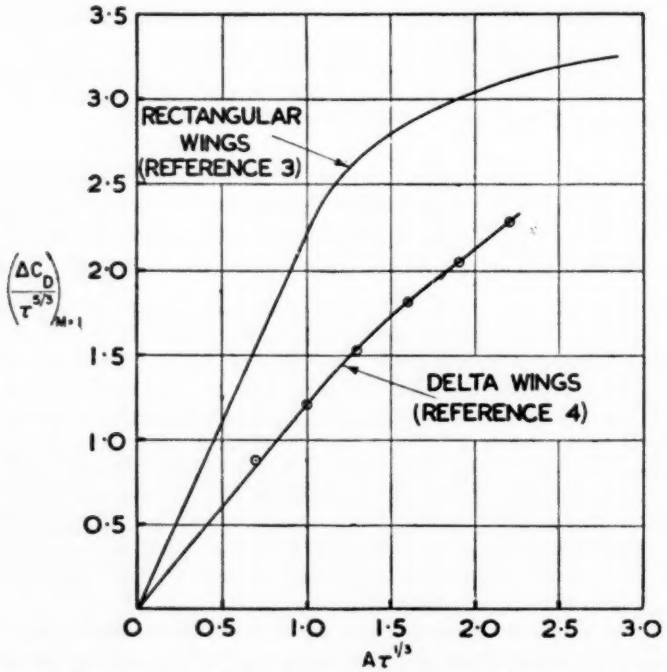

FIGURE 1. Similarity analysis of $(\Delta C_D/\tau^{5/3})_{M=1}$ for wings with N.A.C.A. 63AOXX sections

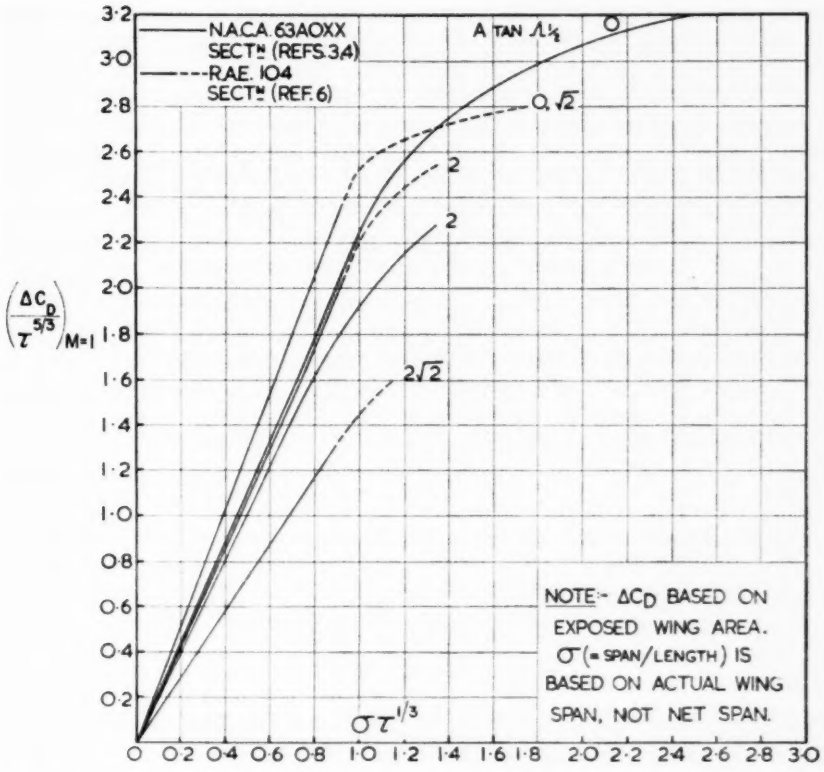

FIGURE 2. Effect of transonic slenderness parameter and $\sigma\tau^{1/3}$ on the sonic wave drag parameter $(\Delta C_D/\tau^{5/3})_{M=1}$.

For rectangular wings Spreiter[3] showed that $(\Delta C_D/\tau^{5/3})_{M=1}$ was a linear function of $A\tau^{1/3}$ for $A\tau^{1/3} < 1$. Page[4] carried out wind tunnel tests on delta wings and obtained a wider range of linearity. These two sets of results are illustrated in Fig. 1. Clearly the scope of these results should be extended to include wings with swept-back trailing edges. Some drag-rise results for a series of swept-back, tapered wings have been obtained at W.R.E. using the free flight technique[6]; the range of linearity was found to become larger as the mid-chord shearback $A \tan \Lambda_{1/2}$ increased and the wing became more "slender." Taper ratio was not an important parameter.

It is possible to obtain a much neater presentation of all this experimental data by introducing the slenderness parameter[6, 7] σ (=span/length) and plotting $(\Delta C_D\tau^{5/3})_{M=1}$ against $\sigma\tau^{1/3}$, as in Fig. 2. Clearly $(\Delta C_D/\tau^{5/3})_{M=1}$ varies linearly with $\sigma\tau^{1/3}$ (or $A\tau^{1/3}$) for all the wings provided that $\sigma\tau^{1/3}$ is less than about unity. This result is a generalisation of Spreiter's result for rectangular wings and is likely to be

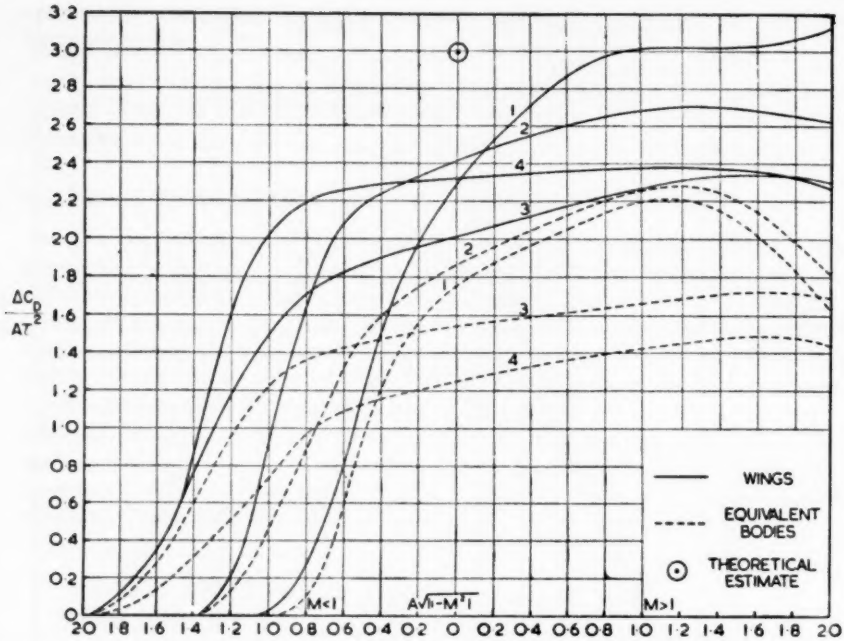

FIGURE 3. Similarity comparison of drag-rise results for wings and equivalent bodies.

applicable to wings of arbitrary plan form. Hence it is suggested that the sonic area rule will be applicable to thin wing and slender body combinations when the wing slenderness parameter $\sigma\tau^{1/3}$ is less than unity.

4. Application to Wings with Round-Nosed Sections

Theoretical investigations of the drag of non-lifting wings with round-nosed sections show that a so-called leading edge drag force exists when the component of free stream Mach number normal to the edge is less than unity. This edge drag is incorporated in the wave drag, deduced from area rule considerations.* However, some additional leading edge drag would appear if the flow in the nose region were no longer of the reversible subsonic type, normal to the leading edge, but was essentially transonic in character. Then an equivalent body of revolution, having the same distribution of cross-sectional area as the wing, would have a lower transonic drag-rise than the wing.

Whitcomb's original statement of the transonic area rule[1] implies that the

*The author is indebted to a referee for pointing out that Ref. 5 is incorrect in assuming that the edge drag should be added to this wave drag. The leading edge drag force is added only to that theoretical wave drag calculated from the integration over the wing of the product of local pressure and local surface slope.

drag-rise of a wing is approximately the same as that of its equivalent body. From the foregoing discussion it can be seen that this would be true only when the wave drag was very much greater than any additional drag-rise of the leading edge force. That there may exist configurations for which this is not true is shown by Fig. 3, which presents the drag-rises[5] of four wings and their equivalent bodies of revolution. These wings had round-nosed R.A.E. 104 sections, with $A\tau^{1/3}$ being 0·841, 1·189, 1·682 for Wings 1, 2, 3 (and 4) respectively. Also, the mid-chord shearback $A \tan \Lambda_{1/2}$ was equal to 2 and the taper ratio was 0·408. The slenderness parameter $\sigma\tau^{1/3}$ varied from 0·50 to 0·96, being less than unity. Thus, from Section 3, the sonic area rule would be expected to be applicable.

A systematic difference between wing and equivalent body drag-rise is evident in Fig. 3. The assumption that any flow separation effects (due to shock wave and boundary layer interaction) are unimportant in drag-rise comparisons has enabled estimates to be made of the additional leading edge drag force. This is found[5] to be about twice the drag-rise of the theoretical leading edge force[8]. It is clear that flow separation effects may be incorporated in the estimate of the additional leading edge drag-rise. Unfortunately, these effects cannot be isolated, since no satisfactory method of allowing for them exists.

Pending a more complete investigation of the effective leading edge drag force it is suggested that, near sonic speed, an additional leading edge drag-rise, equal to twice the theoretically predicted leading edge drag-rise, be incorporated in drag estimates of wings having thickness/chord ratios of about 6 per cent to 9 per cent.

A wave drag estimate, obtained from the theoretical version of the sonic area rule[2], is also shown in Fig. 3. It is not surprising that this estimate is very much greater than the sonic drag-rise of the equivalent body; the essentially supersonic theory of Ref. 2 would not be expected to give satisfactory wave drag estimates at sonic speed.

5. Influence of Body Cross-Sectional Shape

One group of free flight results[5] referred to wing-body combinations having the same distribution of cross-sectional area, but different body shapes. The bodies had

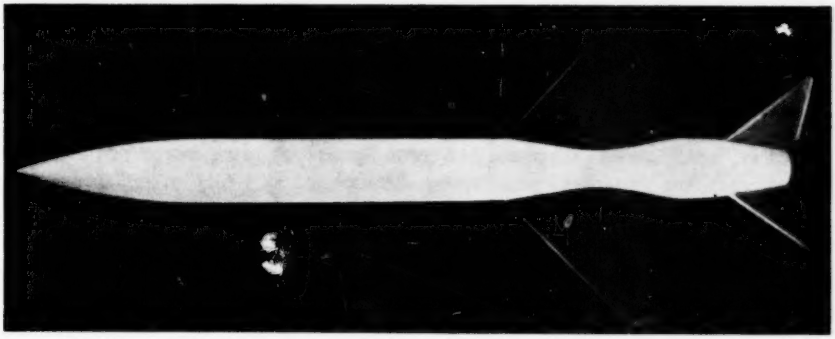

FIGURE 4. Typical test vehicle. (Maximum body waisting in the plane of the wing.)

thickness/length ratios of 8 per cent and so could be considered "slender." A typical test vehicle, with stabilising fins, is shown in Fig. 4. The body shapes used were circular, elliptic with the major axis parallel to the wing plane and elliptic with the major axis normal to the wing plane. A constant total cross-sectional area was maintained in the region of the wing.

The test results[5] showed no significant variations in drag with body shape. Thus body cross-sectional shape has no significant effect on the transonic drag of these wing-body combinations. It is suggested that this result applies to all configurations with smooth bodies that are slender. For non-slender bodies, however, cross-sectional shape may be a significant variable.

Acknowledgment

Publication is made with the permission of the Chief Scientist, Australian Defence Scientific Service, Department of Supply, Melbourne.

References

1. Whitcomb, R. T. A Study of the Zero-Lift Drag-Rise Characteristics of Wing-Body Combinations near the Speed of Sound. N.A.C.A. Report 1273, 1956.

2. Lord, W. T. Notes on the Drag of Wing-Body Combinations at Transonic and Supersonic Speeds. R.A.E. Technical Note Aero 2229, January 1953. (*See also* R. & M. to be issued and R.A.E. Technical Note Aero 2282, 1954.)

3. Spreiter, J. R. On the Range of Applicability of the Transonic Area Rule. N.A.C.A. T.N. 3673, May 1956.

4. Page, W. A. Experimental Determination of the Range of Applicability of the Transonic Area Rule for Wings of Triangular Plan Form. N.A.C.A. T.N. 3872, December 1956.

5. Sheppard, L. M. Some Free Flight Tests on the Sonic Area Rule and Wing-Body Wave Drag. W.R.E. Technical Note HSA 51, June 1959.

6. Sheppard, L. M. Transonic Drag Tests of 32 Wings having R.A.E. 104 sections. W.R.E. Report HSA 12, October 1959.

7. Sheppard, L. M. Experimental Evidence on the Transonic and Supersonic Similarity Laws for the Wave Drag of Non-Lifting Wings. W.R.E. Technical Note HSA 54, November 1959.

8. Jones, R. T. Leading Edge Singularities in Thin Airfoil Theory. *Journal of the Aeronautical Sciences*, Vol. 17, May 1950.

The Stability of the Short-Period Motion of an Airframe Having Non-Linear Normal Force and Pitching Moment Curves

P. A. T. CHRISTOPHER

(*Department of Aerodynamics, The College of Aeronautics, Cranfield*)

SUMMARY: The analysis of the stability of second-order non-linear systems by Poincaré's method of singular points in the phase plane is briefly presented and used to determine stability criteria for the short-period motion of an airframe having non-linear normal force and pitching moment curves. These results are then compared with those obtained by the application of quasi-linear stability theory.

1. Introduction

The linear theory of airframe dynamic stability is based on the assumption that, during a disturbance of the steady motion, powers and time derivatives higher than the first can be neglected (*see* Ref. 1). In some applications the linear theory is invalid, even as a first approximation, since the governing differential equations are markedly non-linear in form. An example of this kind arises in relation to the stability of low aspect ratio wings having a leading edge separation, the separated flow rolling up into approximately streamwise vortices which produce non-linear force and moment variations with incidence. Similar non-linear variations occur in wings at transonic speeds (*see* Ref. 2), on wings and bodies at hypersonic speeds and on most configurations at incidence near the stall.

Except for those cases where it is possible to separate the variables or the equation is exact, no explicit general solutions to non-linear differential equations are known. Between the extremes of the exact solution and the approximate quasi-linear one a variety of higher approximations can be derived; these are usually based on analytic iteration techniques which yield series solutions of differing degrees of accuracy. For equations of the second order and lower the "phase plane" method, which is qualitative, will give considerable insight into the nature and stability of solutions and can, by the use of Liénard's or other constructions, give quantitative solutions. In Ref. 3 the phase plane method is discussed and applied to examples taken from elementary mechanics, structural engineering and electrical machine theory.

Received May 1960

The longitudinal free motion of an airframe is often expressed in terms of a differential equation of at least the fourth order; the principal modes of oscillation, the "short peroid" and "phugoid", are then interrelated (*see* Ref. 1). In some applications, for example many guided missiles, the short-period motion, which is governed by an equation of the second order, is of dominant interest. When the influence of non-linear normal force and pitching moment variations with incidence are included in this equation, it provides an interesting example of the phase plane method.

NOTATION

a, b, c, d constants in Poincaré's theory of singular points

f_1, f_2 functions defined in equation (17)

m airframe mass

q angular velocity about axis of pitch

t time

$v = dx/dt$

w velocity along axis of yaw

x any independent variable, *see* equation (1)

$$z_w = \frac{1}{m}\left(\frac{\partial Z}{\partial w}\right)_{w=0}$$

$$z_q = \frac{1}{m}\left(\frac{\partial Z}{\partial q}\right)_{q=0}$$

$$z_\eta = \frac{1}{m}\left(\frac{\partial Z}{\partial \eta}\right)_{\eta=0}$$

$$m_w = \frac{1}{B}\left(\frac{\partial M}{\partial w}\right)_{w=0}$$

$$m_q = \frac{1}{B}\left(\frac{\partial M}{\partial q}\right)_{q=0}$$

$$m_\eta = \frac{1}{B}\left(\frac{\partial M}{\partial \eta}\right)_{\eta=0}$$

$$m_{\dot{w}} = \frac{1}{B}\left(\frac{\partial M}{\partial \dot{w}}\right)_{\dot{w}=0}$$

$z_3, z_5, \ldots$
$m_3, m_5, \ldots$ } constants in the force and moment relations of equation (12)

$$A_1 = (U_0 + z_q)\, m_w - m_q z_w$$

$$A_3 = (U_0 + z_q)\, m_3 - m_q z_3$$

B moment of inertia about the axis of pitch

$$B_1 = (U_0 + z_q)\, m_{\dot{w}} + m_q + z_w$$

$B_3 = 3z_3$

D the operator d/dt

$G = -2A_1$

$H = B_1\left(1 - \frac{B_3}{B_1}\frac{A_1}{A_3}\right)$

M moment about axis of pitch

Q forcing function of the elevator

U_0 velocity along the axis of roll (longitudinal body axis)

Z force along axis of yaw

η elevator angle

θ angle of elevation

λ root of characteristic equation (9)

ξ ordinate of w referred to singular point

2. The Phase Plane Method

The method is concerned with equations of the form

$$\frac{d^2x}{dt^2} + B(x)\frac{dx}{dt} + C(x) = 0. \quad . \quad . \quad . \quad . \quad (1)$$

or degenerate forms. Writing $v = dx/dt$, then $d^2x/dt^2 = v\,dv/dx$ and (1) becomes

$$v\frac{dv}{dx} + B(x)v + C(x) = 0. \quad . \quad . \quad . \quad . \quad (2)$$

The graphs of the solutions of this equation in the xv-plane, known as the phase plane, are referred to as "integral curves" and through each ordinary point in the plane there passes only one such curve.

Equation (2) may be rewritten as an equivalent pair of equations

$$\left.\begin{aligned}\frac{dv}{dt} &= -C(x) - B(x)v \\ \frac{dx}{dt} &= v,\end{aligned}\right\} \quad . \quad . \quad . \quad . \quad . \quad (3)$$

which define a field vector having components dv/dt and dx/dt; this vector is always tangential to the integral curve and indicates the direction in which t is increasing. When $B(x) \equiv 0$, and $C(x)$ is an anti-symmetric function, the integral curves are closed and the slope of the field vector is

$$\frac{dv}{dt}\Big/\frac{dx}{dt} = \frac{dv}{dx} = \frac{-C(x)}{v}. \quad . \quad . \quad . \quad (4)$$

The variables can be separated and, provided that the integral is soluble, the integral curves may normally be expressed in analytic form. The resulting motion is periodic, this being characteristic of conservative systems. For the general case, explicit integration is not possible and solutions may be obtained by geometric constructions, such as that of Liénard. To examine the stability of the solutions of (2) or (3) it is not necessary to have these explicitly; for this purpose use may be made of Poincaré's theory of singular points, which is now briefly summarised.

3. Singular Points

The stationary positions of equilibrium of equations (2) or (3) correspond with the singularities of the equivalent equation

$$\frac{dv}{dx} = \frac{-C(x) - B(x)\,v}{v} \quad . \quad . \quad . \quad . \quad . \quad . \quad (5)$$

and analysis of the character of these singularities gives considerable insight into the nature of the motion near these points. More generally, consider the singularities of the equation

$$\frac{dv}{dx} = \frac{P(x, v)}{Q(x, v)}, \quad . \quad . \quad . \quad . \quad . \quad (6)$$

which are defined by $P(x, v) = Q(x, v) = 0$. Since the origin can always be changed to correspond with the singular point, then analysis can be restricted to singularities at the origin.

When (6) has a singularity at the origin then it is assumed (Poincaré) that it may be written in series form

$$\frac{dv}{dx} = \frac{ax + bv + p(x, v)}{cx + dv + q(x, v)}, \quad . \quad . \quad . \quad . \quad . \quad (7)$$

where $p(x, v)$ and $q(x, v)$ are the remaining terms of series whose lowest terms are of second degree at least. Further, if the constants obey the inequality

$$\Delta = \begin{vmatrix} a & b \\ c & d \end{vmatrix} = ad - bc \neq 0,$$

then the integral curves behave, in the neighbourhood of the singularity, as if $p(x, v)$ and $q(x, v)$ were absent.

The singularities of the reduced equation

$$\frac{dv}{dx} = \frac{ax + bv}{cx + dv} \quad . \quad . \quad . \quad . \quad . \quad . \quad . \quad (8)$$

are of four distinct types.

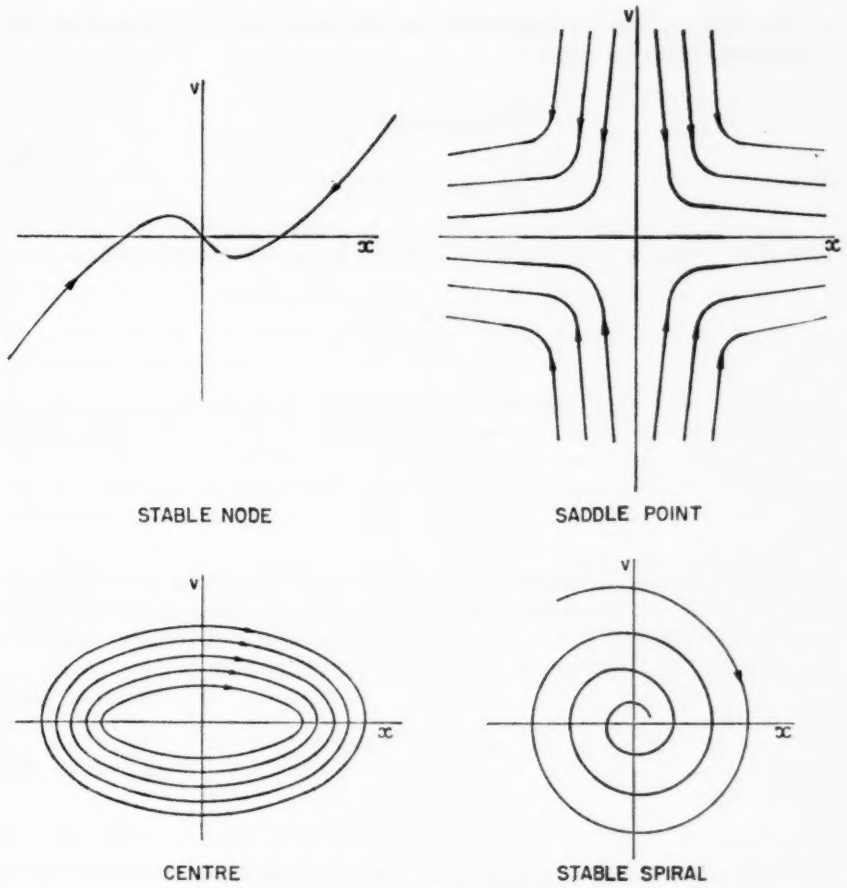

FIGURE 1. Types of singularities.

The four types of singularities are

(*i*) nodal points (or nodes), which are either stable or unstable, ($a=d=0$, $c=1$, $b>0$ or $d=0$, $a=b=c=1$)

(*ii*) centres, which indicate periodic motion, ($b=c=0$, $d=1$)

(*iii*) spiral points, which are either stable or unstable, ($a=1$, $d=-1$, $b=c\neq 0$)

(*iv*) saddle points, which are unstable ($a=d=0$, $c=1$, $b<0$).

The nature of the integral curves in the region of these singularities is shown in Fig. 1. If the singularity does not correspond with one of the four cases (*i*)-(*iv*), then it may be reduced to one of these forms in a new variable by means of non-singular, linear transformations.

Equation (8) may be replaced by the equivalent pair of equations for the components of the field vector

$$\left.\begin{aligned}\frac{dv}{dt}&=\dot{v}=ax+bv\\ \frac{dx}{dt}&=\dot{x}=cx+dv.\end{aligned}\right\} \quad . \quad . \quad . \quad . \quad . \quad . \quad (8a)$$

Also, x and v may be transformed into x_1 and v_1 by the linear transformation

$$x_1=\alpha x+\beta v$$
$$v_1=\gamma x+\delta v,$$

implying that the integral curves are now referred to new oblique co-ordinate axes. A further transformation is now sought which makes the slope of the field vector in the x_1v_1-plane

$$\frac{dv_1}{dx_1}=\frac{\lambda_2 v_1}{\lambda_1 x_1}. \quad . \quad . \quad . \quad . \quad . \quad . \quad (9)$$

This form is directly comparable with certain of those in (*i*)-(*iv*) and it is left to obtain λ_1 and λ_2 in terms of the coefficients in equation (8). Since the transformation is to be non-singular, then $v_1\neq 0$, $x_1\neq 0$ for all values of x and v, and thus $(\alpha\delta-\gamma\beta)\neq 0$. Equation (9) may be written in the equivalent form

$$\left.\begin{aligned}\frac{dv_1}{dt}&=\dot{v}_1=\lambda_2 v_1\\ \frac{dx_1}{dt}&=\dot{x}_1=\lambda_1 x_1\end{aligned}\right\} \quad . \quad . \quad . \quad . \quad . \quad . \quad (9a)$$

and, since $\dot{x}_1=\alpha\dot{x}+\beta\dot{v}$ and $\dot{v}_1=\gamma\dot{x}+\delta\dot{v}$, then, upon substitution for $\dot{x}$, $\dot{v}$, x_1, v_1, $\dot{x}_1$ and $\dot{v}_1$ in (9*a*), there arise the equations

$$\left.\begin{aligned}\alpha(cx+dv)+\beta(ax+bv)&=\lambda_1(\alpha x+\beta v)\\ \gamma(cx+dv)+\delta(ax+bv)&=\lambda_2(\gamma x+\delta v)\end{aligned}\right\} \quad . \quad . \quad . \quad . \quad (9b)$$

Since these must be true for all values of x and v, then the coefficients of x and v must vanish (*i.e.* the coefficient may be equated) giving the equations

$$\left.\begin{aligned}\alpha(\lambda_1-c)-\beta a&=0\\ -\alpha d+\beta(\lambda_1-d)&=0\end{aligned}\right\} \quad . \quad . \quad . \quad . \quad (10a)$$

and

$$\left.\begin{aligned}\gamma(\lambda_2-c)-\delta a&=0\\ -\gamma d+\delta(\lambda_2-b)&=0.\end{aligned}\right\} \quad . \quad . \quad . \quad . \quad (10b)$$

The coefficients α, β, γ and δ are not all zero; therefore (10*a*) and (10*b*) have a common eliminant

$$\begin{vmatrix} (\lambda-c) & -a \\ -d & (\lambda-b) \end{vmatrix} = 0$$

$$\text{or} \quad \lambda^2-\lambda(b+c)-(ad-bc)=0. \qquad . \quad . \quad . \quad (10c)$$

Criteria for distinguishing the type of singularity are obtained from the "characteristic equation" (10*c*) which has the roots

$$\lambda_{1,2}=\tfrac{1}{2}\{(b+c)\pm[(b+c)^2+4(ad-bc)]^{1/2}\}$$

and, since $ad-bc\neq 0$, then λ can never be zero. Three important cases are distinguished, as follows.

Roots real and unequal. These arise when the discriminant is positive. The sub-cases are: if $\Delta>0$ then λ_2/λ_1 is negative and corresponds to a saddle point, and if $\Delta<0$ then λ_2/λ_1 is positive and corresponds to a nodal point. In the second case, if λ_1 and λ_2 are both negative the node is stable, whereas if λ_1 and λ_2 are both positive the node is unstable.

Roots complex conjugate. Complex roots occur when the discriminant is negative. If the real part of the root is negative the integral curves are stable spirals, whereas if the real part is positive the curves are unstable spirals. When the roots are purely imaginary the singularity is a centre; however, under these conditions the singularity of (8) is not necessarily that of (7) and the higher order terms in $p(x, v)$ and $q(x, v)$ have to be considered.

Roots real and equal. The singularity is a node and its stability is governed in the same way as if the roots were unequal.

4. Equations of Longitudinal Motion of an Airframe

In analysing the longitudinal dynamic stability of guided missiles it is customary to consider only the short-period motion, the velocity of flight being assumed constant during a small disturbance. In this case the linear equations of motion become (*see*, for example, Ref. 5)

$$\left.\begin{aligned}(D-z_w)\,w-(U_0+z_q)\,\theta &= z_\eta\eta \\ -(m_wD+m_w)\,w+(D-m_q)\,\theta &= m_\eta\eta\end{aligned}\right\} \quad . \quad . \quad . \quad . \quad (11)$$

For the present problem it is intended to include non-linear variations of the normal force Z and pitching moment M with vertical velocity w and to introduce these effects into equations (11). It is assumed that the force and moment contributions due to w, written $Z(w)$ and $M(w)$ respectively, may be expressed in any of the graphical forms shown in Fig. 2. The important quality of these curves is that they are anti-symmetrical in form, characteristic of most symmetrical configurations. The anti-symmetric character allows the forces and moments to be written as power series in odd powers of w.

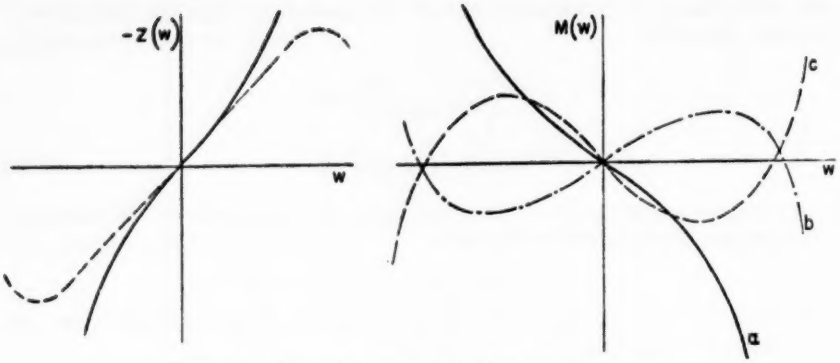

FIGURE 2. Normal force and pitching moment curves.

$$\text{Thus} \qquad \left.\begin{aligned} \frac{Z(w)}{m} &= z_w w + z_3 w^3 + z_5 w^5 \quad + \ldots \\ \frac{M(w)}{B} &= m_w w + m_3 w^3 + m_5 w^5 + \ldots \end{aligned}\right\} \quad . \quad . \quad . \quad (12)$$

When these non-linear expressions are substituted into the equations of motion, they become

$$\dot{w} - (z_w w + z_3 w^3 + \ldots) - (U_0 + z_q)\,\dot{\theta} = z_\eta \eta \quad . \quad . \quad . \quad (13)$$

$$-m_{\dot{w}}\dot{w} - (m_w w + m_3 w^3 + \ldots) + (D - m_q)\,\dot{\theta} = m_\eta \eta. \quad . \quad . \quad (14)$$

Eliminating $\dot{\theta}$ between (13) and (14) then gives

$$(D - m_q)(\dot{w} - z_w w - z_3 w^3 - \ldots) - (U_0 + z_q)(m_{\dot{w}}\dot{w} + m_w w + m_3 w^3 + \ldots) = [z_\eta (D - m_q) - m_\eta (U_0 + z_q)]\,\eta$$

or, upon collecting terms, gives

$$\ddot{w} - [(U_0 + z_q)\, m_{\dot{w}} + m_q + z_w + 3z_3 w^2 \ldots]\,\dot{w} - [(U_0 + z_q)\, m_w - m_q z_w]\, w - - [(U_0 + z_q)\, m_3 - m_q z_3]\, w^3 - \ldots = [z_\eta D - (U_0 + z_q)\, m_\eta - z_\eta m_q]\,\eta \quad (15)$$

This equation may be written in the form

$$\ddot{w} - f_1(w)\,\dot{w} - f_2(w) = Q(\eta) \quad . \quad . \quad . \quad . \quad (16)$$

which, for the case of the free motion, $Q(\eta) \equiv 0$, reduces to

$$\ddot{w} - f_1(w)\,\dot{w} - f_2(w) = 0, \quad . \quad . \quad . \quad . \quad . \quad (17)$$

and is of the same form as (1).

Note: It is important to appreciate that in a non-linear system the principle of linear superposition no longer applies, and the solution of (17) is no longer a complementary function to the complete solution of (16). In linear theory, if the corresponding equation to (17) can be shown to be stable, then the corresponding equation to (16) will also be stable provided that $Q(\eta)$ is of finite magnitude. The stability of (16) and (17) are not related in this simple manner.

The variable w cannot be eliminated between equations (13) and (14) in such a way as to give an equation in θ which is of the same form as (16) and therefore the stability of the θ motion cannot be obtained by the method of singular points.

5. Stability of the Short-Period Motion

Writing $\dot{w}=v$, then (17) becomes

$$\frac{dv}{dw}=\frac{f_2(w)+f_1(w)\,v}{v}, \qquad . \quad . \quad . \quad . \quad . \quad (18)$$

which has singularities when $f_2(w)=0$, $v=0$. The number of singular points depends on the number of unequal roots of the equation

$$f_2(w)=[(U_0+z_q)\,m_w-m_qz_w]\,w+[(U_0+z_q)\,m_3-m_qz_3]\,w^3+\ldots.$$
$$\ldots.+[(U_0+z_q)\,m_{2n-1}-m_qz_{2n-1}]\,w^{2n-1}+\ldots.=0, \quad . \quad (19)$$

and therefore on the number of terms, n, used to represent the force and moment curves. For simplicity only two terms are considered in the remainder of the analysis, although this can readily be extended to any reasonable number of singular points; hence

$$f_2(w)=[(U_0+z_q)\,m_w-m_qz_w]\,w+[(U_0+z_q)\,m_3-m_qz_3]\,w^3=0. \quad . \quad (20)$$

When the coefficients of w and w^3 in (20) are the same sign, then only one singularity exists and this is at the origin, while if the coefficients are of different sign singular points occur at

$$w=\pm\left\{\frac{-(U_0+z_q)\,m_w+m_qz_w}{(U_0+z_q)\,m_3-m_qz_3}\right\}^{1/2}, \qquad v=0, \qquad . \quad . \quad (21)$$

as well as at the origin.

Consider the singularity at the origin and write (18) in the first approximation as

$$\frac{dv}{dw}=\frac{A_1w+B_1v}{v}, \qquad . \quad . \quad . \quad . \quad . \quad (22)$$

where $A_1=(U_0+z_q)\,m_w-m_qz_w$

$B_1=(U_0+z_q)\,m_w+m_q+z_w$,

terms of w^2 and higher degree being neglected. Comparing with the standard form, equation (8), $a \equiv A_1$, $b \equiv B_1$, $c \equiv 0$ and $d \equiv 1$, and the roots of the characteristic equation are

$$\lambda_{1,2} = \tfrac{1}{2}\{B_1 \pm (B_1^2 + 4A_1)^{1/2}\}.$$

The different cases are:—

$B_1 < 0$, $A_1 \ll 0$ such that $B_1^2 + 4A_1 < 0$. The roots are complex conjugate and the singularity is a stable spiral point.

$B_1 < 0$, $A_1 < 0$ such that $B_1^2 + 4A_1 \geq 0$. Both roots are real and negative, corresponding to a stable node.

$B_1 < 0$, $A_1 > 0$. The roots are of opposite sign, giving rise to a saddle point.

From the definition of A_1 and B_1, it can be seen that the sign of A_1 is largely determined by that of m_w and that of B_1 by the sign of z_w. In normal circumstances z_w will be negative and so will B_1. As a first approximation m_w will be proportional to the centre of gravity margin and thus A_1 may be interpreted as a static stability parameter. $A_1 \ll 0$ implies a large amount of static stability which, when combined with $B_1 \ll 0$, the latter condition implying positive damping in the linear case, gives a damped oscillation. Increasing A_1 corresponds with decreasing the static stability, $A_1 = 0$ being the boundary between a stable node and saddle.

The equation of free motion for the linear case is obtained from (15) by neglecting second and higher powers of w and the terms in η, giving

$$\ddot{w} - B_1\dot{w} - A_1 w = 0. \quad . \quad . \quad . \quad . \quad . \quad (23)$$

For stability of the linear equation both B_1 and A_1 must be negative, which is the same criterion as that for a stable singularity at the origin in the case of the non-linear equation.

The singularities away from the origin may have their co-ordinates written as $w = w_s$, $v = 0$ and, referred to these co-ordinates as origin, w may be written

$$w = w_s + \xi. \quad . \quad . \quad . \quad . \quad . \quad . \quad (24)$$

Equation (18) now becomes

$$\frac{dv}{d\xi} = \frac{f_2(w_s + \xi) + f_1(w_s + \xi)\, v}{v} \quad . \quad . \quad . \quad . \quad (25)$$

which, upon substitution for f_1 and f_2, gives

$$\frac{dv}{d\xi} = \frac{A_1(w_s + \xi) + A_3(w_s + \xi)^3 + [B_1 + B_3(w_s + \xi)^2]\, v}{v},$$

where $A_3 = (U_0 + z_q)\, m_3 - m_q z_3$ and $B_3 = 3z_3$.

Expanding,

$$\frac{dv}{d\xi} = \frac{[A_1 w_s + A_1\xi + A_3 w_s^3 + 3A_3 w_s^3\xi + \ldots] + [B_1 + B_3 (w_s + \xi)^2]\, v}{v}.$$

Now $A_1 w_s + A_3 w_s^3 = f_2(w_s) = 0,$

and therefore in the first approximation

$$\frac{dv}{d\xi} = \frac{(A_1 + 3A_3 w_s^2)\,\xi + (B_1 + B_3 w_s^2)\, v}{v}$$

$$\text{or} \quad \frac{dv}{d\xi} = \frac{G\xi + Hv}{v}, \qquad \ldots\ldots\ldots \quad (26)$$

$$\text{where} \quad G = A_1 + 3A_3 w_s^2 = A_1 + 3A_3\left(-\frac{A_1}{A_3}\right) = -2A_1$$

$$\text{and} \quad H = B_1 + B_3 w_s^2 = B_1 - B_3\left(\frac{A_1}{A_3}\right) = B_1\left[1 - \frac{B_3}{B_1}\frac{A_1}{A_3}\right].$$

In order to produce this singularity, A_1 and A_3 must be of opposite sign. Comparison with the standard form, equation (8), in which x is replaced by ξ, gives $a \equiv G$, $b \equiv H$, $c \equiv 0$ and $d \equiv 1$ and the roots of the characteristic equation are

$$\lambda_{1,2} = \tfrac{1}{2}\{H \pm (H^2 + 4G)^{1/2}\}$$

The different cases are:—

$H < 0$, $A_1 < 0$, $A_3 > 0$. Here G is positive and the singularity is a saddle point.

$H < 0$, $A_1 > 0$, $A_3 < 0$. Now G is negative. When $H^2 + 4G < 0$ the singularity is a stable spiral point. When $H^2 + 4G \geqslant 0$ the singularity is a stable node.

The damping of the motion near the origin is dependent on B_1, which in normal circumstances is negative, whereas in the present case H can change sign. Since A_1/A_3 is always negative if the singularity is to exist, then B_3 must be positive if H is to change sign.

Two further cases emerge:—

$H > 0$, $A_1 < 0$, $A_3 > 0$. Here G is positive and the singularity is a saddle point.

$H > 0$, $A_1 > 0$, $A_3 < 0$. G is negative. When $H^2 + 4G < 0$ the roots of the characteristic equation are complex with positive real parts and correspond to an unstable spiral in the phase plane. When $H^2 + 4G > 0$ the roots are real and of different sign and correspond to a saddle point.

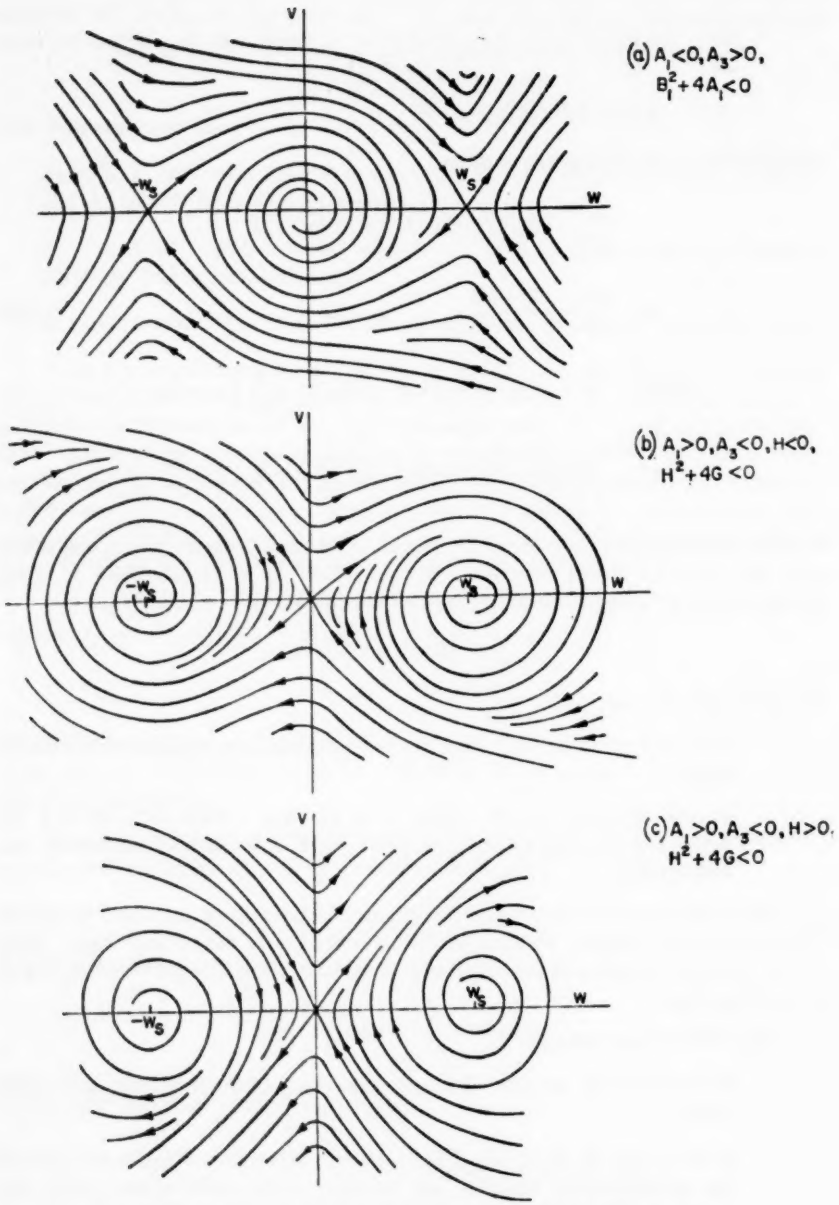

FIGURE 3. Integral curves in the region of the singularities, $B_1 < 0$.

It is now appropriate to plot the integral curves in the phase plane. In the cases where A_1 and A_3 are of the same sign, then the singularity occurs only at the origin and the non-linear terms do not change its character. When A_1 and A_3 are of different sign, then two additional symmetrically disposed singularities arise whose natures depend on the signs of H, A_1, A_3 and the discriminant H^2+4G. The three interesting cases are those where the singularities away from the origin differ from those at the origin and are sketched in Fig. 3.

The curves of Fig. 3(*a*) correspond to an $M(w)$ curve such as c in Fig. 2, and imply that for initial values of w between $\pm w_s$ the airframe will perform a damped oscillation. When z_w, and hence B_1, is large, then $B_1^2+4A_1>0$ and the motion near the origin degenerates into a subsidence. In the quasi-linear approximation m_w will change sign at the minimum in the $M(w)$ curve, and (17) will become unstable when $df_2(w)/dw$ changes sign.

Differentiation gives

$$\frac{df_2(w)}{dw} = (U_0+z_q)\,m_w - m_q z_w + 3\,\{(U_0+z_q)\,m_3 - m_q z_3\}\,w^2,$$

which changes sign when

$$w = \pm\left\{\frac{-(U_0+z_q)\,m_w + m_q z_w}{3\,(U_0+z_q)\,m_3 - m_q z_3}\right\}^{1/2} = w_m. \qquad . \quad . \quad (27)$$

Since the dominant terms in (21) and (27) are those containing m_w and m_3, then it follows that the range of w over which damped oscillations will result from an initial disturbance is greater by a factor of approximately $\sqrt{3}$ than that predicted by the quasi-linear approximation. Any changes of sign of H due to the influence of $B_3=3z_3$ have no influence on the nature of the singularities at $\pm w_s$.

The curves in Figs. 3(*b*) and 3(*c*) correspond with an $M(w)$ curve such as b in Fig. 2. When $H<0$, which it normally will be unless B_3 is large and positive, such that $H^2+4G<0$, then any initial disturbance will cause the airframe to perform damped oscillations about $\pm w_s$. From the quasi-linear theory $df_2(w)/dw$ changes sign at a value of w given by (27) and stability is indicated for larger values of w, provided that B_3 is negative. If B_3 is positive this implies that $f_1(w)$ will also change sign (this corresponds to the stalling of the airframe), which occurs when $f_1(w)=0$ or

$$w = \pm\left\{\frac{(U_0+z_q)\,m_{\dot{w}} + m_q + z_w}{-3z_3}\right\}^{1/2} = w_s \qquad . \quad . \quad (28)$$

If the value of w given by (27) is smaller than that given by (28), there will exist a region between these values for which stability is predicted by quasi-linear theory, whereas if the converse is true no stable region exists. The non-linear theory indicates that if B_3 is such that $H<0$, then the motion will always be stable in the sense that it performs a damped oscillation about $\pm w_s$, whereas the quasi-linear

theory indicates stability about any value of w greater than that given by (27). If B_3 is large and positive such that $H > 0$, then non-linear theory indicates instability for all values of w, while quasi-linear theory indicates a stable region for values of w lying between w_m and w_z, provided that $w_m < w_z$.

6. Conclusions

The important conclusions which may be drawn from this analysis are as follows.

(1) The method is only suitable for a partial determination of the stability of the short-period motion of an airframe with the elevators undeflected. It is partial in the sense that it can only consider the influence of the non-linearities on the equation governing the vertical velocity w (or incidence) and not that involving the angular rate of pitch. In the non-linear problem these two equations differ in form, whereas in the comparable linear problem they do not.

(2) Comparisons with quasi-linear theory (*i.e.* linear theory based on the local slope of the $Z(w)$ and $M(w)$ curves) indicate the following:—

(*a*) The criteria for stability at low incidence is the same for both methods.

(*b*) With airframes having pitching moment curves such as *b* and *c* in Fig. 2, the stability criteria and motions predicted by the two methods differ considerably at moderate to high incidence. With curve *c*, quasi-linear theory predicts instability when w has values outside the range between the maximum and the minimum, whereas non-linear theory indicates a stable region which is greater by a factor of approximately $\sqrt{3}$. With curve *b* and a $Z(w)$ curve whose gradient does not decrease, quasi-linear theory predicts stability when w has values outside the range between the maximum and the minimum; whereas non-linear theory indicates that the only possible motion of the airframe is a damped oscillation about values of $w = w_s$ given by equation (21). With curve *b* and a $Z(w)$ curve having a decreasing slope, which includes the case of the stall, quasi-linear theory indicates a stable region for values of w between those corresponding to zero stiffness w_m and zero damping w_z; non-linear theory indicates instability for all values of incidence.

References

1. Duncan, W. J. *The Principles of the Control and Stability of Aircraft.* Chapter III. Cambridge University Press, 1952.
2. Trilling, L. and Covert, E. E. Quasi-Steady Pitching Oscillations in Transonic Flight. *Journal of the Aeronautical Sciences,* September 1955.
3. Stoker, J. J. *Nonlinear Vibrations in Mechanical and Electrical Systems.* Chapters 2 and 3. Interscience Publishers, New York, 1950.
4. Bieberbach, L. *Theorie Der Differentialgleichungen.* Chapter 4, pp. 74-78. Dover Publications, New York, 1944.
5. Spearman, F. R. J. The Derivation and Use of Aerodynamic Transfer Functions of Airframes. *Journal of the Royal Aeronautical Society,* November 1955.

Design Charts for Transient Temperature and Thermal Stress Distributions in Thermally Thick Plates

J. S. PRZEMIENIECKI, Ph.D., A.F.I.A.S., A.F.R.Ae.S.

(*Bristol Aircraft Limited*)

SUMMARY: A set of design charts is presented for the calculation of transient temperature and thermal stress distributions in thermally thick plates subjected to aerodynamic heating.

The method is particularly useful for determining temperatures and thermal stresses in plates with an arbitrary variation of the heat transfer coefficient and the adiabatic wall temperature of the boundary layer. The present method is based on repetitive applications of the exact analytical solution to a unit triangular variation of the adiabatic wall temperature and a constant heat transfer coefficient. The actual variation of the adiabatic wall temperature is represented as a series of straight lines while the heat transfer coefficient is approximated by a step function. The temperature distribution through the plate is separated into linear and "self-equilibrating" temperature distributions to facilitate thermal stress calculations; these distributions can be obtained directly from the design charts presented in this paper.

The general principle of this semi-numerical method is also applied to thermally thin plates subjected to arbitrary heating conditions.

1. Introduction

In heat transfer calculations for plates subjected to aerodynamic heating or cooling it is often necessary to consider temperature gradients through the thickness of the plate. Whether these gradients are important depends on the magnitude of the heat transfer coefficient h at the exposed surface, the plate thickness d, and the thermal conductivity k. These three variables can be combined into a single non-dimensional parameter usually described as the Biot number $B=hd/k$. It will be assumed here that for $B>0{\cdot}1$ the heated (or cooled) plate can be defined as "thermally thick", which is a plate in which temperature gradients through the thickness are not negligible, while for $B<0{\cdot}1$ the plate can be defined as " thermally thin", in which temperature gradients are negligible. It should, however, be emphasised that this division is somewhat arbitrary and it is only introduced to facilitate practical calculations.

Received May 1960.

The one-dimensional heat flow by conduction in a medium whose thermal properties do not vary with temperature is governed by the partial differential equation

$$\frac{\partial^2 T}{\partial x^2} = \frac{1}{\kappa} \frac{\partial T}{\partial t} \quad . \quad . \quad . \quad . \quad . \quad . \quad (1)$$

where T is the temperature, x is the distance, κ is the thermal diffusivity and t is the time. In problems involving aerodynamic heating of plates the boundary conditions are usually taken as

$$k \frac{\partial T}{\partial x} = h(t)\,[T_{w_0}(t) - T]; \quad x = d. \quad . \quad . \quad . \quad . \quad (2)$$

and

$$\frac{\partial T}{\partial x} = 0; \quad x = 0, \quad . \quad . \quad . \quad . \quad . \quad . \quad . \quad (3)$$

where k is the thermal conductivity, $h(t)$ is the heat transfer coefficient and T_{w_0} is the adiabatic wall temperature. In the first boundary condition the rate of heat absorption by the material at the heated surface at $x = d$ is equated to the rate of heat input by forced convection (aerodynamic heating), while the second condition assumes that the surface at $x = 0$ is insulated (zero heat transfer).

The heat transfer coefficient h is usually evaluated as a function of time, depending on the variation of aerodynamic conditions just outside the boundary layer. For more accurate calculations, however, the variation of h with the surface temperature should also be included, particularly in heat transfer calculations for turbulent flow[1].

The arbitrary variation of $h(t)$ and $T_{w_0}(t)$ in practical design problems rules out any possibility of a successful analytical solution for the temperature distribution; only solutions to relatively simple cases can be obtained. Solutions to the problems with a constant heat transfer coefficient and a suddenly applied temperature T_{w_0} are known and furthermore the case of arbitrary variation of T_{w_0} can be solved using Duhamel's integral. Kaye and Yeh[2] obtained a solution for the temperature distribution assuming that the heat flux through one surface varies as a quadratic function of time. Chen[3] represented the heat transfer coefficient and the adiabatic wall temperature by constants and exponential functions and solved the differential equation by means of the Laplace transformation method.

Several objections may be made to the use of the analytical methods such as those given in Refs. 2 and 3. Firstly, solutions may not be sufficiently realistic, due to the various simplifications which are necessary to get any solution at all; secondly, the analytical expressions are usually extremely complicated for practical applications; and thirdly, the analytical solutions usually converge poorly near $t = 0$ unless special asymptotic solutions are employed for small values of time.

The numerical methods are based essentially on step-by-step integration of the heat conduction equation. These methods have the additional advantage over

analytical methods that the variation of thermal properties of the material with temperature and the temperature dependence of the heat transfer coefficients can be included. Similarly any radiation losses and other non-linear effects, *e.g.* free convection, can be included in the solution. Numerical methods applied to heat transfer problems are, in general, time-consuming and require relatively small intervals of time. On the other hand, they can be programmed for automatic computation and several such programmes for digital computers are already in existence.

The semi-numerical method described in this paper is based on repetitive application of the exact analytical solution to the response to a triangular variation of T_{w0} over a relatively large time interval. This is possible because of the linear character of equations (1), (2) and (3). The heat transfer coefficient h is assumed here to be constant in any given time interval, while the variation of T_{w0} is represented by a series of straight lines. A similar approach has been used in Ref. 4, where the adiabatic wall temperature T_{w0} was also represented by a finite series of unit triangles. The main advantage of this method is that the computing time is appreciably reduced, compared with standard numerical methods, if special charts are available for the temperature distribution due to linear variation of T_{w0}. Such charts are presented in this paper and they can be used for calculating either the temperature or the thermal stress distributions.

To facilitate calculations involving thermal stresses, the temperature distribution through the thickness of a plate is separated into linear and "self-equilibrating" temperature distributions[1]; the linear distribution contributes to the overall deformation, either curvature or expansion in the plane of the plate, while the self-equilibrating distribution produces zero overall deformations.

Notation

$T(x, t), T(z, t)$ temperature distribution

$T(n, N)$ temperature distribution (in non-dimensional distance and time)

T_{w0} adiabatic wall temperature

T_τ adiabatic wall temperature at time N_τ

$T_m(t), T_m(N)$ mean temperature

$\Delta T(t), \Delta T(N)$ temperature gradient

$T^\star(z,t), T^\star(n,N)$ self-equilibrating temperature distribution

x distance measured from the insulated surface

$z = x - d/2$, distance measured from the middle surface

$n = x/d$, non-dimensional distance

d plate thickness

t time

$\kappa = k/(\rho c)$, thermal diffusivity

k thermal conductivity

h heat transfer coefficient

$N=\kappa t/d^2$, non-dimensional time

δ non-dimensional time interval

$N_r=r\delta$

r, j integers

$B=hd/k$, Biot number

$\Phi=ad^2/\kappa$

a rate of increase of T_{w_0}, defined by equation (11)

E Young's modulus

α coefficient of thermal expansion

ν Poisson's ratio

σ thermal stress

ρ density

c specific heat

w_j j^{th} positive root of $w_j \tan w_j = B$

$F(N_r, B_r)$ temperature functions for $B=B_r$ and $N=N_r$

B_r Biot number at N_r

$R(N_r)$ temperature response at N_r

$\overline{T}=\int_0^\infty T e^{-pN}\,dN$, transformed temperature (Laplace transform)

p function in the Laplace transform

$\exp(\ )$ exponential function

$\operatorname{erfc}(\ )$ complementary error function

$i^r \operatorname{erfc}(\ )$ r^{th} repeated integral of the complementary error function

$i^r \operatorname{erfc}(0)=2^{-r}/\Gamma(1+r/2)$

$\Gamma(\ )$ gamma function

2. Temperature Distribution, Self-Equilibrating Temperature

The solution of equation (1) can be separated into linear and self-equilibrating temperature distributions[1], *i.e.*

$$T(z,t)=T_m(t)+\Delta T(t)\frac{z}{d}+T^{\star}(z,t), \quad . \quad . \quad . \quad (4)$$

where $$z=x-d/2 \quad . \quad . \quad . \quad . \quad . \quad . \quad . \quad . \quad (5)$$

is the distance measured from the middle surface towards the heated surface at $x=d$,

$T_m(t)$ is the mean temperature, $\Delta T(t)$ is the linear temperature gradient and $T^\star(z, t)$ is the self-equilibrating temperature distribution, for which

$$\int_{-d/2}^{d/2} T^\star \, dz = \int_{-d/2}^{d/2} T^\star z \, dz = 0. \quad . \quad . \quad . \quad . \quad . \quad (6)$$

Thus only the first two terms on the right hand side of equation (4) contribute to the overall deformation of the plate. T_m and ΔT terms produce thermal stresses in the presence of edge restraints. On the other hand, stresses due to $T^\star$ occur even if all edges are completely free.

Using equations (4) and (6), it follows that

$$T_m = \frac{1}{d}\int_{-d/2}^{d/2} T \, dz \quad . \quad . \quad . \quad . \quad . \quad (7)$$

and

$$\Delta T = \frac{12}{d^2}\int_{-d/2}^{d/2} Tz \, dz. \quad . \quad . \quad . \quad . \quad . \quad (8)$$

Alternatively, ΔT could be obtained by equating the first moment of the temperature $T(z, t)$ to the first moment of the $\Delta T(t)\, z/d$ distribution about the middle plane.

For a plate with all edges free, the thermal stress distribution through the thickness of the plate, away from the edges, is given by

$$\sigma = \frac{\alpha E}{(1-\nu)}\left\{-T + \frac{1}{d}\int_{-d/2}^{d/2} T \, dz + \frac{12}{d^2}\frac{z}{d}\int_{-d/2}^{d/2} Tz \, dz\right\}. \quad . \quad . \quad (9)$$

Obviously, the stresses given by equation (9) fall to zero in a narrow "boundary layer" along the edges.

Now, using equations (4), (7) and (8), it follows that the thermal stresses given by equation (9) are proportional to the self-equilibrating temperature distribution $T^\star$, *i.e.*

$$\sigma = -\alpha E T^\star/(1-\nu). \quad . \quad . \quad . \quad . \quad . \quad (10)$$

The mean temperature T_m induces thermal stresses only if one or more edges are restrained against expansion in the plane of the plate. In such cases compressive or tensile stresses are induced if the plate is respectively heated or cooled more rapidly than its surrounding structure. The effect of the temperature gradient ΔT is to produce a uniform curvature in the plate and therefore, in the absence of any edge restraints, the plate bends into a spherical surface. Because of the restraint along the edges, which prevents the edges from leaving the plane of the supports, the temperature gradient ΔT produces certain reactions along the boundaries and bending stresses in the plate. Ref. 1 gives a full discussion of thermal stresses due to temperature components T_m, ΔT and $T^\star$.

3. Linearly Varying Adiabatic Wall Temperature T_{w0}

If the adiabatic wall temperature varies linearly with time and the initial temperature is assumed to be zero, then

$$T_{w0} = at, \quad . \quad . \quad . \quad . \quad . \quad . \quad (11)$$

where a is the rate of temperature increase. The assumption $T_{w0}=0$ at $t=0$ does not affect the results because it is always possible to measure T_{w0}, and hence the temperature distribution in the plate, from some initial equilibrium temperature. It is shown in Appendix I that, for a constant heat transfer coefficient h and a linearly varying T_{w0}, the temperature distribution is given by

$$\frac{T(n,N)}{\Phi} = N + \tfrac{1}{2}(n^2 - 1 - 2B^{-1}) + 2\sum_j \frac{\sin w_j \cos w_j n}{w_j^2 (w_j + \sin w_j \cos w_j)} \exp(-w_j^2 N) \quad . \quad (12)$$

where the w_j are the positive roots of the transcendental equation

$$w_j \tan w_j = B. \quad . \quad . \quad . \quad . \quad . \quad (13)$$

The parameters Φ, n, N and B used in equation (12) are defined as follows:—

$$\Phi = ad^2/\kappa \quad . \quad . \quad . \quad . \quad (14)$$

$$n = x/d \text{ (non-dimensional distance)} \quad . \quad . \quad . \quad . \quad (15)$$

$$N = \kappa t/d^2 \text{ (non-dimensional time)} \quad . \quad . \quad . \quad . \quad (16)$$

$$B = hd/k \text{ (Biot number)} \quad . \quad . \quad . \quad . \quad (17)$$

Using now equations (4), (7), (8) and (12), it is found that

$$\frac{T_m(N)}{\Phi} = N - \tfrac{1}{3} - B^{-1} + 2\sum_j \frac{\sin^2 w_j}{w_j^3 (w_j + \sin w_j \cos w_j)} \exp(-w_j^2 N) \quad . \quad . \quad . \quad (18)$$

$$\frac{\Delta T(N)}{\Phi} = \tfrac{1}{2} - 24\sum_j \frac{1}{w_j^2} \frac{\sin w_j}{(w_j + \sin w_j \cos w_j)} \left(\frac{1-\cos w_j}{w_j^2} - \frac{\sin w_j}{2w_j}\right) \exp(-w_j^2 N) \quad (19)$$

$$\frac{T^\star(n,N)}{\Phi} = \frac{1}{12}(6n^2 - 6n + 1) - 2\sum_j \frac{\sin w_j}{w_j^2 (w_j + \sin w_j \cos w_j)} \left[\frac{\sin w_j}{w_j} - \cos w_j n - \right.$$

$$\left. - 12\left(n - \tfrac{1}{2}\right)\left(\frac{1-\cos w_j}{w_j^2} - \frac{\sin w_j}{2w_j}\right)\right] \exp(-w_j^2 N). \quad (20)$$

In general, the complete temperature distribution through the thickness of the plate is not required and for design purposes only the following quantities are of practical interest: surface temperatures $T(0,N)$ and $T(1,N)$, mean temperature $T_m(N)$, temperature gradient $\Delta T(N)$ and the self-equilibrating temperatures $T^\star(0,N)$ and $T^\star(1,N)$. These component temperatures have been plotted in

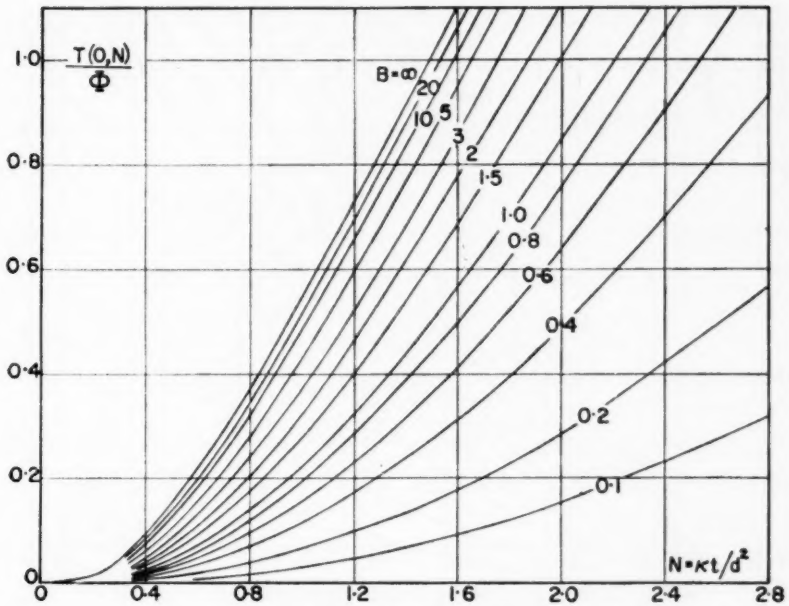

FIGURE 1. Surface temperature at $n=0$ (insulated surface).

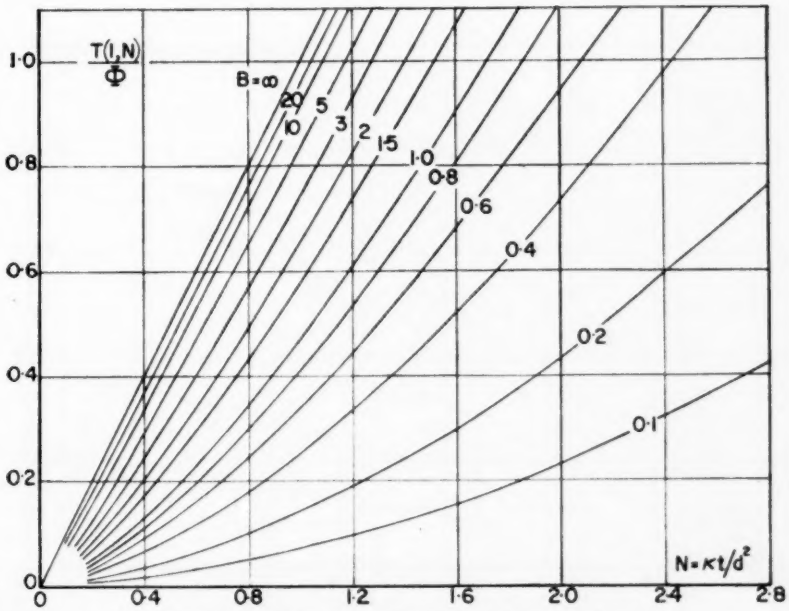

FIGURE 2. Surface temperature at $n=1$ (heated surface).

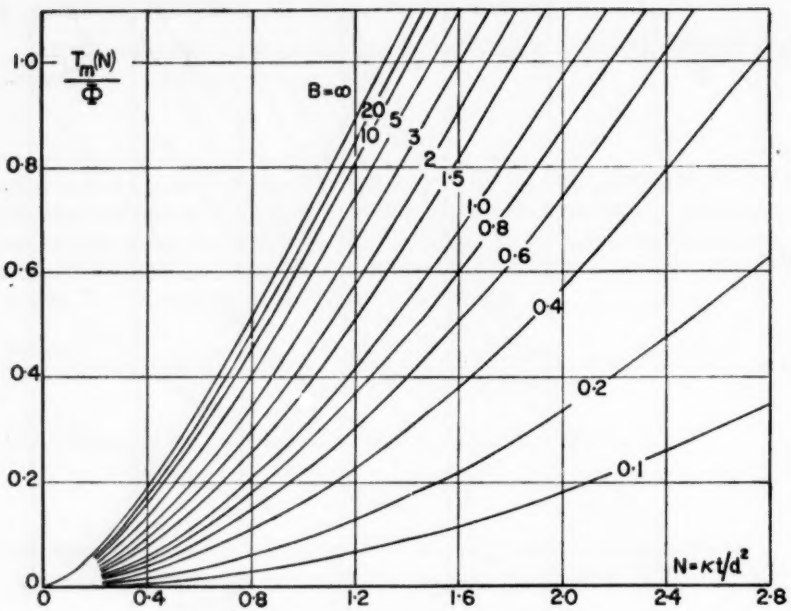

FIGURE 3. Mean temperature T_m (N).

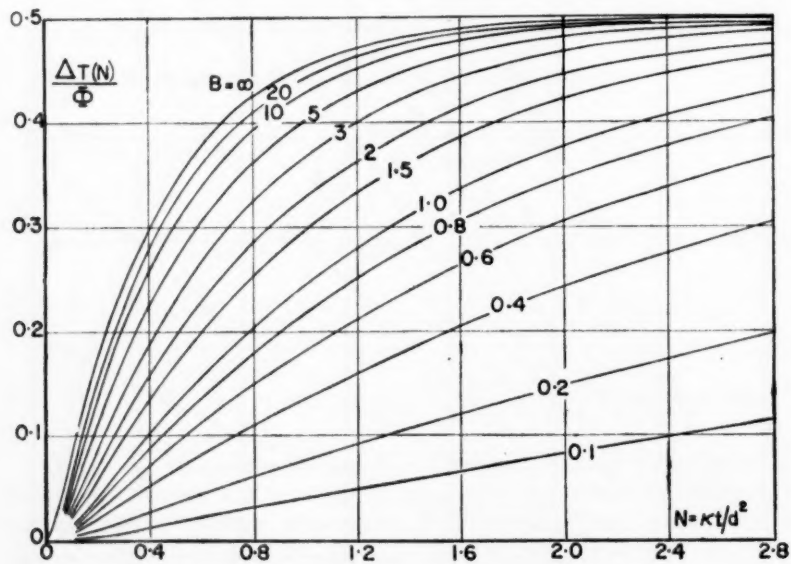

FIGURE 4. Temperature gradient ΔT (N).

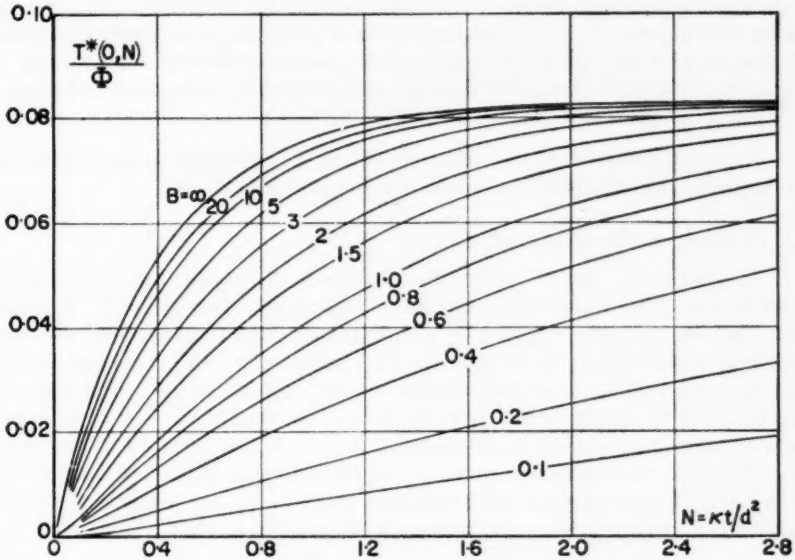

FIGURE 5. Self-equilibrating temperature at $n=0$ (insulated surface).

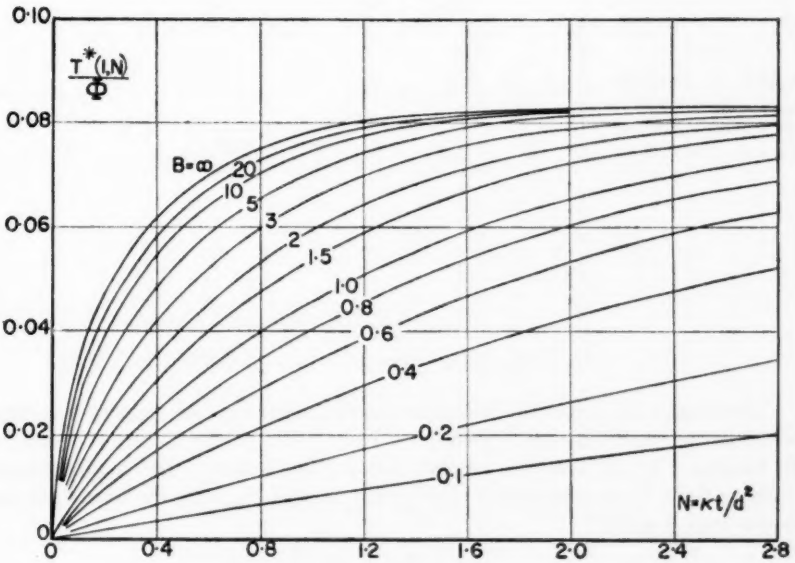

FIGURE 6. Self-equilibrating temperature at $n=1$ (heated surface).

Figs. 1 to 6 as functions of the non-dimensional time $N=\kappa t/d^2$ for a range of values of the Biot number $B=hd/k$. In general, for $B<0{\cdot}1$ the plate can be regarded as thermally thin, for which any temperature gradients through the thickness are negligible. For such cases, only the mean temperature T_m is required and it can be calculated by means of equation (26) given in Section 5.

For small values of the non-dimensional time N, asymptotic expressions derived in Appendix II can be used for various temperature components.

4. Arbitrary Variation of T_{w_0}

In practice T_{w_0} can be represented by a series of straight lines constructed by contributions from elementary triangular variations, as shown in Fig. 7. It is easily seen that the triangular variation is obtained from three separate linear variations starting at times N equal to N_{r-1}, N_r and N_{r+1} respectively. This triangular variation may be regarded also as a "temperature impulse" applied to the heated surface of the plate. The magnitude of T_{w_0} at the time N_r is denoted by T_r and the average heat transfer coefficient in the time interval N_{r-1} to N_{r+1} is assumed to be given by h_r. Thus the corresponding value of the Biot number can be calculated from $B_r=h_rd/k$. For simplicity it will be assumed that $N_r-N_{r-1}=\delta$ (constant), or $N_r=r\delta$; but it should be emphasised that unequal intervals of time could also be used.

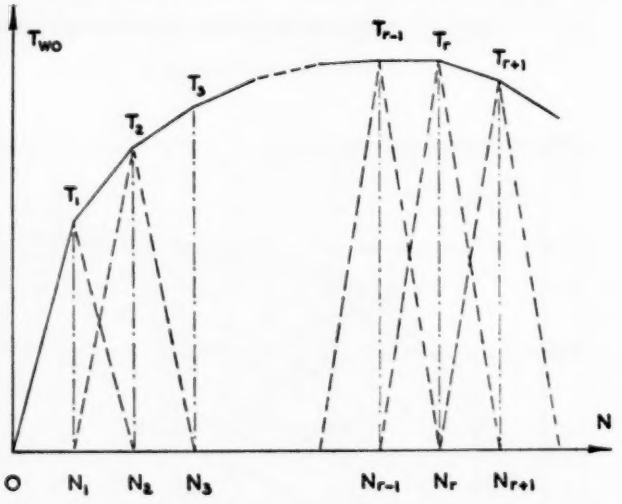

FIGURE 7. Straight line approximation for T_{w_0} by a series of triangular variations.

Assuming that any of the non-dimensional temperature parameters represented on the design charts in Figs. 1 to 6, *i.e.* $T(0, N)/\Phi$, $T(1, N)/\Phi$, etc., is denoted by the function $F(N, B)$, which is a known function of N and B, then the temperature response $R(N)$ to the application of a linearly varying T_{w_0} after the time N_1 is given by (*see* Figs. 7 and 8)

$$R(N_1)=\frac{T_1}{\delta}F(N_1, B_1). \quad . \quad . \quad . \quad . \quad . \quad (21)$$

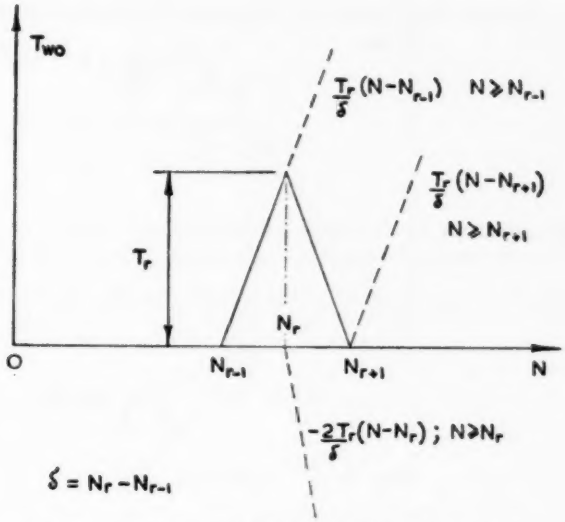

FIGURE 8. Triangular variation of adiabatic wall temperature.

After the time N_2 has elapsed

$$R(N_2) = \frac{T_1}{\delta} F(N_2, B_1) - \frac{2T_1}{\delta} F(N_1, B_1) + \frac{T_2}{\delta} F(N_1, B_2). \quad . \quad . \quad (22)$$

while for N_3

$$R(N_3) = \frac{T_1}{\delta} F(N_3, B_1) - \frac{2T_1}{\delta} F(N_2, B_1) + \frac{T_1}{\delta} F(N_1, B_1) + \frac{T_2}{\delta} F(N_2, B_2) -$$

$$- \frac{2T_2}{\delta} F(N_1, B_2) + \frac{T_3}{\delta} F(N_1, B_3). \quad . \quad (23)$$

For the time N_r the general formula becomes

$$\begin{aligned}
\delta R(N_r) = {} & T_1 [F(N_r, B_1) - 2F(N_{r-1}, B_1) + F(N_{r-2}, B_1)] + \\
& + T_2 [F(N_{r-1}, B_2) - 2F(N_{r-2}, B_2) + F(N_{r-3}, B_2)] + \\
& + T_3 [F(N_{r-2}, B_3) - 2F(N_{r-3}, B_3) + F(N_{r-4}, B_3)] + \\
& + . \quad . \quad . \quad . \quad . \quad . \quad . \quad . \quad . \quad . \quad . \quad . \quad . \quad . \quad . \quad . \quad . \quad . \quad + \\
& + T_{r-2} [F(N_3, B_{r-2}) - 2F(N_2, B_{r-2}) + F(N_1, B_{r-2})] + \\
& + T_{r-1} [F(N_2, B_{r-1}) - 2F(N_1, B_{r-1})] + \\
& + T_r [F(N_1, B_r)]. \quad . \quad . \quad . \quad . \quad (24)
\end{aligned}$$

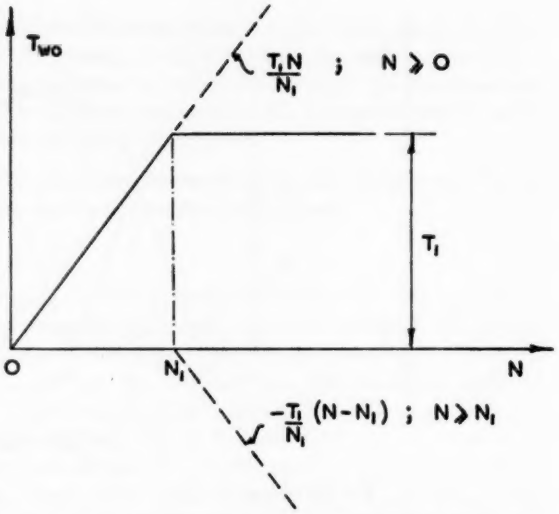

FIGURE 9. Step variation of adiabatic wall temperature.

Equation (24) can be arranged in a tabular form and any required temperature components can then be computed rapidly with the aid of the design charts shown in Figs. 1–6. The method is sufficiently accurate for engineering purposes, even if large time intervals are used.

It should be emphasised that $T_1, T_2, \ldots T_r$ can be either positive or negative, depending on whether the case considered represents acceleration or deceleration.

If the adiabatic wall temperature T_{w_0} increases linearly from $T_{w_0}=0$ to T_1 in time N_1, thereafter remaining constant, then this variation can be represented as a difference of two linear variations, as shown in Fig. 9. If, in addition, the Biot number B does not vary with time, then the response function can be simply expressed as

$$R(N)=\frac{T_1}{N_1}F(N,B); \quad N \leqslant N_1 \qquad . \quad . \quad . \quad . \quad (25a)$$

and $$R(N)=\frac{T_1}{N_1}[F(N,B)-F(N-N_1,B)]; \quad N \geqslant N_1. \qquad . \quad . \quad . \quad . \quad (25b)$$

5. Thermally Thin Plates

It is usually assumed that for $B < 0{\cdot}1$ plates can be regarded as thermally thin and any temperature gradients across the thickness are negligible. It can be shown that for linearly varying adiabatic wall temperature $T_{w_0}=at$, the mean temperature T_m of a thermally thin plate is given by

$$\frac{T_m(N)}{\Phi}=N-B^{-1}[1-\exp(-BN)]. \qquad . \quad . \quad . \quad (26)$$

For large values of N equation (26) reduces to a straight line variation

$$\frac{T_m(N)}{\Phi} = N - B^{-1} \quad . \quad . \quad . \quad . \quad . \quad (27)$$

$$\text{or} \qquad T_m = T_{w_0} - \frac{a\rho cd}{h} \quad . \quad . \quad . \quad . \quad . \quad . \quad (27a)$$

where $a\rho cd/h$ represents the temperature difference between the adiabatic wall temperature and the mean temperature in the steady state.

The mean temperature in a thick plate for large values of N can be obtained from equation (18).

$$\text{Hence} \quad \frac{T_m(N)}{\Phi} = N - \tfrac{1}{3} - B^{-1} \quad . \quad . \quad . \quad (28)$$

$$\text{or} \qquad T_m = T_{w_0} - \frac{a\rho cd}{h}(1 + \tfrac{1}{3}B). \quad . \quad . \quad . \quad . \quad (28a)$$

It is therefore clear that equation (26) overestimates the mean temperature, if used for thick plates. Equations (27*a*) and (28*a*) become identical only for $B = 0$.

Equations (26) can be used for calculating the mean temperature due to a triangular variation of T_{w_0} and hence the semi-numerical method described in previous sections is also applicable to thin plates.

ACKNOWLEDGMENT

The author wishes to acknowledge the permission of Bristol Aircraft Limited to publish this paper.

Appendix I

SOLUTION OF THE DIFFERENTIAL EQUATION OF HEAT FLOW

The basic equation (1), together with the boundary conditions (2) and (3) and linear variation of the adiabatic wall temperature, can be expressed in non-dimensional form as

$$\frac{\partial^2 (T/\Phi)}{\partial n^2} = \frac{\partial (T/\Phi)}{\partial N} \quad . \quad . \quad . \quad . \quad . \quad (29)$$

$$\frac{\partial (T/\Phi)}{\partial n} = B\,[N - (T/\Phi)] \;; \quad n = 1 \quad . \quad . \quad (30)$$

$$\frac{\partial (T/\Phi)}{\partial n} = 0; \quad n = 0 \quad . \quad . \quad . \quad (31)$$

$$\text{and} \qquad T/\Phi=0 \quad \text{at} \quad N=0, \qquad . \quad . \quad . \quad . \quad (32)$$

where the last equation implies zero temperature at $N=0$. In practical applications, however, the initial temperature at $N=0$ is constant and therefore the temperature distribution $T(n, N)$ represents temperature increase above the initial temperature.

Introducing the single-tailed Laplace transform

$$\overline{T}=\int_0^\infty T\,e^{-pN}\,dN, \qquad . \quad . \quad . \quad . \quad . \quad (33)$$

equations (29), (30) and (31) can be transformed into

$$\frac{d^2(\overline{T}/\Phi)}{dn^2}=pN \qquad . \quad . \quad . \quad . \quad . \quad . \quad (34)$$

$$\frac{d(\overline{T}/\Phi)}{dn}=B\left[\frac{1}{p^2}-(\overline{T}/\Phi)\right]; \quad n=1 \qquad . \quad . \quad . \quad (35)$$

$$\text{and} \qquad \frac{d(\overline{T}/\Phi)}{dn}=0 \; ; \; n=0, \qquad . \quad . \quad . \quad . \quad . \quad . \quad (36)$$

where equation (32) has been used in deriving equation (34). The solution of equation (34) with the boundary conditions (35) and (36) is given by

$$(\overline{T}/\Phi)=\frac{\cosh p^{1/2}n}{p^2\left[(p^{1/2}/B)\sinh p^{1/2}+\cosh p^{1/2}\right]} \qquad . \quad . \quad (37)$$

Applying now the inversion theorem to equation (37) it can be shown that

$$\frac{T(n, N)}{\Phi}=N+\tfrac{1}{2}(n^2-1-2B^{-1})+2\sum_j \frac{\sin w_j \cos w_j n}{w_j^2\,(w_j+\sin w_j \cos w_j)}\exp(-w_j^2 N), \qquad . \quad (12)$$

where the w_j are the positive roots of the transcendental equation

$$w_j \tan w_j = B. \qquad . \quad . \quad . \quad . \quad . \quad (13)$$

The first six roots w_j of equation (13) are given in Ref. 5 for a range of values of the Biot number B.

Appendix II

Solution for Small Values of Non-Dimensional Time

For small values of the non-dimensional time N, the parameter p in equation (37) must be large[6] and hence $\sinh p^{1/2} \simeq \cosh p^{1/2} \simeq \tfrac{1}{2}\exp p^{1/2}$. The values of $\overline{T}/\Phi$ at $n=0$ and 1 from equations (37) can therefore be approximated by the following equations.

$$\frac{\overline{T}}{\Phi} \simeq \frac{2\exp(-p^{1/2})}{p^2(1+p^{1/2}B^{-1})}\ ;\quad n=0 \qquad (38)$$

and

$$\frac{\overline{T}}{\Phi} \simeq \frac{1}{p^2(1+p^{1/2}B^{-1})}\ ;\quad n=1. \qquad (39)$$

In view of the invariance properties of the Laplace transform with respect to the second variable (distance), equations (7) and (8) can be used for calculating the transformed mean temperature $\overline{T}_m$ and temperature gradient $\Delta\overline{T}$. Thus, substituting equation (37) into (7) and (8), it follows that

$$\frac{\overline{T}_m}{\Phi} = \frac{1}{p^{5/2}(1+p^{1/2}B^{-1})} \qquad (40)$$

and

$$\frac{\Delta\overline{T}}{\Phi} = \frac{6}{p^{5/2}(1+p^{1/2}B^{-1})} - \frac{12}{p^3(1+p^{1/2}B^{-1})} + \frac{24\exp(-p^{1/2})}{p^3(1+p^{1/2}B^{-1})} \qquad (41)$$

Using now the table of Laplace transforms from Ref. 5, it can be shown that

$$\frac{T(0,N)}{\Phi} = 2B^{-2}\left\{\sum_{r=0}^{r=2}(-1)^r B^r (4N)^{r/2}\, i^r\,\mathrm{erfc}\left(\frac{1}{2N^{1/2}}\right) - \right.$$

$$\left. -\exp(B+B^2N)\,\mathrm{erfc}\left(\frac{1}{2N^{1/2}}+BN^{1/2}\right)\right\}. \qquad (42)$$

$$\frac{T(1,N)}{\Phi} = B^{-2}\left\{\sum_{r=0}^{r=2}(-1)^r B^r (4N)^{r/2}\, i^r\,\mathrm{erfc}\,(0) - \exp(B^2N)\,\mathrm{erfc}\,(BN^{1/2})\right\} \qquad (43)$$

$$\frac{T_m(N)}{\Phi} = B^{-3}\left\{\sum_{r=0}^{r=3}(-1)^{r-1} B^r (4N)^{r/2}\, i^r\,\mathrm{erfc}\,(0) + \exp(B^2N)\,\mathrm{erfc}\,(BN^{1/2})\right\} \qquad (44)$$

$$\frac{\Delta T(N)}{\Phi} = 3BN^2 + 6(B^{-3}+2B^{-4})\left\{\sum_{r=0}^{r=4}(-1)^{r-1} B^r (4N)^{r/2}\, i^r\,\mathrm{erfc}\,(0) + \right.$$

$$\left. +\exp(B^2N)\,\mathrm{erfc}\,(BN^{1/2})\right\} + 24B^{-4}\left\{\sum_{r=0}^{r=4}(-1)^r B^r (4N)^{r/2}\, i^r\,\mathrm{erfc}\left(\frac{1}{2N^{1/2}}\right) - \right.$$

$$\left. -\exp(B+B^2N)\,\mathrm{erfc}\left(\frac{1}{2N^{1/2}}+BN^{1/2}\right)\right\}, \qquad (45)$$

where $i^r\,\mathrm{erfc}\,(\ )$ is the r^{th} repeated integral of the complementary error function erfc ( ).

The self-equilibrating temperature components can be calculated now from equations (42) to (45) and equation (4). Hence

$$T\star(0,N)/\Phi = \{(T(0,N) - T_m(N) + \tfrac{1}{2}\Delta T(N))\}/\Phi \qquad (46)$$

and

$$T\star(1,N)/\Phi = \{(T(1,N) - T_m(N) - \tfrac{1}{2}\Delta T(N))\}/\Phi. \qquad (47)$$

No definite rule can be laid down for the maximum value of N up to which the approximate expressions can be used instead of the exact expressions given by equations (12) to (20). If the approximate expressions are used they should always be checked against the exact values for the maximum value of the non-dimensional time N likely to be used in the calculations.

REFERENCES

1. PRZEMIENIECKI, J. S. Design of Transparencies. *Journal of the Royal Aeronautical Society*, Vol. 63, pp. 620-636, November 1959.

2. KAYE, J. and YEH, V. C. M. Design Charts for Transient Temperature Distributions Resulting from Aerodynamic Heating at Supersonic Speeds. *Journal of the Aeronautical Sciences*, Vol. 22, pp. 755-762, 786, November 1955.

3. CHEN, S. Y. Transient Temperature and Thermal Stresses in Skin of Hypersonic Vehicle with Variable Boundary Conditions. *Trans. A.S.M.E.*, Vol. 80, No. 7, pp. 1389-1394, October 1958.

4. HILL, P. R. A Method of Computing the Transient Temperature of Thick Walls from Arbitrary Variation of Adiabatic Wall Temperature and Heat Transfer Coefficient, N.A.C.A. T.N. 4105, October 1957.

5. CARSLAW, H. S. and JAEGER, J. C. *Heat Conduction in Solids*. Oxford University Press. pp. 377 and 380-381, 1947.

6. HEISLER, M. P. Transient Thermal Stresses in Slabs and Circular Pressure Vessels. *Journal of Applied Mechanics*, Vol. 20, pp. 261-269, June 1953.

Further Comments on High-Lift Testing in Wind Tunnels with Particular Reference to Jet-Blowing Models*

S. F. J. BUTLER and J. WILLIAMS

(*Royal Aircraft Establishment, Farnborough*)

SUMMARY: This paper discusses some of the special problems of wind-tunnel testing which arise with high-lift jet-blowing models, supplementing earlier comments[1]. Further detailed remarks are made about recent developments on tunnel-wall interference, test rigs and methods of minimising constraints from air-feeds to models, and on general test and model design techniques.

1. Introduction

Some of the special problems encountered in wind-tunnel testing of high-lift models were discussed by Anscombe and Williams[1] nearly three years ago, largely in terms of early experience gained by the R.A.E. and N.P.L. low-speed tunnel staffs. Since then, further research and development have been carried out in connection with tests on models incorporating plane jets (boundary layer control or jet flaps) and round jets. In particular, the half-model techniques already described previously for three-component force measurements with jet-blowing have now been thoroughly proved[2, 3, 4] and widely used. Furthermore, at R.A.E., a special technique has been developed for six-component measurements on complete models with jet-blowing, and tunnel "lift-constraint" corrections have been derived theoretically[5] for three-dimensional wings with full-span jet flaps.

Further detailed comments are made on tunnel-wall interference with jet-blowing models, on test rigs and methods of minimising constraints from air-feeds to models, and on the measurement and evaluation of jet-blowing parameters. Earlier remarks on accuracy of manufacture requirements are supplemented by comments on blowing slot and duct design and on realistic representation of practical aircraft configurations.

NOTATION

a local velocity of sound

A wing aspect ratio

*Based on a paper prepared for the AGARD Wind-Tunnel Panel Meeting, Brussels, March 1959.

Received February 1960.

A_t area of slot throat or convergent nozzle exit

b breadth of tunnel, in spanwise direction

c wing chord

C cross-sectional area of tunnel working section

C_J jet-reaction coefficient
C_μ jet-momentum coefficient
} *see* Section 4.1

C_Q jet-flow coefficient

C_L lift coefficient

C_m pitching-moment coefficient

C_T thrust coefficient

d_j diameter of round-jet exit

D diameter of circular wing

h height of tunnel working section, normal to wing

h_f height of jet exit above tunnel floor

J static jet thrust

M_j jet mass-flow rate

p_D jet (or duct) stagnation pressure

p_0 main stream static pressure

q_0 main stream dynamic head

R_e chord Reynolds number

S wing reference area

T_D jet (or duct) stagnation temperature

T_0 main stream temperature

v_j jet velocity

V_0 main stream velocity

x streamwise distance

z distance below wing

α wing incidence relative to main stream

γ ratio of specific heats for air

δ, δ' tunnel "lift-constraint" correction factors (*see* Ref. 9)

ε angle of downwash relative to main stream

ε_∞ angle of downwash at infinity downstream

θ jet angle relative to wing chord line

ρ_0 density of main stream

η_t tailplane angle

2. Choice of Model

The need to minimise tunnel-wall interference, because corrections are inevitably approximate, tends to limit the size of the model relative to that of the working section. On the other hand, the requirements of test Reynolds number, pressure-plotting, and accuracy of manufacture usually demand as large a model as possible. Tunnel-wall interference is discussed further in Section 2.1 and a few additional remarks about Reynolds number effects are made in Section 2.2. Although pressure-plotting and accuracy of manufacture does not warrant any further comment, the importance of good slot and duct design and of realistic representation of practical aircraft configurations seems worth mention (*see* Section 2.3). Other conflicting factors which must be taken into account in model design, such as the provision of air-feeds to the model for blowing (and suction), the associated type and size of model support, the model strength, and the best use of available air supplies, are discussed in Section 3 of this paper and of Ref. 1.

2.1. Tunnel Interference

The various interference corrections and the corresponding limitations on model size were considered in Section 2.2 of Ref. 1. With boundary layer control models[7], where the sectional lift coefficient is unlikely to be much greater than 4, interference considerations should be little different from those associated with normal testing. The ratio of wing chord to tunnel height is usually kept below one-third and the ratio of wing span to tunnel breadth below three-quarters. However, with models incorporating a large jet efflux at a high angle to the main stream, and in particular for tests at the higher lift coefficients associated with jet-flap schemes[8], the interference can assume formidable proportions unless the models are much smaller than normal; the classical Glauert corrections[9] may also be considerably in error. The following discussion refers to closed working sections, although some of the comments are of more general interest. Theoretically, partially ventilated working sections (slotted or perforated walls) can offer much reduced lift-constraint corrections and small blockage. However, the correction factors are particularly sensitive to the assumed effective open area, which can vary appreciably from the simple geometric value over a range of high lift tests.

2.1.1. *Plane-Jet Models (Jet Flaps)*

With regard to lift-constraint corrections for finite aspect ratio jet-flap models, the effects of induced curvature of the stream over the wing chord can probably be neglected as usual, but significant effects can undoubtedly arise from the alterations in the curvature of the jet sheet. Hence, the classical correction factors based on simple Glauert theory may be appreciably in error at large values of the jet momentum coefficient C_μ and jet angle θ, when the circulation about the wing is controlled mainly by the effectiveness of the jet sheet rather than by wing incidence or camber. Maskell[5] has recently extended the classical lift-constraint theory to jet-flap wings, following his treatment of the effects of finite aspect ratio for thin full-span jet-flap wings in an inviscid free stream[6]. This extended theory, for closed working sections, assumes that the tunnel constraint is small, and that the bulk of

the bound vorticity over the wing and jet is confined within a distance from the tunnel centre which is small compared with the linear dimensions of the working section. The constraint correction can then be conveniently represented by an increment $\Delta\alpha$ to the geometrical wing incidence α, similar but not identical to the classical correction, together with an increment ΔC_μ to the jet-momentum coefficient. This latter arises because of the upwash distribution induced at the centre line of the tunnel by the image system, causing higher curvature of the jet sheet and hence higher vorticity than would exist in an unrestricted stream.

The corrections to the measured wing incidence, jet-momentum coefficient, wing lift and thrust coefficients, to give equivalent free stream conditions, are as follows:—

$$\Delta\alpha = \frac{1}{1+(2C_\mu/\pi A)}\,\delta\,\frac{S}{C}\,C_L, \quad \text{(no tail)},$$

$$\Delta C_\mu = \frac{C_\mu \Delta\alpha}{\theta+\alpha-\varepsilon_\infty}, \quad \text{where} \quad \varepsilon_\infty = \frac{2C_L}{\pi A + 2C_\mu},$$

$$\Delta C_L = \Delta C_\mu \sin(\theta+\alpha) + C_T \Delta\alpha,$$

$$\Delta C_T = \Delta C_\mu \cos(\theta+\alpha) - C_L \Delta\alpha.$$

The measured distribution of downwash angle $\varepsilon(x, z)$ must be corrected by the amount

$$\Delta\varepsilon = \left(1+\frac{\delta'}{\delta}\,\frac{x}{h}\right)\Delta\alpha;$$

this leads to the normal pitching-moment correction formula for tail-on results,

$$\Delta C_m = -\frac{\partial C_m}{\partial \eta_t}\,\frac{\delta'}{\delta}\,\frac{x}{h}\,\Delta\alpha,$$

and a correction to the measured jet path,

$$\Delta z = x\left(1+\frac{\delta'}{\delta}\,\frac{x}{2h}\right)\Delta\alpha,$$

with a corresponding correction to tail height.

The symbols S and C denote the reference wing area and the cross-sectional area of the tunnel working section, respectively; δ and δ' represent the classical constraint-correction factors as tabulated in Ref. 9. It will be noted that the correction $C_T\Delta\alpha$ to lift, frequently ignored in conventional testing, can be quite significant with jet-flap models. In the corrections given, the use of the jet-reaction coefficient $C_J\,[\equiv J/(q_0 S)]$, might be preferred to the slot momentum coefficient $C_\mu\,[\equiv M_j v_j/(q_0 S)]$, provided that the measured static thrust could reasonably be assumed to represent the jet momentum leaving the trailing edge with wind-on conditions (*see* Section 4.1). Furthermore, when thrust at small jet angles is being

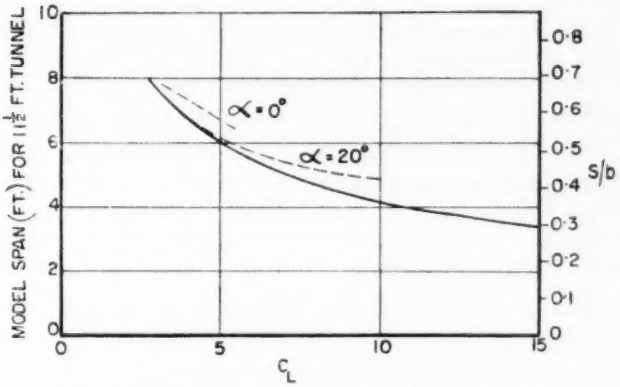

——— $\Delta\alpha = 2°$, using classical tunnel constraint corrections.
— — — $\Delta\alpha = 2°$, using new jet-flap constraint corrections, with a full-span 60° jet flap.

FIGURE 1. Effect of tunnel wall interference on permissible model size. Rectangular-wing aspect-ratio-6 model in an 11½ ft. × 8½ ft. tunnel.

studied, careful evaluation of $(\theta + \alpha - \varepsilon_t)$ is necessary, as discussed later in this section. Finally, the foregoing corrections correspond strictly to the case of full-span jet-flap wings with an elliptic spanwise distribution of loading, so discretion must be used in their application to part-span jet-flap models.

It was suggested in Ref. 1 that the model size should be limited to keep the incidence correction $\Delta\alpha$ below 2° up to the maximum value of C_L to be tested, say 10 for S.T.O.L. research investigation. The corresponding correction, $\Delta\varepsilon$, to the angle of downwash at a normal tailplane location might be double this value. Fig. 1 plots the appropriate limit in size against C_L (with $\Delta\alpha = 2°$) for a rectangular wing of aspect ratio 6 with a full-span jet flap, mounted horizontally in an R.A.E. 11½ ft. × 8½ ft. closed tunnel; curves corresponding to both classical and Maskell's new corrections are included. It is seen that the new corrections permit a slightly larger span. More important, perhaps, is the better accuracy of the new corrections, so that the suggested restriction on $\Delta\alpha$ might be somewhat relaxed if its magnitude were the sole criterion. However, much broader considerations are desirable, particularly if an assessment of thrust efficiency forms an important part of the research experiments. This can conveniently be illustrated by a brief examination of the new lift-constraint corrections for the model and tunnel of Fig. 1.

If the span of the aspect-ratio-6 model is limited to 5 ft., to give $\Delta\alpha \leqslant 2°$ for $C_L \leqslant 10$, then the correction ΔC_L to the measured C_L is not likely to exceed $0{\cdot}05\ C_L$; thus any error in this correction will not be particularly serious as regards lift. However, the corresponding correction $-C_L \Delta\alpha$ to the measured thrust coefficient C_T could well be as much as $0{\cdot}1\ C_\mu$ at high C_L-values, and an even higher proportion of C_T. This could be particularly important at high C_μ-values and jet angles, when errors in the correction could give misleading answers about the net thrust available under S.T.O.L. conditions. Again, although the further correction

$\Delta C_\mu \cos(\theta+\alpha)$ [$\equiv C_\mu \Delta\alpha \cos(\theta+\alpha)/(\theta+\alpha-\varepsilon_\infty)$] to the measured C_T is likely to be less than 0·05 C_μ for jet angles of 30° and above, the proportion could be higher and the correction more inaccurate at small jet angles, because of possible errors in the evaluation of the denominator $(\theta+\alpha-\varepsilon_\infty)$. In such cases, it is probably more accurate to express C_L, ε_∞, $\Delta\alpha$ and $(\theta+\alpha-\varepsilon_\infty)$ all as specific linear functions of θ and α for the evaluation of this correction at small θ and α.

Thus, in limiting the model size to allow for the inevitably approximate nature of the lift-constraint corrections, the magnitude of $\Delta\alpha$ and $C_L \Delta\alpha/C_\mu$ should be examined for the maximum value of C_L envisaged at least, together with the magnitude of $\Delta C_\mu/C_\mu$ for a representative range of values of C_L and C_μ.

Additional interference effects can arise when the jet angle and momentum coefficient are so large that the jet sheet approaches close to the floor of the tunnel. Clearly, the foregoing lift-constraint corrections ought then to be modified because the jet cannot reasonably be assumed to lie along the centre line of the tunnel. The sensitivity of the constraint correction factors δ and δ' to offset from the tunnel centre line can be assessed using Ref. 10, but there is also a further significant effect associated with "jet-constraint" on the tunnel main stream flow between the lower surface of the wing and the tunnel floor. This usually leads to a reduction in the measured lift for a particular configuration, in contrast to normal lift-constraint effects; pitching moment, downwash, and drag changes also become embarrassing. As suggested in Ref. 1, effects should be small with a wing chord not exceeding one-sixth the tunnel height, at least for jet angles θ up to 60° with C_μ-values up to 4 (Ref. 11). At larger θ and C_μ, say up to 90° and 10 respectively, a wing chord as little as one-tenth the tunnel height could be needed[12]*. Fortunately, for our deliberations, the lift-constraint rather than jet-constraint limitations are usually the more significant in practical cases. For example, the representative aspect-ratio-6 model in the 11½ ft. × 8½ ft. tunnel is limited by lift-constraint considerations to 60 in. span, so that the 10 in. chord is only one-tenth the tunnel height. More guidance on the effect of proximity of the jet sheet to the tunnel floor should be obtained from current R.A.E. tests on a jet-flap complete model with various ground heights.

2.1.2. *Round-Jet Models*

Tunnel interference corrections for models with round jets at large angles to the main stream have so far received little attention, since the problem is a fairly novel and difficult one. If the jets are of sufficient spanwise extent to produce substantial jet-flap effects, then the foregoing arguments could of course be applied qualitatively. In many practical cases, however, the pressure lift generated on the external wing surface due to the jet efflux is only a fraction of, rather than many times, the gross jet thrust and may even be negative. The path of the jet is then primarily a function of the ratio v_j/V_0 of jet to tunnel speed and is not intimately associated with increased bound vorticity on the wing, as in the jet-flap case. The tunnel interference is therefore mainly associated with the round jets hitting or approaching

*Mounting the model above the tunnel centre line should alleviate the jet-constraint effect but would introduce further complications and unknowns.

close to the floor, so that conventional lift-constraint arguments become quite inappropriate. In the absence of theoretical guidance, test results on ground effect could again be interpreted to suggest limitations on model size, but unfortunately the available information is almost all restricted to zero forward speed.

With wing areas only slightly larger than the jet exit area, the ground interference at zero forward speed can be mainly attributed to back pressure on the jet and the lower wing surface. For most test purposes, this effect is probably negligible when the jet exit diameter $d\,[=\sqrt{(4A_j/\pi)}]$ is less than one-half the height h_j of the jet exit above the floor, *i.e.* less than one-quarter the tunnel height for a centrally-mounted model. With gross wing areas several times the jet exit area, the interference at zero forward speed largely arises from suctions on the wing lower surface associated with flows induced by entrainment with the jet. In R.A.E. tests on wings of circular and equilateral plan forms, having a centrally mounted jet with a ratio D/d of wing to jet diameter exceeding 4, Wyatt has shown that the ratio of the downward suction S_T on the wing surface to the gross thrust T of the jet is mainly a function of D/h_t. The ratio S_T/T decreased from about 0·2 to 0·06 as D/h_t was reduced from 4 to 1·6, and probably would have been less than 0·02 with $D/h_t < 1/3$. With annular rather than circular jets, the interference problem becomes somewhat more complex, since downward suction on the peripheral wing surface and back pressure on the central fairing or hub can be present simultaneously. Again, if air intakes are represented on the jet-blowing model, they may be subject to interference due to re-circulation of the jet efflux and, in this respect at least, the roof of the tunnel can also play an important part.

When the main stream speed is non-zero, tunnel interference effects on net thrust and pitching moment will be equally as important as those on lift. In the absence of adequate information, it seems reasonable to conjecture that serious interference is unlikely for most practical cases if the wing chord does not exceed one-third of the height of the jet exit above the tunnel floor, *i.e.* one-sixth of the tunnel height. This limitation satisfies the jet-constraint restriction associated with jet-flap arguments, should meet most lift-constraint restrictions associated with pressure lift (and drag) on the wing arising from partial jet-flap effects or wing incidence, and should give static lifts correct to within one or two per cent. Admittedly, it may be rather severe for many model tests with round jets and often may have to be relaxed, particularly for wing-fan models. Each case has naturally to be considered on its own merits, both in respect of the information needed and the accuracy required. Check tests can be made by varying the height of a ground-board but, as stressed in Section 3.3 of Ref. 1, care is needed to ensure that the different blockages in the two compartments of the tunnel do not lead to misleading results.

To provide further information on tunnel interference with round-jet models, some tunnel tests are being made at the R.A.E. on a simple single-jet model at various heights above the tunnel floor and with various ground-board heights. In addition, some of the more complex powered-lift models now being used for basic research in the 11½ ft. × 8½ ft. and 13 ft. × 9 ft. tunnels at R.A.E. are also being briefly tested in the 24 ft. diameter open-jet tunnel to give a check on tunnel interference effects.

2.1.3. *"Blockage" Corrections*

In high-lift testing, solid and wake blockage corrections to the tunnel dynamic head are usually only of secondary importance when choosing model scale. Nevertheless, they should not be overlooked, particularly if good absolute accuracy is required in, say, the determination of $C_{L\,max}$ or the thrust coefficient. Solid blockage, associated with the volume of model in the bounded main stream, can be readily estimated using classical methods[9], but "wake blockage" can arise in several novel forms with jet-blowing high-lift models.

When the flow is unseparated on conventional models, the wake blockage correction to the main stream dynamic head q_0 can conveniently be expressed in terms of the rig drag coefficient C_{Dr} and the model profile drag coefficient C_{D_0}, as follows:—

$$\Delta q_0/q_0 = \tfrac{1}{2}(S/C)(C_{Dr}+C_{D_0}).$$

For completely stalled flows, unpublished work by Maskell at the R.A.E. suggests the relation

$$\Delta q_0/q_0 = \tfrac{1}{2}(S/C)(C_{Dr}+C_{D_0}) + \tfrac{1}{2}K(S/C)(C_D - C_{Di} - C_{D_0}),$$

where C_{D_0} again represents the profile drag coefficient with unseparated flow, C_{Di} represents the induced drag coefficient $(C_L^2/\pi A)$, C_D denotes the measured total drag coefficient under the relevant test conditions, and K is an empirical constant of about 5 for aspect ratios up to 10. For intermediate cases, where some degree of separation is present although the flow is not completely stalled, the choice of a K-value (between 5 and 1) is not a straightforward one and will depend on whether the separation is of the trailing-edge or nose-bubble type.

On jet-blowing models, apart from such low velocity wakes, consideration is also necessary of the high-velocity jets which are being fed into the tunnel main stream. These jets steadily grow in width and decrease in maximum velocity as mixing takes place with the lower velocity main stream. In the particular case of jet flaps, any separation on the wing upper surface usually reattaches forward of the trailing edge and the thickened boundary layer is completely absorbed by the jet emerging close to or at the trailing edge; the resulting "thick wake" is quite different in character from that behind a conventional aerofoil. The problem of blockage corrections with jet-blowing models would therefore appear to be rather complex and to warrant further investigation.

2.2. Reynolds Number

The earlier remarks[1] concerning the requirements of test Reynolds number have been well substantiated. In the absence of appreciable flow separation on the wing upper surface, variation of wing Reynolds number has had no significant effect on jet-blowing wing performance over the range tested ($R_c = 0{\cdot}5\times10^6$ to 2×10^6). The main stream Mach number, although low, seems likely to be more important, since sonic flow can occur over the wing surface at high lifts. The tailplane (or fin), on the other hand, may be working at extremely low Reynolds numbers and over a

wide range of downwash angles, if fixed, so it is probably subject to considerable scale effect and should be used only as a mean downwash (or sidewash) meter. The full-scale tailplane (or fin) characteristics should then be estimated using full-scale lift slopes and stalling angles.

It is worth adding that the maximum possible test Reynolds number for any prescribed value of the jet-momentum coefficient C_μ is independent of the model scale, if the available air supply is being used to its limit. Likewise, the maximum possible lift and thrust forces on the model are also independent of scale, if C_μ is the parameter governing the effectiveness of blowing on a specific configuration; however, the corresponding moments will be proportional to model scale.

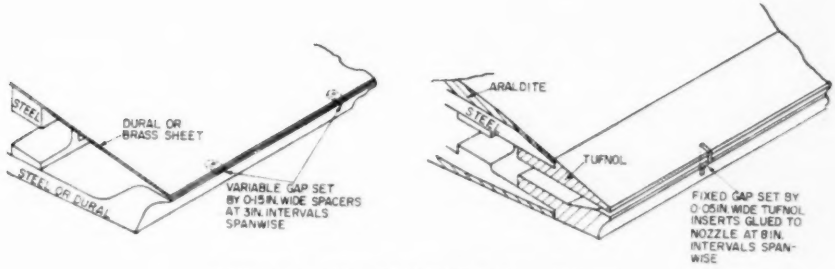
STEEL
DURAL OR BRASS SHEET
STEEL OR DURAL
VARIABLE GAP SET BY 0·15 IN. WIDE SPACERS AT 3 IN. INTERVALS SPANWISE
ARALDITE
STEEL
TUFNOL
FIXED GAP SET BY 0·05 IN. WIDE TUFNOL INSERTS GLUED TO NOZZLE AT 8 IN. INTERVALS SPANWISE

FIGURE 2. Typical jet-blowing slot arrangements.

2.3. MODEL DESIGN

Simple convergent blowing slots have worked well over a wide range of pressure ratios and, with most models, the incorporation of complex convergent-divergent slots for supercritical pressure ratios is probably unnecessary. Some typical slot designs are shown in Fig. 2; Tufnol and Araldite have often proved more convenient materials than steel. Usually it is convenient to have a short parallel length of slot at the exit so as to ensure that the jet is directed properly, and also to accommodate the simple spacers needed to maintain the correct slot width. Much larger parallel lengths than about five slot widths are undesirable in view of the losses due to the slot boundary layer. The spacers should be as small and as widely-spaced as practicable, consistent with maintaining the desired slot width; say, not more than 0·25 in. wide at spanwise intervals not less than 3 in., giving an overall blockage less than 10 per cent, particularly for boundary layer control at large flap angles. The slot upper lip can advantageously be kept thin and ridges on the flap upper surface should be kept as small as possible. Simple cylindrical ducts are adequate to maintain a satisfactory spanwise distribution of slot velocity if the chordwise cross section of the duct is large enough to keep the duct spanwise velocity below about two-tenths of the slot velocity. Where this is not possible, careful tapering of the duct is required to ensure a uniform spanwise distribution of duct static pressure, and corner vanes are needed to turn the air chordwise if total loss of duct dynamic head on turning cannot be tolerated.

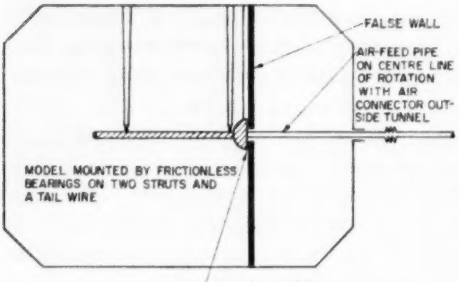
FALSE WALL
AIR-FEED PIPE ON CENTRE LINE OF ROTATION WITH AIR CONNECTOR OUTSIDE TUNNEL
MODEL MOUNTED BY FRICTIONLESS BEARINGS ON TWO STRUTS AND A TAIL WIRE
CLEARANCE ABOUT 0·2 IN.

FIGURE 3. Horizontal half-model rig for a simple three-component overhead balance (N.P.L.)

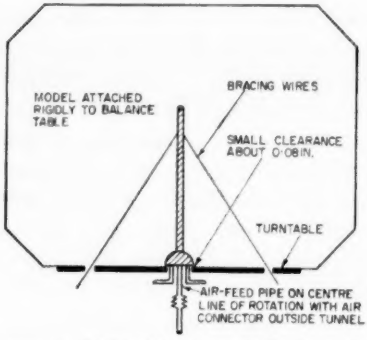
MODEL ATTACHED RIGIDLY TO BALANCE TABLE
BRACING WIRES
SMALL CLEARANCE ABOUT 0·08 IN.
TURNTABLE
AIR-FEED PIPE ON CENTRE LINE OF ROTATION WITH AIR CONNECTOR OUTSIDE TUNNEL

FIGURE 4. Vertical half-model rig for a six-component virtual-centre floor balance (R.A.E.)

In testing models of specific aircraft configurations, the effect of essential practical features should be examined; for example, flap gaps, flap cut-outs, and extensive blockage of the slot such as might arise from the flap operating mechanism. The effects of air brakes, undercarriage assemblies and stores can also vary significantly with jet-blowing.

3. Various Test Rigs and Methods of Air-Feed

3.1. HALF-MODELS

The advantages of using a half-model are that a larger-scale model can be installed, that the manufacturing time is considerably reduced, and that the problems of model support, method of air-feed, and carriage of pressure-plotting tubes are all greatly simplified. The disadvantages are that the model cannot be yawed, so that the measurements are therefore restricted to lift, drag, pitching moment, and possibly rolling moment, at zero angle of yaw.

The two half-model techniques described in Section 3.1 of Ref. 1 have now been used successfully for a variety of blowing tests, including jet-flap models. Basically, the N.P.L. method (Fig. 3) is designed for a simple three-component balance, with the model mounted horizontally on struts or wires, and a vertical false wall inserted in the tunnel. The horizontal air-feed is aligned with the model pitch axis, being designed to minimise air-feed constraint effects on lift, drag, and pitching moment. Variants of this method have been used for similar tests in several other wind tunnels in Great Britain, with equal success. The R.A.E. method (Fig. 4) is suitable for a virtual-centre balance, preferably a floor balance, with the model mounted rigidly from the moment table*, using the tunnel floor as a reflection plane. The vertical air-feed on the model pitch axis is again designed to minimise air-feed constraints on the relevant force measurements.

*With a virtual-centre balance, the model can of course be connected to the moment table in any convenient way, frictionless mountings being unnecessary. This is especially advantageous with air-feeds to the models.

As regards air-feed connectors for half models, the "necked canvas-hose" and "two-faced air-bearing" types developed at R.A.E. and N.P.L. respectively have already been described in Ref. 1. Some other types are mentioned in the general discussion on air-feed connectors in Appendix I.

The results obtained from half-model tests have shown good agreement with the corresponding results obtained on complete models. However, comparative high-lift experiments on a half-model and a similar complete model in the same tunnel are still lacking. From the broad comparisons available, which include in one case a jet-blowing configuration, it would appear that the tail-off lift, drag, and pitching moments are generally in good agreement, although significant differences can arise in zero-lift drag and pitching moment. The downwash ε at the tail and $d\varepsilon/d\alpha$, as determined by using the tailplane as a mean downwash meter, agree within experimental accuracy. However, as might be expected, tail power may be different, because of wall boundary-layer effects on the half-model, and possibly to scale effect. In any case, as discussed in Section 2, it is advisable to use the tail mainly as a downwash meter.

The reflection-plate boundary layer is normally of little concern, provided that the half-model has a fuselage thickness rather more than three times that of the boundary layer, and provided that the static pressure gradient in the tunnel is not sensibly affected. For tests on a half-wing without a fuselage, it may be necessary to thin the reflection-plate boundary layer, at least near the wing root. This could be achieved by using suction to remove the boundary layer or a vortex-generator system to deflect it.

Clearly, the half-model technique can yield valuable results in less time than the complete model. However, to enable lateral stability in sideslip and asymmetrical aircraft configurations to be studied, it is also essential to develop complete-model rigs suitable for six-component measurements on jet-blowing models.

3.2. Complete Models

The additional difficulties which arise in designing a complete-model rig with jet blowing are quite appreciable, particularly as regards achieving completely satisfactory model support and air-feed arrangements. Some possible solutions based on recent R.A.E. experience are therefore discussed.

3.2.1. *R.A.E. Jet-Blowing Complete-Model Rig and Test Technique*

The jet-flap complete-model rig briefly mentioned at the end of Section 3.2 of Ref. 1* has now been fully developed and in satisfactory operation for more than two years; the rig also permits tests on floor-mounted half-models over a 40° incidence range. Complete models are mounted horizontally (Fig. 5) on a single hollow strut from the virtual-centre lower balance of the No. 2 11½ ft. × 8½ ft. tunnel, the air for jet-blowing being fed to the model through a "four-faced

*Mr. A. Anscombe was responsible for the initial design of the rig.

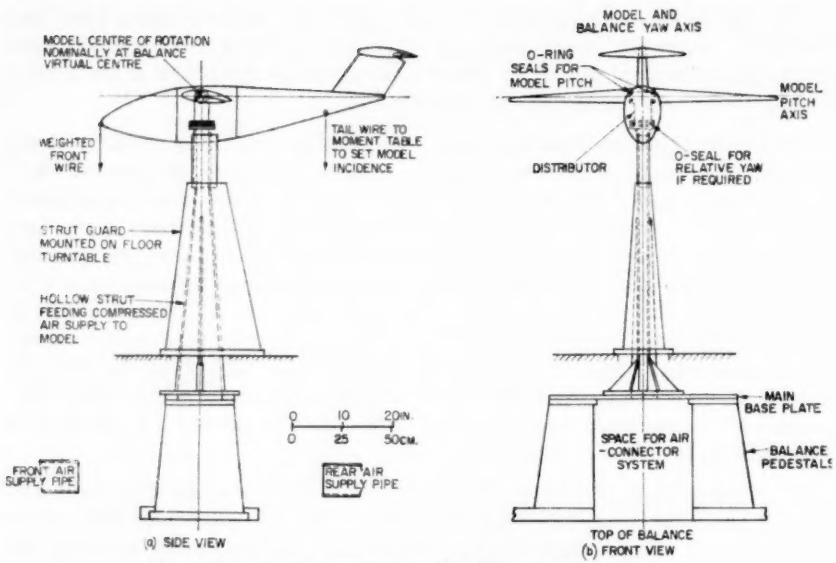
MODEL CENTRE OF ROTATION NOMINALLY AT BALANCE VIRTUAL CENTRE
WEIGHTED FRONT WIRE
TAIL WIRE TO MOMENT TABLE TO SET MODEL INCIDENCE
STRUT GUARD MOUNTED ON FLOOR TURNTABLE
HOLLOW STRUT FEEDING COMPRESSED AIR SUPPLY TO MODEL
0 10 20IN.
0 25 50CM.
FRONT AIR SUPPLY PIPE
REAR AIR SUPPLY PIPE
(a) SIDE VIEW
MODEL AND BALANCE YAW AXIS
O-RING SEALS FOR MODEL PITCH
MODEL PITCH AXIS
DISTRIBUTOR
O-SEAL FOR RELATIVE YAW IF REQUIRED
MAIN BASE PLATE
SPACE FOR AIR-CONNECTOR SYSTEM
BALANCE PEDESTALS
TOP OF BALANCE
(b) FRONT VIEW

FIGURE 5. General arrangement of R.A.E. complete-model rig.

air-bearing" connector specially devised to minimise the constraint effects on all six components. Details of this air-bearing connector are given in Appendix II. The tunnel balance, briefly described in Chapter V of Ref. 9, is also unusual in that it, too, is supported on compressed-air bearings.

The main features of the complete-model rig, apart from the air-bearing connector, are concerned with the pitching and yawing mechanisms at the centre of the model, frictionless bearings being unnecessary since a virtual-centre balance is being used†.

The model is pivoted on a hollow central distributor (Fig. 5) and can be pitched relative to the distributor. To ensure rotatable leak-proof connections, O-ring seals are incorporated between the twin output pipes of the distributor and the main wing ducts which rotate with the model. The distributor is bolted by its base flange to the top flange of the hollow support strut, slotted holes in the flange permitting up to $\pm 15°$ yaw of model and distributor relative to the strut; a dowel can be used to set relative yaw at 0°. An O-ring seal is again used to avoid leaks. The strut access hole in the bottom of the fuselage is sealed by a roller blind to avoid possible " bomb bay " flow interference effects. The top of the strut, which is exposed during longitudinal stability tests, is faired to a low-drag 40 per cent aerofoil section and the strut is mounted on a main base plate spanning the balance pedestals, which have been placed side by side for convenience. The strut guard is mounted independently on the floor turntable.

---

†See footnote on p. 294.

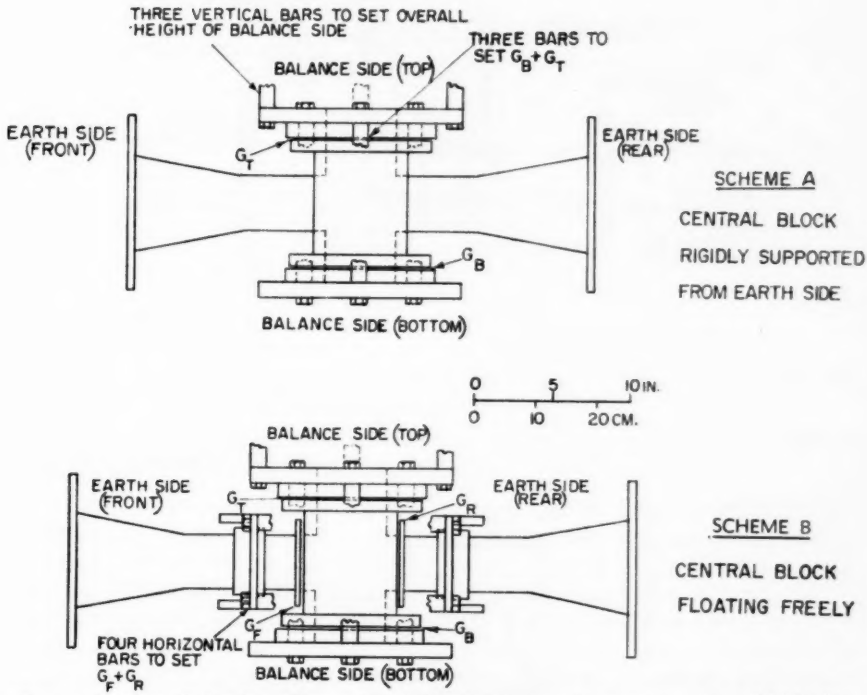

FIGURE 6. Two air-bearing schemes tested for six-component measurements on jet-blowing models. Along-wind sections.

The air-bearing connector is isolated from the model and strut by the main base plate, so that strut deflections under load are not transmitted directly to the balance side of the connector; this occupies the space below the base plate and between the pedestals. Appendix II contains details of the final arrangement (*see* Figs. 6 and 7).

During longitudinal stability tests over an incidence range at zero sideslip, the model incidence is controlled by a tail wire connected to a capstan mounted on the balance, with a loaded front wire to return the model towards negative incidence. The results are corrected for drag and pitching-moment tares due to the exposed portion of the strut and the wires.

During lateral stability tests, the model incidence is fixed by a dowel-pin and the front wire and tail wire are removed. It has been found preferable, with current jet-flap models, to extend the strut guard so as to cover the whole of the exposed strut, and to rotate the model and strut together by yawing the moment table*. In

*At the model design stage, it was not known whether the moment table could be yawed without introducing serious air-feed constraint effects on one or more of the freedoms; so the internal yawing joint was included.

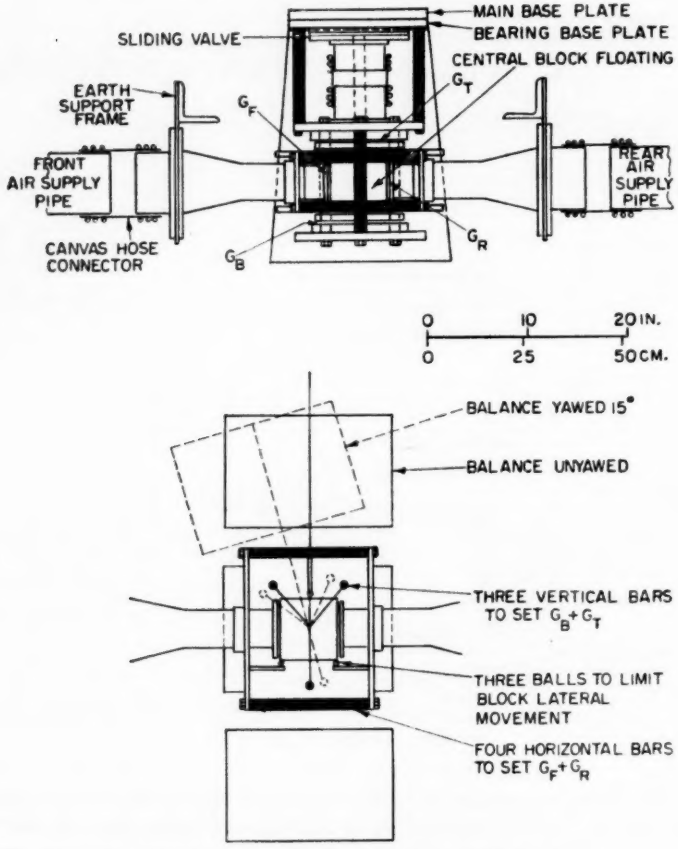

FIGURE 7. General arrangement of final air-bearing system (Scheme B).

this way, strut tare effects on side force and rolling moment are avoided, and the moments are measured about yawed axes directly. Moreover, the balance zeros do not vary greatly with yaw angle, as would be the case if the model were yawed relative to the strut. Although the interference of the extended strut guard on the fin and tail must be larger than that of the exposed strut, it has been shown to be small.

The position of the strut guard giving least interference, as indicated by pressure plotting on the strut, is virtually along wind. Unfortunately, the size of the strut guard permits only 7° yaw relative to the strut, so that at large model yaw angles the strut guard is somewhat misaligned from the optimum. By comparative tests at a fixed model yaw angle, with a range of strut guard yaw angles, the measured results can be extrapolated to the zero strut guard yaw condition. For the present

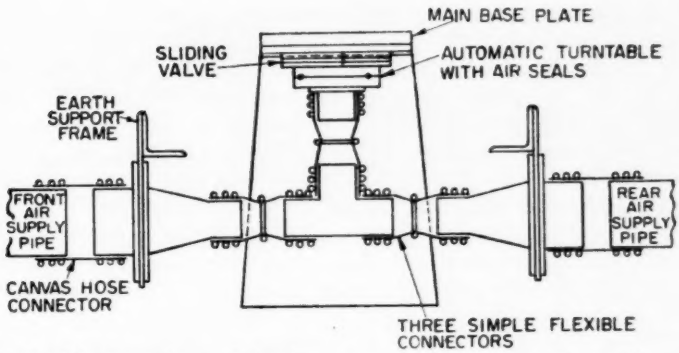

FIGURE 8. Possible alternative to air-bearing system of Fig. 7, using simple flexible connectors.

model, the errors due to misalignment were relatively insignificant, even with the model at incidence and with the fin and tail on.

The tunnel results are corrected in all cases for the calibrated effects of shift of the model centre of rotation relative to the balance virtual-centre, since the model support strut can deflect under load. On the present model the deflections involved are small, generally less than 0·020 in. Another small correction is applied for the calibrated misalignment of the model centre of rotation and balance virtual-centre in rigging. Balance zeros are taken with the correct static pressure in the air-feed connector, the supply being sealed off from the model blowing ducts by an isolating valve.

Since the zeros do not change rapidly with internal static pressure for the final system, the resulting zeros are only slightly less accurate than those for the basic balance. It has also been established that the balance calibration is not affected appreciably by the presence of the connector, and that the constraint effects due to the connector remain the same when loads are applied to the model. Such questions would, of course, require examination with any connector system; it cannot be tacitly assumed that the presence of the air connector will merely affect the basic zeros.

3.2.2. *Possible Extensions of the R.A.E. Complete-Model Rig to other Balance Systems*

Since the R.A.E. complete-model rig has proved very satisfactory in practice, some possible modifications to permit six-component measurements for jet-blowing models on other balance systems seemed worth mention.

With a virtual-centre balance, either above or below the tunnel, the R.A.E. rig should require little modification, provided the moment table can be assumed to return to sensibly the same position and attitude when balanced under typical aero- one further degree of rotational freedom in pitch, as discussed later, in order to dynamic loads as when balanced at zero load. It may be necessary otherwise to add permit slight misalignments of the "balance side" relative to "earth side" in each of

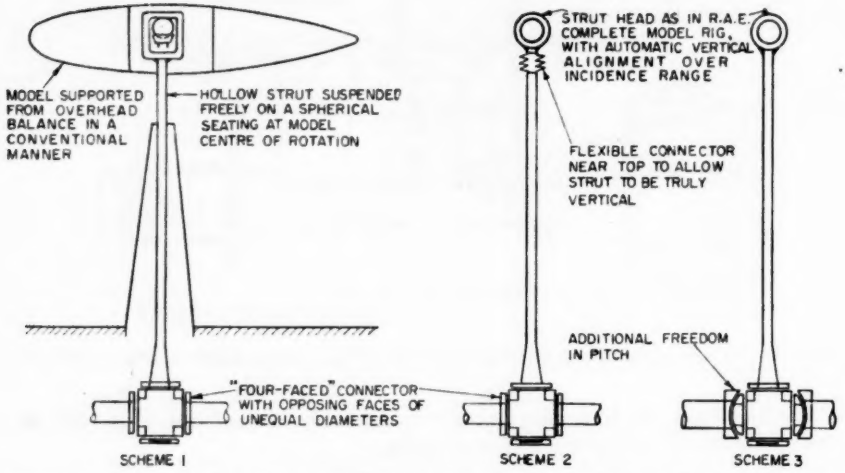
MODEL SUPPORTED FROM OVERHEAD BALANCE IN A CONVENTIONAL MANNER
HOLLOW STRUT SUSPENDED FREELY ON A SPHERICAL SEATING AT MODEL CENTRE OF ROTATION
"FOUR-FACED" CONNECTOR WITH OPPOSING FACES OF UNEQUAL DIAMETERS
STRUT HEAD AS IN R.A.E. COMPLETE MODEL RIG, WITH AUTOMATIC VERTICAL ALIGNMENT OVER INCIDENCE RANGE
FLEXIBLE CONNECTOR NEAR TOP TO ALLOW STRUT TO BE TRULY VERTICAL
ADDITIONAL FREEDOM IN PITCH
SCHEME 1
SCHEME 2
SCHEME 3

FIGURE 9. Some possible air-feed arrangements for use with conventional (not virtual-centre) six-component balances.

the three translational and three rotational senses without introducing substantial constraints. Again, when the table displacements are large, inside and outside diameters of opposing faces of the air-bearing connector may have to be made unequal. The air-bearing connector could probably be replaced by an arrangement using three flexible connectors, such as bellows or necked canvas sleeves, as shown in Fig. 8, provided larger constraints were acceptable; a turntable would have to be incorporated on the "balance side" or "earth side" to permit the balance to be yawed. This system could also completely avoid the air leak present with air-bearing connectors or labyrinth seals*.

With a conventional balance (not the virtual-centre type), the air must be fed directly to the model through a frictionless connector. Furthermore, greater movements of the model under load will usually occur, both in translation and in rotation. Some possible arangements using air-bearing connectors are outlined in Fig. 9, for models supported from an overhead balance in the conventional manner.

The first scheme employs a hollow strut, suspended from the model by a spherical air-bearing at the model centre of rotation. A "four-faced air-bearing" connector (or bellows system) is used at the foot of the strut, with unequal inner and outer diameters on opposing faces to permit substantial relative translational movements without appreciable alteration in force constraints. Thus, as the model moves, the strut will remain vertical, with its weight acting through the model centre of rotation, while the spherical bearing allows for model rotational movements, including those due to model distortion under aerodynamic loads. The main

*With air-bearing connectors, the leak could be prevented, if desired for mass flow calibration, by incorporating inflatable rubber seals in the plane faces of the air-bearings.

objection is the aerodynamic interference which could arise due to the air leak from the spherical bearing inside the model; the mass flow calibration in itself should cause no difficulty since it could be carried out on a special rig or after sealing the air gaps. The second scheme employs the same lower part, but the spherical bearing inside the model is replaced by a cylindrical joint and O-seals, as in the R.A.E. complete model. Preferably, the top of the strut should be maintained vertical automatically as the model incidence is altered. Bellows or a necked-canvas joint would be incorporated as near the top as possible, so that the lower part of the strut would be able to align itself truly vertically with its c.g. practically below the model centre of rotation, even if the top of the strut were slightly misaligned in pitch or roll from the vertical. The third scheme dispenses with the flexible joint, but might require the additional rotational freedom in pitch, if the lower part of the strut cannot be aligned sufficiently accurately.

All these schemes appear rather complicated, but would at least be expected to result in relatively small air-feed constraints on the model, and for that reason would prove preferable to cruder schemes involving larger constraints. The advantages of virtual-centre balances for six-component measurements on jet-blowing models are obvious in view of the increased complexity otherwise involved in the air-feed connector system.

3.3. Two-Dimensional Aerofoil Models

Investigation of two-dimensional characteristics, to check basic theory and to study specific fundamental aspects, usually requires overall force measurements as well as pressure plotting and wake traverses. The characteristics could be derived from results obtained on a finite aspect ratio model, but the analysis is likely to be difficult and unreliable unless the aerofoil is mounted with reflection plates at its ends. Some of the problems which arise in testing such a model between reflection plates at high lift coefficients, have already been discussed in Section 3 of Ref. 1. If the model completely spans the tunnel from wall to wall, then wall boundary-layer separations and flow through the air gaps at the ends of the aerofoil are two possible sources of trouble. When it is impracticable to span the tunnel, because of limitations of model strength or air supply, separate end-plates can be used as false walls bridging the tunnel from roof to floor (assuming a horizontal model). Difficulties then arise in ensuring a uniform flow through the central compartment acting as a "new working section," and in determining the correct main stream velocity*. If the end-plates are much smaller, so that comparting the tunnel is avoided, the aerofoil rig becomes only quasi-two-dimensional in the sense that the chordwise loading is sensibly independent of spanwise position but downwash effects are still present (*see* Appendix IV of Ref. 1).

A better test arrangement comprises an aerofoil spanning the smaller dimension of the tunnel, with the centre section of the span mounted and fed independently of

*These difficulties could be avoided by fitting a complete "two-dimensional" contraction and diffuser to the false walls so that the whole of the tunnel main stream flow passes through the new working section. But special care is then needed to avoid flow separation in the diffuser and deterioration in the tunnel fan performance.

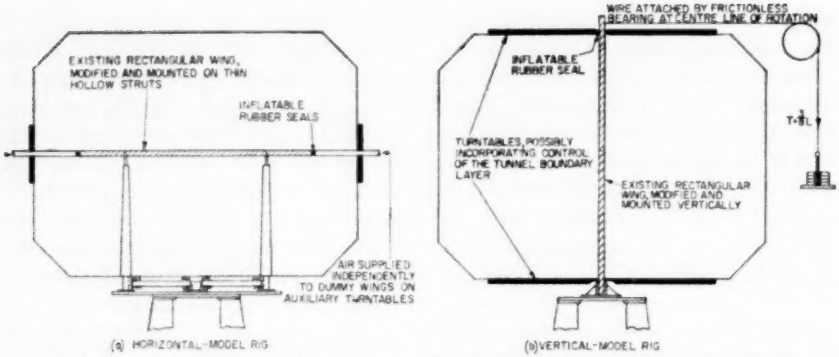
EXISTING RECTANGULAR WING, MODIFIED AND MOUNTED ON THIN HOLLOW STRUTS
INFLATABLE RUBBER SEALS
AIR SUPPLIED INDEPENDENTLY TO DUMMY WINGS ON AUXILIARY TURNTABLES
(a) HORIZONTAL-MODEL RIG
WIRE ATTACHED BY FRICTIONLESS BEARING AT CENTRE LINE OF ROTATION
INFLATABLE RUBBER SEAL
TURNTABLES POSSIBLY INCORPORATING CONTROL OF THE TUNNEL BOUNDARY LAYER
EXISTING RECTANGULAR WING, MODIFIED AND MOUNTED VERTICALLY
T-SEL
(b) VERTICAL-MODEL RIG

FIGURE 10. Possible two-dimensional test arrangements for R.A.E. virtual-centre floor balance.

the twin outboard (dummy) sections, but with the spanwise distribution of aerofoil shape and jet blowing as uniform as possible. The small gaps between the centre and outboard sections should be sealed, without introducing significant constraints when balance measurements are being taken (Section 3.3.2 of Ref. 1). Moreover, the associated breaks in the spanwise extent of the blowing slot should be kept as small as possible, about the same size as the width of spacer being used to set the slot gap. Since the outboard sections are intended to avoid tunnel-wall boundary-layer effects on the centre section, the geometrical aspect ratio of the whole aerofoil must be kept as large as possible (say, at least 2), commensurate with the need for a large chord, because of Reynolds number, pressure plotting, and manufacturing considerations. In any case, flow separation at the tunnel walls should be minimised by auxiliary boundary-layer control on the walls themselves. The chief difficulties likely to arise with this type of two-dimensional rig are the support of the centre section independent of the outboard ones, the separate air-feed to the centre section, and the accurate alignment of the centre and outboard sections. These difficulties can be somewhat eased by keeping the geometrical aspect ratio of the whole aerofoil low, commensurate with the needs already mentioned and with limitations of chord/height ratio because of tunnel interference.

Some of the rigs designed for two-dimensional jet flap tests in the R.A.E. No. 2 $11\frac{1}{2}$ ft. $\times 8\frac{1}{2}$ ft. tunnel are now briefly outlined, by way of illustration. In a rig designed and built about four years ago, the model span had to be limited because of air-feed and strength considerations, and end-plates spanning the tunnel were used. The arrangement proved unsatisfactory for accurate measurements, largely because the size and blockage of the outer tunnel compartments were considerably different from those of the central one containing the jet-flap aerofoil. Since then no further balance measurements have been made on two-dimensional models. But possible new rigs spanning the tunnel have been considered, taking advantage of the higher air-feed pressure ratios which should soon be available (up to 7·5:1). The geometrical aspect ratio of the aerofoil needs to be at least $6b/h$, to meet the limitation $c/h < 1/6$ of Section 2.1.1.

The horizontal-model rig shown in Fig. 10(*a*) closely approximates to the ideal

arrangement just discussed, except in that h is the smaller dimension (8½ ft.) of the tunnel. The centre test wing could be supported by two hollow metal struts, suitably covered by strut guards; the wing would be able to pitch, using a similar arrangement of metal bearings and O-seals as for the R.A.E. complete model, with the air supplied through the struts. Large total head losses would be involved, and further losses would be introduced if throttling of the model blowing duct were essential to obtain a uniform spanwise distribution. The spanwise location of the struts is chosen to maintain the extremities of the test rig horizontal with uniform spanwise loading. The calculated deflections under load are very small (less than 0·01 in. at $C_L = 5$, $V_0 = 100$ ft./sec.), and it should not be necessary to adjust the vertical height of the outer wings. The latter would be mounted on auxiliary turntables with independent air supplies and inflatable rubber seals could be incorporated at the joints of the wing and flap contours.

The vertical-model rig shown in Fig. 10(*b*) is a simple extension of the normal half-model arrangement, and makes h the larger tunnel dimension (11½ ft.). However, the deflections would be embarrassingly large, about 2 in. at the tip at $C_L = 5$, $V_0 = 100$ ft./sec., unless a restraining load were applied. Since both ends of the model are located in the tunnel boundary layer, repeat balance measurements with the model reduced in span and one dummy wing would be desirable, to determine the appropriate corrections.

4. Measurement of Jet-Flow Parameters

The main parameters and their experimental determination were discussed fully in Section 4 of Ref. 1, formulae for the jet-momentum coefficient and notes on accuracy of measurement being also included in Appendix V of Ref. 1. Some qualifications of the earlier comments are made here in the light of more recent experience.

4.1. Definition of the Main Parameters

The jet-momentum coefficient $C_\mu [\equiv M_j v_j/(q_0 S)]$, rather than the jet-quantity coefficient $C_Q [\equiv M_j/(\rho_0 V_0 S)]$ or the velocity ratio v_j/V_0, has been established as a satisfactory non-dimensional parameter for the correlation of basic studies on plane jets with arbitrary slot width*. This procedure has been justified for both subsonic and supersonic blowing, even up to pressure ratios as high as 5 and with simple convergent nozzles. However, some elaboration may be necessary when the pressure ratio is so low that the jet velocity is only about twice the main stream velocity V_0 and barely exceeds the local stream velocity V near the slot exit. For example, in boundary layer control studies, the rate of mixing is important and the relative velocity $v_j - V$ becomes more significant than v_j itself; in fact low-pressure boundary layer control results tend to correlate better with those at high pressure ratio if we take

$$\dot{C}_\mu \equiv M_j (v_j - V)/(q_0 S) = C_\mu - 2C_Q (V/V_0).$$

*For basic studies, mean sectional coefficients are usually derived by taking the wing reference area as that corresponding to the spanwise extent of the blowing slot. For performance studies, comparing differing extents of blowing, overall coefficients may be preferable, based on the same gross wing area as the overall force coefficients.

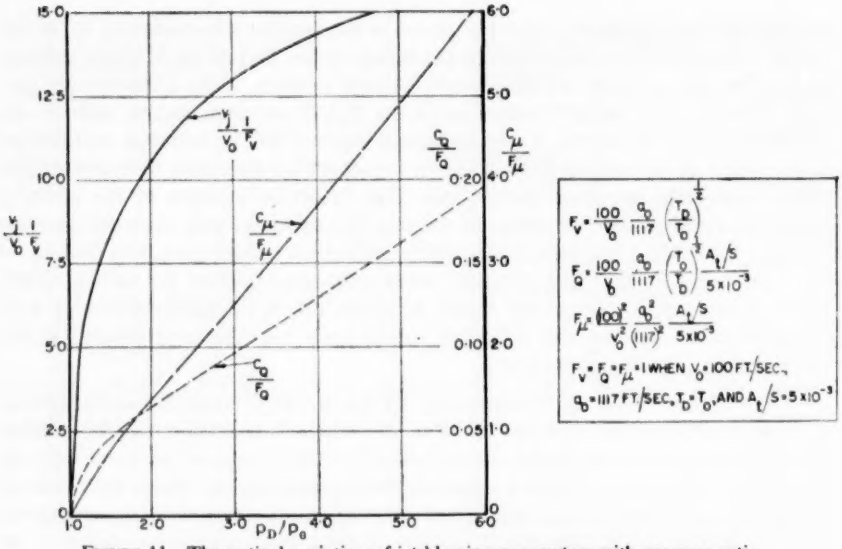

FIGURE 11. Theoretical variation of jet-blowing parameters with pressure ratio.

Unfortunately, the difficulty arises in specifying the values of V/v_j or V/V_0, particularly since V can vary rapidly chordwise near the slot exit or over the flap knee.

For the evaluation of C_μ, the blowing velocity v_j is perforce determined theoretically, by assuming isentropic expansion from the total pressure p_D (and temperature T_D) in the slot throat or duct to the main stream static pressure p_0. Total head variation across the width of the slot due to slot boundary layer growth is not usually significant from high-lift aspects if the slot is well designed (*see* Section 2.3), but should not be overlooked when a precise assessment of thrust losses has to be undertaken. The mass flow rates can likewise be estimated theoretically for the prescribed pressures, slot temperature, and slot throat area A_t. However, in experimental work, the mass flow is best taken as that actually fed to the model duct, so that errors due to throat area determination and viscous effects are avoided.

For completeness, Fig. 11 illustrates the variation of v_j/V_0 with blowing pressure ratio p_D/p_0, at representative conditions of main stream speed ($V_0 = 100$ ft./sec.), ratio of slot temperature to main stream temperature ($T_D/T_0 = 1$) and the speed of sound in the main stream ($a_0 = 1{,}117$ ft./sec.), taking $\gamma = 1{\cdot}4$. The corresponding values of C_μ and C_Q are also shown for a representative ratio of slot area to wing area ($A_t/S = 5 \times 10^{-3}$) and the procedure for scaling to other conditions is indicated.

The jet-reaction coefficient C_J [$\equiv J/(q_0 S)$] is sometimes used instead of C_μ, where J represents the total jet reaction measured wind-off with a correction added for the measured pressure drag round the model arising from the local flows induced by the jet stream. With trailing-edge slots, or simple round nozzles, C_J should be

only two or three per cent different from C_μ, but the difference may be appreciable if the air is ejected over a trailing-edge flap, because of skin friction losses. The value of C_J yields the installed static thrust and, subject to some qualifications, signifies the effective jet momentum leaving the trailing edge. For example, the flap-drag correction can be quite appreciable (about 0·05 C_μ) and its determination on a three-dimensional model is not easy, particularly if a body is present. Furthermore, the momentum leaving the trailing edge wind-on is not necessarily the same as that wind-off, for a prescribed practical condition. The value of C_μ yields, by definition, the mass flow and total pressure required at the slot with wind-on conditions and, subject to the specification of v_j, signifies the momentum ejected from the slot.

It is commonly argued that, provided the jet-momentum or reaction coefficient is correctly represented, temperature differences between the jet and main stream are of secondary importance as regards model force measurements. While this may well be true over the temperature range of 15°C to 50°C normally practicable in tunnel testing without special precautions, the extrapolation of such test results to full-scale jet temperatures certainly needs further justification. In fact, the whole question of the interpretation of test results at very low forward speeds warrants careful examination when the jet velocity and temperature are substantially different from full-scale values.

4.2. Experimental Determination of Momentum Coefficient

Measurements have to be made of the total head in the slot or nozzle (for the evaluation of v_j) and of the rate of mass flow M_j to the model, as discussed in Section 4.2 of Ref. 1. The spanwise variation of slot total head can be determined accurately by traversing a flattened Pitot located in the parallel slot exit, provided the slot is wide enough for the purpose, say, 0·01 in. or more. At the same time, the spanwise variation of slot width can usefully be checked with feeler gauges, preferably over the same range of jet pressure and temperature as in the tunnel tests. A static pressure tapping in the low velocity duct can be used as a convenient datum for setting the nominal pressure ratio. If the slot width is too small to admit entry of a flattened Pitot, the mean pressure ratio, as indicated by several such pressure tappings, has to be used. In this case, it is especially important that the duct velocity should be low enough to ensure negligible losses and a uniform spanwise distribution of slot total head.

Although the mass flow can be readily measured by an orifice plate in the delivery line between the pump and the model, its determination to within an absolute accuracy of ± 1 per cent over a wide range of test conditions is no easy matter. Fortunately, a lower absolute accuracy suffices for most purposes, provided the comparative accuracy can be maintained at this figure (*see* Appendix V of Ref. 1). The precise assessment of thrust losses, particularly under cruising conditions, represents one case where a good absolute accuracy in the measurement of M_j and C_μ may be essential.

If the mass flow meter has to be installed in non-standard conditions, as often happens because of space limitations, then it must be recalibrated *in situ* and any

leaks downstream of the meter must be sealed or allowed for. The measured thrust characteristics of a simple circular nozzle of about the same exit area also form a useful standard of reference against which to compare $M_j v_j$. Finally, it is advisable to measure the mass flows for the prescribed duct reference pressures under completely representative model and wind-on conditions. For example, with subsonic blowing over flaps at large deflection angles, the mass flow can be noticeably affected by the variation of the static pressure just outside the slot with the main stream velocity and flap angle.

Appendix I

Some General Remarks on the Choice of Air-Feed Connectors

In view of the variety of possible air-feed connectors, the merits of some known to the authors are discussed briefly here. Clearly, no single type will provide a universal solution for all model tests, but the following remarks may assist in the selection of a suitable type for a particular application.

A mercury seal is attractive when sufficient vertical height is available, since this limits the blowing pressure ratio which can be tolerated. Difficulties may arise from the weight of mercury involved and the problem of maintaining the strut in a truly vertical position. Significant tare forces could also occur from the internal static pressure, and from vertical momentum and static pressure changes along the strut associated with surface friction and separation, if the velocity is high. A simple rubber tube hanging in a U-shape may likewise be adequate if sufficient vertical depth is available, particularly when the air can be supplied at high pressure so that the tube diameter can be small. Measurable constraints seem inevitable in this case.

A quite different approach is to use a hollow strain-gauge sting for the model support. Here the principal objections are the necessity for suitable electronic equipment, the problem of adequate accuracy over a wide range, including difficulties associated with heating effects of the air supply, and possibly the lengthy development time.

A multiple arrangement of bellows and gimbal rings would seem attractive, but the authors have no personal experience as to the magnitude of the resulting constraints, or as to whether substantial model movements could be tolerated. The simple "necked-canvas sleeves," mentioned in Appendix II of Ref. 1, are essentially flexible bellows and could be employed along the lines suggested in Section 3.2.2 to permit six-component force measurements. Appreciable constraints could arise, but with good design they should be repeatable and could be allowed for. The resulting system should be robust as well as simple and probably quite adequate for most purposes.

Air-bearing connectors are discussed in detail in Appendix III of Ref. 1 and Appendix II of this paper. A possible disadvantage, compared with bellows or hose-type connectors, arises from the inherent air leak, but this need not be troublesome, except perhaps when the air-bearing has to be located inside the model itself. Although appearing somewhat complex at first sight, the parts required are reasonably straightforward to make with a lathe and shaper, provided that flat faces only are needed. Those developed to date at the R.A.E. and N.P.L. have proved quite satisfactory and well worth the extra effort required. The likely advantages comprise trouble-fee operation if the air supply is filtered, small and repeatable air-feed constraints to the model, and compactness. Furthermore, the air-bearing connector can sometimes be designed to incorporate the required rotations of the balance side of the connector relative to the earth side arising when the model is yawed or pitched, thus avoiding the necessity for an auxiliary turntable

Appendix II

DETAILS OF "FOUR-FACED" AIR-BEARING CONNECTOR FOR R.A.E. COMPLETE-MODEL RIG

(Suitable for six-component measurements using a null-movement virtual-centre balance)

An air-bearing connector suitable for three-component tests had already been developed at N.P.L. (*see* Appendix III of Ref. 1). In the R.A.E. jet-flap complete-model rig (*see* Fig. 5) the air-feed connection had to be chosen to minimise the constraint effects on all six components. Small constraints were acceptable, as long as they were repeatable and measurable. Since it was desired to continue testing half-models on the same balance, the chosen system had to permit the balance to yaw over a total range of about 40°, without serious constraint variations for half-model tests. Two main schemes were tried in turn (*see* Figs. 6 and 7), each using air-bearing connectors.

In Scheme A (Fig. 6) two horizontal air-bearings were used, as in the N.P.L. three-component rig. The "earth side" supported a hollow Dural central block, which was arranged with its top and bottom faces truly horizontal. The "balance side" faces of the air-bearing were formed by two machined circular pads, spaced apart by three shouldered round bars and hung from the base plate by three like bars.

However, it was found that, with this scheme, the lift-zero varied rapidly with differential gap ($G_B - G_T$) at a fixed internal pressure. For example, a change of 0·001 in. in ($G_B - G_T$) altered the lift constraint by 10 lb. at an internal pressure of two atmospheres (gauge). The other constraints did not vary with ($G_B - G_T$) and were solely functions of internal pressure; they were large but not intolerable, as seen from the following table.

BALANCE ZERO CONSTRAINTS AT INTERNAL PRESSURE OF TWO ATMOSPHERES GAUGE

	Lift (lb.)	*Drag* (lb.)	*Side force* (lb.)	*Pitching moment* (lb. ft.)	*Rolling moment* (lb. ft.)	*Yawing moment* (lb. ft.)
A	Variable	<0·5	<0·5	<10	<5	<0·2
B	<0·5	<0·5	<0·5	< 2	<4	<0·2

In view of the indeterminate lift-zero constraint with Scheme A, Scheme B was next tried. Here, two vertical air-bearings were added (Fig. 6) so that the block now floated freely between the balance side and the earth side. As in the first scheme, the air-bearings were supplied by direct leak from the main internal feed; however, for convenience, two rings of holes in the bottom pad were supplied from the interior to start the block floating. From the table, it is clear that the additional freedom is beneficial, since the lift constraint is now small and determinate. The constraints on pitching and rolling moment, which are further reduced, largely arise from small drag and side force constraints, which produce appreciable moment constraints at the balance virtual centre, about which the moment changes are measured. As pressurised zeros are taken before and after each run, there is no appreciable overall reduction in balance accuracy. Scheme B requires the block to be stable to small displacements. Except as far as lateral translational displacements are concerned, the system is inherently stable, since the local pad pressure increases automatically as the gap decreases at a given internal pressure, so that restoring forces and moments are produced. The lateral movement of the block, however, had to be restricted by a set of three balls running freely in sockets.

Scheme B has now functioned successfully for more than two years.

Appendix III

A Jet-Path Visualisation Technique

The path of deflected plane jets or circular jets can be visualised quite simply by means of fluid injection method. Streams of a suitable liquid, for example, water or paraffin, fed by gravity from a static tank reservoir above the tunnel, are injected into the centre of the jet just outside the slot. The liquid is dispersed as a cloud of fine drops, and rapidly spreads across the jet as it is carried downstream. Elevation or plan views of the path of the jet can be obtained with conventional lighting, and transverse sections by projecting a plane of light normal to the main stream direction.

The method is particularly suitable for jet speeds above 500 ft./sec. The effect of model configuration changes can be studied in as much detail as required, and no particular precautions are necessary, apart from mopping up the liquid puddles which form on the tunnel floor! To visualise a flow of 1 lb./sec. of air, from one wing of a jet-flap complete model with a slot area of about $30 \times 0{\cdot}05$ in., eleven tubes of 0·05 in. internal diameter were regularly spaced along the span, together with an extra tube of 0·10 in. diameter to visualise the tip vortex. About one gallon (10 lb.) of water sufficed for 10 minutes' continuous running.

References

1. Anscombe, A. and Williams, J. Some Comments on High-Lift Testing in Wind Tunnels with Particular Reference to Jet-Blowing Models. *Journal of the Royal Aeronautical Society*, Vol. 61, p. 529, 1957.

2. Butler, S. F. J. and Guyett, M. B. Low-Speed Wind-Tunnel Tests on the De Havilland Sea Venom with Blowing Over the Flaps. R. & M. 3129, 1956.

3. Williams, J. and Alexander, A. J. A Preliminary Note on a Wind-Tunnel Investigation of Trailing-Edge Flap Blowing on a 5 per cent thick 60° Delta Wing. Unpublished N.P.L. Paper, 1957.

4. Alexander, A. J. and Williams, J. Interim Note on Wind-Tunnel Experiments on a Rectangular-Wing Jet-Flap Model of Aspect-Ratio 6. Unpublished N.P.L. Paper, 1958.

5. Maskell, E. C. The Interference on a Three-Dimensional Jet-Flap Wing in a Closed Wind Tunnel. Unpublished Ministry of Supply Report.

6. Maskell, E. C. and Spence, D. A. A Theory of the Jet Flap in Three Dimensions. *Proc. Roy. Soc.* A, Vol. 251, p. 407, 1959.

7. Williams, J. British Research on Boundary-Layer Control for High-Lift by Blowing. *Zeitschrift für Flugwissenschaften*, Vol. 6, No. 5, p. 143, 1958.

8. Williams, J. British Research on the Jet-Flap Scheme. *Zeitschrift für Flugwissenschaften*, Vol. 6, No. 6, p. 170, 1958.

9. Pankhurst, R. C. and Holder, D. W. *Wind-Tunnel Technique*. Pitman, London, 1952.

10. Silverstein, A. and White, J. A. Wind-Tunnel Interference with Particular Reference to Off-Centre Positions of the Wing and Downwash at the Tail. N.A.C.A. Rep. 547, 1935.

11. Huggett, D. J. The Ground Effect on the Jet Flap in Two Dimensions. *The Aeronautical Quarterly*, Vol. X, February 1959.

12. Vogler, R. D. and Turner, T. R. Wind-Tunnel Investigation at Low Speeds to Determine Flow Field Characteristics and Ground Influence on a Model with Jet-Augmented Flaps. N.A.C.A. T.N. 4116, 1957.

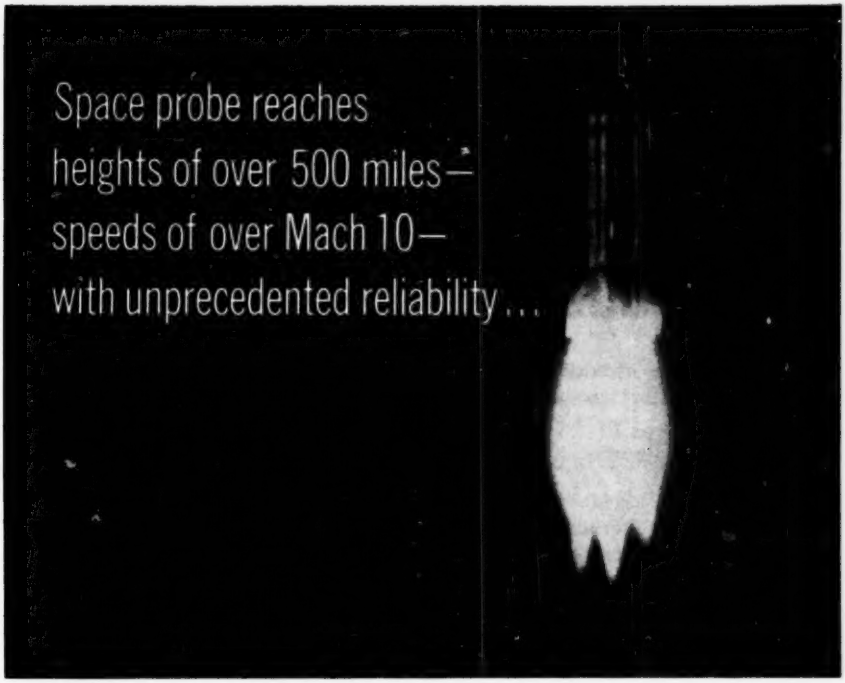

...AND BRISTOL SIDDELEY SUPPLY THE POWER

One of the largest manufacturers of motive power units in the world, Bristol Siddeley Engines Limited produce the Gamma. A liquid propellent rocket engine, the Gamma powers the Saunders-Roe Black Knight, Britain's highly successful space research vehicle. An extremely reliable powerplant, the Gamma produces a total sea-level thrust of 16,400 lb (7,438 kg) and nearly 19,000 lb (8,618 kg) outside the earth's atmosphere, for a total powerplant weight of under 700 lb.

At the Woomera rocket range in Australia, the Gamma has sent Black Knight over 500 miles into space at speeds in excess of Mach 10 with unprecedented reliability. For, to date, every Black Knight vehicle has been launched successfully.

Since Bristol Siddeley's rocket division began work in 1946, it has developed a wide range of components. *By combining these components in single or multi-chamber layouts, thrust requirements from 500 lb up to 100,000 lb can be met.*

Bristol Siddeley products currently in production include:—

AERO:

TURBOJETS: Olympus; Sapphire; Orpheus; Viper.

TURBOPROPS: Proteus; Double Mamba.

ROCKETS: Gamma and others.

RAMJETS: Thor 1 & 2.

INDUSTRIAL & MARINE:

DIESELS: Maybach.

GAS TURBINES: Proteus.

OTHER PRODUCTS: Gas bearing compressors; Beaver ball screws and splines.

BRISTOL SIDDELEY ENGINES LIMITED

BRISTOL Aircraft

OPPORTUNITIES FOR WORK ON NEW PROJECTS AT BRISTOL

Bristol Aircraft Limited offer excellent and progressive careers with their research, development and design teams at FILTON to young men or women who have a degree or a Higher National Certificate or Diploma.

Bristol are known throughout the world for their successful turboprop BRITANNIA and the BLOODHOUND Guided Missile.

They can offer interesting and challenging careers on the projects of the future.

Structures Design Engineers
Mechanical Engineers
Dynamics Engineers
Mathematicians **Draughtsmen**
Physicists **Designers**
Aerodynamicists
Systems Engineers
Electrical/Electronic Engineers

If you are interested, write to:-

J. Raimes, Personnel Manager,
Room FW/10/AQ
Bristol Aircraft Limited, FILTON, Bristol,

giving full details of your education, experience and position in which you are interested.

MEMBER COMPANY OF BRITISH AIRCRAFT CORPORATION

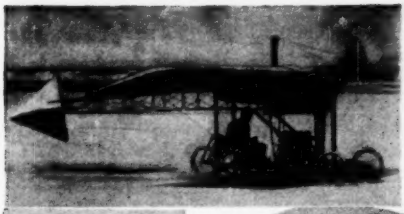

50

50 years of experience are behind the Blackburn NA.39

1909 Robert Blackburn designed, built and flew his first aircraft at Marske Sands in Yorkshire.

1959 Latest of a long line, the Blackburn NA.39 Strike Aircraft, which first flew on its target date in April, 1958, is now in production. Of this aircraft the Ministry of Defence has stated "In the low-level strike role, the NA.39 is ahead of any aircraft in the world."

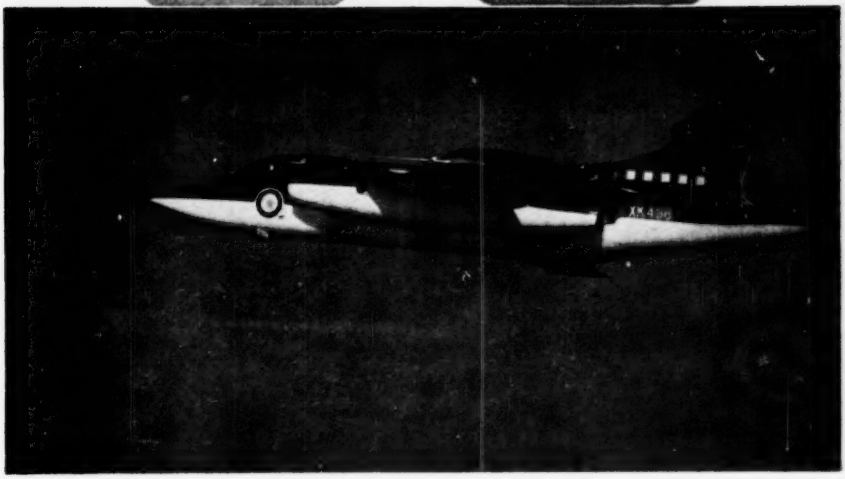

If you are an A.F.R.Ae.S. or possess an equivalent qualification, please write to the Technical Staff Manager, when we shall be pleased to give you details of the opportunities available to experienced men within our technical organisation.

Blackburn Aircraft Limited, Brough, Yorkshire

A128/d

CHAPMAN AND HALL

Published under the authority of the
Royal Aeronautical Society

AIRCRAFT HYDRAULICS

edited by

H. G. CONWAY

Volume I—Hydraulic Systems

Size 10 in. x 6 in. 146 pages 107 illustrations

35s. net

Volume II—Component Design

Size 10 in. x 6 in. 216 pages 120 illustrations

45s. net

INSTRUMENTATION IN TESTING AIRCRAFT

by C. N. JAQUES

Size 8¾ in. x 5½ in. 292 pages 117 illustrations

45s. net

LANDING GEAR DESIGN

by H. G. CONWAY

Size 10 in. x 6 in. 342 pages 366 illustrations

56s. net

AIRCRAFT ELECTRICAL ENGINEERING

edited by

G. G. WAKEFIELD

Size 10 in. x 6 in. 350 pages 201 illustrations

50s. net

37 ESSEX STREET - LONDON WC2

NOTICE TO CONTRIBUTORS

1. All communications should be addressed to the Editor, The Aeronautical Quarterly, 4 Hamilton Place, London, W.1.

2. Papers for consideration should be typewritten with double spacing and be accompanied by a summary of not more than 250-300 words. *Papers must be as short as possible*, otherwise considerable delay in publication will result, and in any case they should not be longer than twenty foolscap pages. Full descriptions and complete results of work, as written for an internal report, are not suitable for publication in *The Aeronautical Quarterly*, and such reports need to be rewritten in concise form. Only necessary equations should be included in the text; routine mathematics should be omitted or given as an Appendix to the paper. Illustrations should be reduced to a minimum. The titles of papers should be kept short—with sub-titles if necessary.

3. Only simple symbols and formulae should be typewritten. All others should be written clearly in ink. Greek letters should be indicated and a clear distinction drawn between capital and small letters. Particular attention should be paid to the use of alpha and *a*, kappa and *k*, mu and *u*, nu and *v*, eta and *n*. The letter *l* must be distinguished from the numeral 1, and the letter *O* from the zero 0.

   The use of dots, bars, and so on, over letters, or the use of dots as multiplication signs and bars for brackets should be avoided as far as possible.

   Suffixes and prefixes must be indicated clearly and complicated suffixes and prefixes should be avoided.

4. A list of *all* symbols used, both in the illustrations and text, *must* be given whether they are standard or not.

5. *Clear* diagrams or sketches must be submitted for redrawing by the Society's draughtsman.

   Photographs must be not less than half plate size and must be clear black and white glossy prints.

6. References should be given in the form:—
   WARD, G. N. Calculation of Downwash Behind a Supersonic Wing. *The Aeronautical Quarterly*, Vol. I, pp. 35-38, May 1949.

7. The copyright of every paper printed in *The Aeronautical Quarterly* is the property of The Royal Aeronautical Society. Permission to reprint or to use any paper will not be unreasonably refused.

8. It is a condition of publication that the author shall have obtained consent where necessary to use any material in his paper which is copyright or the property of any other person or his employers.

9. Authors will be entitled to 20 reprints of their papers free of charge. This number will be shared between joint authors.

The Aeronautical Quarterly is published at the Offices of The Royal Aeronautical Society, 4 Hamilton Place, Piccadilly, London, W.1, at 15s. 0d. net for a single number to non-members and 7s. 6d. net for a single number to members of The Royal Aeronautical Society. Instructions for Contributors are given above. None of the papers must be taken as expressing the opinion of the Council of The Royal Aeronautical Society unless such is definitely stated to be the case. All communications for publication or advertisement in The Quarterly should be addressed to—The Editor, The Aeronautical Quarterly, 4 Hamilton Place, W.1.

Telephone: Grosvenor 3515 (5 lines). Telegraphic Address: Didaskalos, Audley, London

CHAPMAN AND HALL

Published under the authority of the
Royal Aeronautical Society

AIRCRAFT HYDRAULICS

edited by

H. G. CONWAY

Volume I—Hydraulic Systems

Size 10 in. x 6 in. 146 pages 107 illustrations

35s. net

Volume II—Component Design

Size 10 in. x 6 in. 216 pages 120 illustrations

45s. net

INSTRUMENTATION IN TESTING AIRCRAFT

by C. N. JAQUES

Size 8¾ in. x 5½ in. 292 pages 117 illustrations

45s. net

LANDING GEAR DESIGN

by H. G. CONWAY

Size 10 in. x 6 in. 342 pages 366 illustrations

56s. net

AIRCRAFT ELECTRICAL ENGINEERING

edited by

G. G. WAKEFIELD

Size 10 in. x 6 in. 350 pages 201 illustrations

50s. net

37 ESSEX STREET - LONDON WC2

NOTICE TO CONTRIBUTORS

1. All communications should be addressed to the Editor, The Aeronautical Quarterly, 4 Hamilton Place, London, W.1.

2. Papers for consideration should be typewritten with double spacing and be accompanied by a summary of not more than 250-300 words. *Papers must be as short as possible*, otherwise considerable delay in publication will result, and in any case they should not be longer than twenty foolscap pages. Full descriptions and complete results of work, as written for an internal report, are not suitable for publication in *The Aeronautical Quarterly*, and such reports need to be rewritten in concise form. Only necessary equations should be included in the text; routine mathematics should be omitted or given as an Appendix to the paper. Illustrations should be reduced to a minimum. The titles of papers should be kept short—with sub-titles if necessary.

3. Only simple symbols and formulae should be typewritten. All others should be written clearly in ink. Greek letters should be indicated and a clear distinction drawn between capital and small letters. Particular attention should be paid to the use of alpha and *a*, kappa and *k*, mu and *u*, nu and *v*, eta and *n*. The letter *l* must be distinguished from the numeral 1, and the letter *O* from the zero 0.

   The use of dots, bars, and so on, over letters, or the use of dots as multiplication signs and bars for brackets should be avoided as far as possible.

   Suffixes and prefixes must be indicated clearly and complicated suffixes and prefixes should be avoided.

4. A list of *all* symbols used, both in the illustrations and text, *must* be given whether they are standard or not.

5. *Clear* diagrams or sketches must be submitted for redrawing by the Society's draughtsman.

   Photographs must be not less than half plate size and must be clear black and white glossy prints.

6. References should be given in the form:—
   WARD, G. N. Calculation of Downwash Behind a Supersonic Wing. *The Aeronautical Quarterly*, Vol. I, pp. 35-38, May 1949.

7. The copyright of every paper printed in *The Aeronautical Quarterly* is the property of The Royal Aeronautical Society. Permission to reprint or to use any paper will not be unreasonably refused.

8. It is a condition of publication that the author shall have obtained consent where necessary to use any material in his paper which is copyright or the property of any other person or his employers.

9. Authors will be entitled to 20 reprints of their papers free of charge. This number will be shared between joint authors.

The Aeronautical Quarterly is published at the Offices of The Royal Aeronautical Society, 4 Hamilton Place, Piccadilly, London, W.1, at 15s. 0d. net for a single number to non-members and 7s. 6d. net for a single number to members of The Royal Aeronautical Society. Instructions for Contributors are given above. None of the papers must be taken as expressing the opinion of the Council of The Royal Aeronautical Society unless such is definitely stated to be the case. All communications for publication or advertisement in The Quarterly should be addressed to—The Editor, The Aeronautical Quarterly, 4 Hamilton Place, W.1.

Telephone: Grosvenor 3515 (5 lines). Telegraphic Address: Didaskalos, Audley, London

THE AERONAUTICAL QUARTERLY

It is the aim of *The Aeronautical Quarterly* to attract not only original papers contributing to aeronautical science and engineering, and papers developing new or improved methods of analysis and experimental techniques, but also papers on allied sciences which have a bearing on aeronautical problems. *The Aeronautical Quarterly* is open to authors of any nationality and is not restricted to members of the Society.

Most papers can be published within nine months of receipt. Short papers, of not more than 2,000 words, are published much more quickly.

VOLUME XI

Volume XI of *The Aeronautical Quarterly* will be published in four parts, in February, May, August and November 1960. The prices, *including postage and packing*, are:—

	To Members of the Society		*To Non-Members*	
	£ s. d.		£ s. d.	
Per Part	8 0	($1.15)	15 6	($2.20)
Subscription (4 parts)	1 12 0	($4.50)	3 2 0	($8.70)

PRINTED BY THE LEWES PRESS, WIGHTMAN & CO. LTD., LEWES, SUSSEX, ENGLAND, AND PUBLISHED BY THE ROYAL AERONAUTICAL SOCIETY, 4 HAMILTON PLACE, LONDON, W.1, ENGLAND.